

T H E U N I V E R S I T Y O F A L B E R T A

RELEASE FORM

NAME OF AUTHOR: DENNIS E. PUF AHL
TITLE OF THESIS: THE BEHAVIOR OF THAWING SLOPES IN PERMAFROST
DEGREE FOR WHICH THESIS WAS PRESENTED: DOCTOR OF PHILOSOPHY
YEAR THIS DEGREE GRANTED: 1976

Permission is hereby granted to THE UNIVERSITY OF ALBERTA LIBRARY to reproduce single copies of this thesis and to lend or sell such copies for private, scholarly or scientific research purposes only.

The author reserves other publication rights, and neither the thesis nor extensive extracts from it may be printed or otherwise reproduced without the author's written permission.

(Signed)

D. E. Pufahl.....

PERMANENT ADDRESS:


Department of Civil Engineering
University of Saskatchewan
Saskatoon, Saskatchewan S7N 0W0

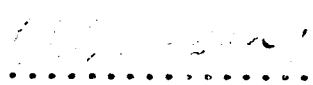
DATED: .Sept..1/76.....

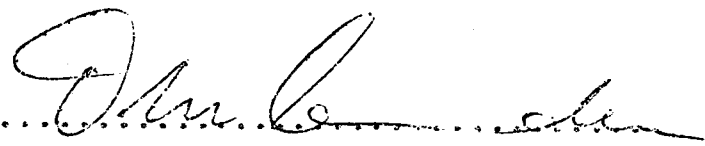
THE UNIVERSITY OF ALBERTA

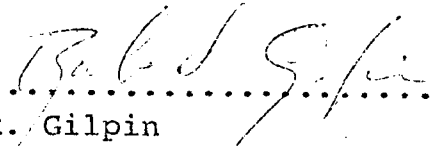
FACULTY OF GRADUATE STUDIES AND RESEARCH

The undersigned certify that they have read, and recommend to the Faculty of Graduate Studies and Research for acceptance, a thesis entitled "THE BEHAVIOR OF THAWING SLOPES IN PERMAFROST" submitted by Dennis E. Pufahl in partial fulfilment of the requirements for the degree of Doctor of Philosophy in Civil Engineering.

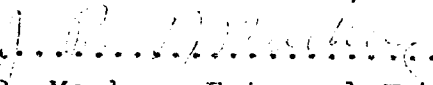

.....
N.R. Morgenstern, Supervisor


.....
S. Thomson


.....
D. Cruden


.....
R. Gilpin

Date: Sept 1, 1976


.....
J.R. Mackay, External Examiner

THE UNIVERSITY OF ALBERTA

THE BEHAVIOR OF THAWING SLOPES IN PERMAFROST

by

DENNIS E. PUFAHL

A THESIS

SUBMITTED TO THE FACULTY OF GRADUATE STUDIES

AND RESEARCH IN PARTIAL FULFILMENT OF THE

REQUIREMENTS FOR THE DEGREE OF

DOCTOR OF PHILOSOPHY

DEPARTMENT OF CIVIL ENGINEERING

EDMONTON, ALBERTA

FALL, 1976

ABSTRACT

Slope instability is one of the major considerations in the choice of route location across terrain underlain by permafrost. A field reconnaissance has established the state-of-the-art of cut slope design, construction and performance in the Western Canadian Arctic and Alaska. It is apparent that limited instability of backslope cuts in fine grained frozen soils may be encountered in almost all of these regions. Emphasis has been placed on establishing the geological history, the land form, and the associated soil and ground ice characteristics.

Flow dominated failures on natural slopes and cut slopes are common in regions of permafrost. A means of stabilizing these failures is proposed. The method utilizes insulation to control the rate of thaw and the generation of excess pore water pressures. A sand/gravel surcharge load helps to stabilize the slope by increasing the normal effective stress disproportionately to the shearing stress. Design charts are provided and recommendations for installation are included.

Uncontrolled thawing of backslope cuts in fine grained ice rich soil generally results in the formation of bimodal flows common to periglacial regions. A prerequisite for the development of rational methods of control of these features is the establishment of the energetics of exposed melting permafrost. The theory is developed and verified by field experiments and thus provides the basis for controlling the rate of thaw of exposed permafrost.

Recommendations for the design and construction of cut slopes in frozen soils are outlined. Some control methods are suggested that incorporate sand/gravel and other types of higher quality insulation in a variety of different configurations.

ACKNOWLEDGEMENTS

The activities and research presented in this thesis were carried out under the direction of Dr. N.R. Morgenstern, University of Alberta. The author is grateful and indebted to him for his suggestions regarding the topic, for his help in interpreting and presenting the data, and especially for his seemingly limitless enthusiasm for the research project. The help of Dr. Stan Thomson was also warmly received.

Sincere appreciation is extended to the University of Alberta support staff which include Messrs. O. "Woody" Woods, Roy Gitzel, Al Muir, and Don Nordheimer.

This research project was sponsored by the Department of Energy, Mines and Resources, the Defense Research Board, and the National Research Council of Canada. The Department of Public Works, Government of Can., Northwest Territories and the Yukon Territory, the Alaska Department of Highways in Fairbanks, and the State Materials Laboratory in College Alaska all receive recognition for their suggestions, participation and interest in the project.

Personal financial assistance from the Transportation Development Agency, the Roads and Transportation Association of Can., and the North American Life Canadian Council of Professional Engineers was gratefully received.

In addition the author wishes to acknowledge the support and encouragement offered by wife, Idoline Ann, during the first year and a half in Edmonton. Sincere apologies are extended to her for any economic, social or emotional deprivation that may have resulted from this undertaking.

Finally, the unflagging^d interest and help from Mr. Bill Roggensack during those endless miles of dust and rain and gravel will always be remembered. His editorial assistance was invaluable and the personal friendship and support provided by him and his wife, Muriel, made the completion of this thesis possible.

TABLE OF CONTENTS

	Page
Release Form	i
Title Page	ii
Approval Sheet	iii
Abstract	iv
Acknowledgements	v
Table of Contents	vii
List of Tables	xv
List of Figures	xvi
 CHAPTER I	
INTRODUCTION	
1.1 General	1
1.2 Scope of Thesis	3
 CHAPTER II	
BEHAVIOR OF EXISTING CUTS IN PERMAFROST	
2.1 Objectives	5
2.2 Route	6
2.3 Alaska Highway [Mile 222 (from Dawson Creek, B.C.) 57°58'N latitude; 122°46' W longitude]	7
2.3.1 Summary	8
2.4 Dempster Highway	10
2.4.1 Location and Background	10
2.4.2 Mile 0 - Mile 80	12
2.4.3 Mile 80 - Mile 154	14
2.4.4 Mile 154 - Mile 178	16
2.4.5 Fort McPherson to Arctic Red River Mile 330 to Mile 365	18
2.4.6 Mile 178 - Mile 330	19

	Page
2.5 Mackenzie Highway (Inuvik to Arctic Red River)	19
2.6 Alaska Reconnaissance	20
2.6.1 General	20
2.6.2 TAPS Haul Road	20
2.6.3 Copper River Basin	23
2.7 Conclusions	24
CHAPTER III STABILIZATION OF PLANAR LANDSLIDES IN PERMA-FROST	
3.1 Introduction	33
3.2 Thaw Consolidation Pore Water Pressures	33
3.3 Stability Analysis of Infinite Thawing Slopes	37
3.4 Numerical Procedure for Design	41
3.5 Design Charts	46
3.6 Example Problem	47
3.7 Recommendations for Installation	53
3.8 Long term Performance	55
3.9 Choice of Insulation	55
CHAPTER IV THE ENERGY BALANCE	
4.1 Basic Concepts	70
4.2 Radiative Components on a Horizontal Surface	71
4.2.1 General	71
4.2.2 Direct Beam Clear Sky Solar Radiation	73
4.2.3 Diffuse Clear Sky Radiation	76

	Page
4.2.4 The Effect of Clouds	79
4.2.5 Summary of Short Wave Radiation	83
4.2.6 Short Wave Radiation Reflected by the Surface of the Earth	83
4.2.7 Net Short Wave Radiation	84
4.2.8 Longwave Radiation Emitted by The Ground Surface	86
4.2.9 Longwave Radiation From the Atmos- phere to the Ground	88
4.2.10 Net Longwave Radiation	93
4.3 Radiative Components on a Sloping Sur- face	98
4.3.1 General	98
4.3.2 Direct Beam Radiation	99
4.3.3 Diffuse Radiation	103
4.3.4 Short Wave Component Reflected to the Surface by Surrounding Surfaces	106
4.3.5 Short Wave Component of Radiation Reflected by the Surface	108
4.3.6 Downward Longwave Component of Radiation Falling on the Slope	109
4.3.7 Downward Longwave Component Reflected to the Surface by Surrounding Sur- faces	110
4.3.8 Upward Component of Long Wave Rad- iation Reflected onto the Slope by Surrounding Surfaces	110
4.3.9 Long wave Radiation Emitted by the Surface	111
4.3.10 Summary of Components	111
4.4 Turbulent Transfer Processes	114
4.5 Evaporation and Condensation	114

	Page
4.6 Sensible Heat Transfer	120
4.7 Energy Transfer Due to Precipitation	126
4.8 Soil Heat Transfer	127
4.9 Summary of Heat Balance	128
 CHAPTER V	
HEAT FLUX MEASUREMENTS AT THE HEAD SCARP	
5.1 Introduction	129
5.2 Site Location and Description	129
5.3 Ablation Rates	142
5.3.1 Measurement Techniques	142
5.3.2 Magnitude and Heat Requirements	144
5.4 Radiation Balance	151
5.4.1 Short Wave Radiation	151
5.4.2 Net Short Wave Radiation	152
5.4.3 Net Long Wave Radiation	152
5.4.4 Net All wave Radiation	156
5.5 Radiation Field Instrumentation	156
5.6 Data Acquisition System	157
5.7 Measured Total Short Wave Radiation	162
5.8 Measured Net Radiation	166
5.9 Latent Heat Transfer	173
5.10 Evaporation Quantities	185
5.11 Sensible Heat Transfer	187
5.12 Ablation and the Heat Balance	189

	Page
CHAPTER VI	CONTROL OF THAWING IN EXPOSED PERMAFROST
6.1	Head Scarp Geometry of Bimodal Flows 205
6.2	Basis for Control 206
6.3	Suggested Methods of Control 209
6.4	Recommended Practice for Cut Slope Design 214
6.4.1	Self Healing Cut Slopes 214
6.4.2	Non Self-Healing Cut Slopes 217
CHAPTER VII	CONCLUDING REMARKS 222
	LIST OF REFERENCES 227
APPENDIX A	DETAILS OF FIELD RECONNAISSANCE
A.1	Alaska Highway (Mile 222 (from Dawson Creek, B.C.) 57°58'N Latitude; 122°46'W Longitude) 236
A.1.1	Physiography 236
A.1.2	Climate 236
A.1.3	Permafrost 236
A.1.4	Bedrock Geology 237
A.1.5	Surficial Geology 237
A.1.6	Highway Details (Mile 222) 238
A.2	Dempster Highway 238
A.2.1	Dempster Highway (Mile 0 to Mile 80) 239
A.2.2	Climate 239
A.2.3	Permafrost 240
A.2.4	Bedrock Geology 240
A.2.5	Surficial Geology 240

	Page
A.2.6 Highway Details	240
A.3 Dempster Highway (Mile 80 to Mile 154)	241
A.3.1 Physiography	241
A.3.2 Climate	242
A.3.3 Permafrost	242
A.3.4 Bedrock Geology	242
A.3.5 Surficial Geology	242
A.3.6 Highway Details	243
A.3.6.1 Highway Details (Mile 80 - Mile 96)	243
A.3.6.2 Highway Details (Mile 96 to Mile 123)	243
A.3.6.3 Highway Details (Mile 114)	244
A.3.6.4 Highway Details (Mile 120.7)	244
A.3.6.5 Highway Details (Mile 123 to Mile 154)	244
A.3.7 Summary	245
A.4 Dempster Highway (Mile 154 to Mile 178)	245
A.4.1 Physiography	245
A.4.2 Climate	246
A.4.3 Permafrost	246
A.4.4 Bedrock Geology	246
A.4.5 Surficial Geology	246
A.5 Highway Details	247
A.5.1 Highway Details (Mile 168)	247
A.5.2 Highway Details (Mile 175)	247
A.5.3 Summary	248

	Page
A.6 Dempster Highway (Fort McPherson to Arctic Red River, Mile 330 to Mile 365)	249
A.6.1 Physiography	249
A.6.2 Climate	249
A.6.3 Permafrost	249
A.6.4 Bedrock Geology	249
A.6.5 Surficial Geology	249
A.6.6 Highway Details	250
A.7 Dempster Highway (Mile 178 to Mile 330)	251
A.7.1 Physiography	251
A.7.2 Climate	251
A.7.3 Permafrost	251
A.7.4 Bedrock Geology	251
A.7.5 Surficial Geology	252
A.7.6 Observations	252
A.7.7 Summary	252
A.8 Mackenzie Highway (Inuvik to Arctic Red River)	253
A.9 Alaska Reconnaissance	253
A.9.1 General	253
A.9.2 Physiography	254
A.9.3 Climate	255
A.9.4 Permafrost and Vegetation	255
A.9.5 Bedrock Geology	255
A.9.6 Surficial Geology	256
A.9.7 Highway Details	256
A.9.7.1 Highway Details (Mile 14)	256

	Page
A.9.7.2 Highway Details (Mile 19.6)	257
A.9.7.3 Highway Details (Mile 20.3 to Mile 20.5)	257
A.9.7.4 Highway Details (Mile 22.9)	257
A.9.7.5 Highway Details (Mile 23.4)	258
A.9.7.6 Highway Details (Mile 33.0 to Mile 33.4)	259
A.9.7.7 Highway Details (Mile 42.8)	259
A.9.7.8 Highway Details (Mile 53.5)	259
A.9.7.9 Highway Details (Mile 54.4)	259
A.9.8 Summary	260
A.10 Copper River Basin	260
A.10.1 Physiography	260
A.10.2 Climate	261
A.10.3 Permafrost	261
A.10.4 Bedrock Geology	261
A.10.5 Surficial Geology	261
A.10.6 Highway Details	261
A.11 Conclusions	262
APPENDIX B COMPUTER PROGRAM AND EXAMPLE PROBLEM OF SLOPE STABILIZATION TECHNIQUE	272
APPENDIX C	
C.1 Computer program to calculate the length of a shadow cast by an obstruction on sloping ground	289

	Page
C.2 Computer program to compute the direct beam and total solar daily radiation on a sloping surface from values monitored on a horizontal surface	231
C.3 Procedure for calculating the amount of reflected diffuse radiation from one surface to another	292

APPENDIX D

D.1 Computer program for computing vapor pressures, vapor pressure gradients and temperature gradients from wet and dry bulb temperatures	308
-------------------------------------------------------------------------------------------------------------------------------------------	-----

Radiation data in Table D-1

LIST OF TABLES

Table	Page
2.1 Summary of Soil Data	29
2.2 Summary of Cuts	30
3.1 Physical and Thermal Properties of Various Insulating Methods	42
3.2 Soil, Insulation and Climate Information for Example Problem	48
3.3 Thaw Depth and Insulation and Surcharge Requirements for Example Problem	51
3.4 Comparison of Factors of Safety by Different Methods of Computation	52
4.1 Albedo of Various Surfaces	85
4.2 Infrared Emissivities	87
4.3 Air Temperature, Relative Humidity, and Vapour Pressure	118
4.4 Snow Melt Due to Sensible & Convective Heat Transfer and Bowen's Ratio (After U.S. Army Corps of Eng., 1956)	124
5.1 Summary of Soil Data at Fort Simpson Landslide	139
5.2 Short Wave Radiation Quantities for Slopes at Different Orientations and Inclinations for Fort Simpson Region	195
5.3 Net Longwave Radiation for Different Slopes Computed from Equation 4.53	197(a)
5.4 Net Radiation for Slopes at Different Orientations and Inclinations for Fort Simpson Region	198
5.5 Daily and Accumulated Total Radiation on a Horizontal Surface at the Fort Simpson Test Site	200
5.6 Net Radiation at the Fort Simpson Test Site	201
5.7 Comparison of Predicted Values and Measured Values of Net Radiation	203
5.8 Lysimetric Data	204
D.1 Radiation Data (Fort Simpson Test Site)	

LIST OF FIGURES

Figure		Page
2.1	Transportation Facilities - 1972 Northwestern Canada	8
2.2	Permafrost in Canada (After Brown, 1967)	9
2.3	Location of the Dempster Highway, Dawson City, Yukon Territory to Arctic Red River, N.W.T.	11
2.4	Physiographic Regions of the Yukon Territory	13
2.5	Location of Mile 90 to Mile 180 of the Dempster Highway	15
2.6	TAPS Haul Road; Livengood to the Yukon River Alaska	21
3.1	Thaw Depth vs Time and Thaw Depth vs $\sqrt{\text{Time}}$ for an Insulated Thawing Slope	36
3.2	Pore Pressure at the Thaw Front of a Thawing Infinite Slope	38
3.3	Balance of Forces on a Thawing Infinite Slope	38
3.4	Pore Pressure Factor (R') for Different Thaw Consolidation Ratios (R) After Morgenstern & Nixon (1971)	40
3.5	Pore Pressure Factor (R'') for Different Thaw Consolidation Ratios (R) After Morgenstern & Nixon (1971)	40
3.6	Design Chart for Stabilization of Planar Landslides	58
3.7	Design Charts for Stabilization of Planar Landslides	59
3.8	Design Charts for Stabilization of Planar Landslides	60
3.9	Design Charts for Stabilization of Planar Landslides	61
3.10	Design Charts for Stabilization of Planar Landslides	62
3.11	Design Charts for Stabilization of Planar Landslides	63
3.12	Design Charts for Stabilization of Planar Landslides	64
3.13	Design Charts for Stabilization of Planar Landslides	65
3.14	Design Charts for Stabilization of Planar Landslides	66
3.15	Design Charts for Stabilization of Planar Landslides	67
3.16	Design Charts for Stabilization of Planar Landslides	68

Figure		Page
3.17	Design Charts for Stabilization of Planar Landslides	69
4.1	Monochromatic Emissive Power for Several Temperatures vs Wavelength (After Wiebelt (1966))	72
4.2	Atmospheric Transmission Chart (After Kimball 1928)	78
4.3	Extraterrestrial Daily Radiation Received on a Horizontal Surface (After Lui and Jordan, 1960)	80
4.4	The Ratio of the Monthly Ave. Daily Diffuse Radiation to the Monthly Ave. Daily Total Radiation as a Function the Cloudiness Index K_T (After Lui & Jordan, 1960)	80
4.5	Ratio of Direct to Diffuse Radiation Received at the Ground Surface (%) After London (1957)	81
4.6	Saturated Vapour Pressure vs Temperature	117
4.7	Convection Melt (computed) (After U.S. Army Corps of Eng., 1956)	123
4.8	Condensation Melt (computed) (After U.S. Army Corps of Eng., 1956)	123
5.1	Aerial View of Fort Simpson Landslide	130
5.2	Bank Profile of Mackenzie River Immediately East of Fort Simpson Landslide	131
5.3	Plan View of Fort Simpson Landslide	133
5.3(a)	Description of Sediments of Fort Simpson Landslide	133(a)
5.4	Aerial View of East Flank of Fort Simpson Landslide	134
5.5	Plan View and Instrumentation of Headscarp of Bimodal Flow at Fort Simpson Landslide	136
5.6	View of Headscarp (July 1974)	137
5.7	Mudflow at the Base of the Headscarp	137
5.8	Soil Profile Zone 1, 2 & 3 (Oct. 1973)	141
5.9	Soil in Zone 3	141
5.10	Frozen Core Removed From Zone 4	141
5.11	Schematic Arrangement of Ablation Measurement Technique	143

Figure		Page
5.12	Ablation Measurement Technique	145
5.13	Accumulated Ablation at Sta. 1	145
5.14	Accumulated Ablation at Sta. 2	146
5.15	Accumulated Ablation at Sta. 3	146
5.16	Accumulated Ablation at Sta. 4	147
5.17	Accumulated Ablation at Sta. 5	147
5.18	Accumulated Ablation at Sta. 6	148
5.19	Water Content vs. Relative Frequency Curve	148
5.20	$\cos \Lambda$ vs. Time for a Sloping Surface	153
5.21	$\cos \Lambda$ vs. Time for a Horizontal Surface	153
5.22	Net Radiometer (Fritchen Model)	158
5.23	Net Radiometers Around Headscarp	158
5.24	Typical Variation of Radiation Intensity with Time	160
5.25	Schematic Sketch of Radiation Instrumentation	165
5.26	Data Acquisition System	165
5.27	Total Shortwave Radiation on a Horizontal Surface for the Period of Observation	165
5.28	Net Radiation for the Period of Observation (Sta. 1)	167
5.29	Net Radiation for the Period of Observation (Sta. 2)	168
5.30	Net Radiation for the Period of Observation (Sta. 3)	169
5.31	Net Radiation for the Period of Observation (Sta. 4)	170
5.32	Net Radiation on a Horizontal Surface for the Period of Observation (Sta. 5)	171
5.33	Accumulated Net Radiation for the Period of Observation	172

Figure		Page
5.34	Permafrost Lysimeter	175
5.35	Permafrost Lysimeter	176
5.36	Tray from Permafrost Lysimeter (weighed with standard load cell)	176
5.37	Portable Crane and Permafrost Lysimeter	177
5.38	Product of Average Wind Speed and Relative Humidity vs. Latent Heat of Condensation	180
5.39	Wet and Dry Bulb Temperature Sensors	182
5.40	Typical Vapour Pressure Gradients Above the Headscarp	184
5.41	Daily Evaporation Rates at Test Site	186
5.42	Typical Temperature Gradients above the Headscarp	188
5.43	Heat Balance at the Headscarp of the Fort Simpson Landslide	191
6.1	Gravel Thickness, Ground Surface Thawing Index and Headscarp Retreat for Ice	212
6.2	Gravel and Artificial Insulation Configuration for Steep Slopes	218
6.3	Gravel and Artificial Insulation Configuration for Moderately Steep Slopes	218
6.4	Gravel and Rock Filled Gabions with Artificial Insulation on Moderately Steep Slope	220
6.5	Gravel and Artificial Insulation on Low Angle Slope	220
A.1	Mile 222 Alaska Highway (Backslope instability during construction, July 1973).	263
A.2	Mile 50 Dempster Highway (Headwaters of the East Blackstone River. Road built at very modest geometric design standards)	263
A.3	Mile 124 Dempster Highway (Typical view of the Ogilvie physiographic unit)	263
A.4	Mile 80 Dempster Highway (Improved geometric design standards)	264

Figure		Page
A.5	Mile 109 Dempster Highway (Biangular profile of backslope due to permafrost degradation)	264
A.6	Mile 114 Dempster Highway (Large thermal degradation scar - 150 ft. wide and 15 to 20 ft. deep)	264
A.7	Mile 120.7 Dempster Highway (Ten ft. cut with 2:1 backslopes made into ice rich organic silt)	265
A.8	Mile 153 Dempster Highway (Melting of large ice wedges caused slope degradation)	265
A.9	Mile 153 Dempster Highway (View from top dressed backslope)	266
A.10	Mile 175 Dempster Highway (Backslope and shoulder failure due to melting of a large ice lense)	266
A.11	Mile 175 Dempster Highway (Severe cracking of shoulder due to differential thermal subsidence caused by construction)	266
A.12	Mile 343 Dempster Highway - Large cut between Arctic Red River and Fort McPherson (looking west)	267
A.13	Mile 343 Dempster Highway - Stabilized backslope. (Hand placed vegetation to control rate of thaw)	267
A.14	Bimodal flow in the Richardson Mountains	267
A.15	Approach cut to Mackenzie River crossing at Arctic Red River	268
A.16	Typical vegetation patterns at southern end of TAPS Haul Road	268
A.17	Mile 14 TAPS Haul Road (July 1973)	268
A.18	Mile 20 TAPS Haul Road - Typical Bore Hole Log (After Smith & Berg 1972)	269
A.19	Mile 1916 (31.6 km) TAPS Haul Road (July 1973)	269
A.20	Mile 20.3 (32.6 km) TAPS Haul Road (July 1973)	269
A.21	Mile 22.9 TAPS Haul Road (April 1970) (After Smith & Berg 1972)	270
A.22	Mile 22.9 TAPS Haul Road (July 1973)	270
A.23	Mile 23.4 TAPS Haul Road. Approach to Hess Creek (April 1970)	270

Figure		Page
A.24	Mile 23.4 TAPS Haul Road. Approach to Hess Creek (July 1973)	271
A.25	Mile 33 TAPS Haul Road (July 1973)	271
A.26	Mile 54.4 TAPS Haul Road (July 1973)	271
C.1	Shadow Cast by Obstruction on Sloping Ground	290
C.2	Relation of a Small Surface dA_2 to a Diffusely Reflecting Large Surface A_1 (After Threlkeld, 1963)	292

CHAPTER I

INTRODUCTION

1.1 General

The increased demand for energy and raw materials within the last decade has resulted in the exploitation of many frontier reserves of minerals, oil, and natural gas. The Canadian and Alaskan Arctic are presently the center for much of this activity. The development of natural resources in these regions requires the construction of various transportation facilities over terrain underlain by discontinuous and continuous permafrost. One of the major problems associated with route location for these facilities is that of slope instability.

Research activities by Capps (1919), Eakin (1919), Taber (1943), and Sigafos and Hopkins (1952) provided a substantial quantity of qualitative information regarding slope instability in periglacial regions. The proposed pipeline construction in the Mackenzie valley added new impetus to this aspect of Arctic research. Hardy and Morrison (1972), Hughes (1972), Issacs and Code (1972) and MacKay and Mathews (1973) provided greater insight into the mechanisms of mass movements in the arctic regions.

McRoberts (1973) classified the different types of mass movements encountered along the Mackenzie River valley and its tributaries. He successfully attempted to explain the mechanisms of failure of thawing permafrost slopes in quantitative geotechnical terms. Thaw consolidation excess pore water pressures due to self weight were included in his analysis of an infinite thawing slope. This equation was

$$F_s = \gamma'/\gamma \left(1 - \frac{1}{1 + \frac{1}{2R^2}} \right) \frac{\tan \phi'}{\tan \theta} \quad - - - [1.1]$$

(After McRoberts and Morgenstern, 1974)

where F_s = factor of safety of the slope
 γ' = effective unit weight of the soil
 γ = total unit weight of the soil
 ϕ' = angle of internal friction of the soil
 θ = angle of the slope
 R = thaw consolidation ratio

This relationship adequately explained soil movements on low angle slopes that would have otherwise been stable if only steady state seepage pore water pressures had been present. It was apparent that any stabilization techniques would require the alteration of the thaw-consolidation ratio (R) which includes both thermal and physical properties of the soil as well as the imposed step temperature at the surface. This thesis proposes a method for stabilizing planar landslides on thawing slopes.

The geotechnical implications of uncontrolled retreat of bi-modal flows was recognized and attention was drawn to the hazards involved with artificial cuts in ice rich soil (ibid). A simple model used to relate the rate of ablation to heat flux at the surface is of the form:

$$V = F/L \quad - - - [1.2]$$

(Carslaw and Jaeger, 1947)

where V = the steady state velocity of the ablation surface
 F = the heat flux available at the surface
 L = the volumetric latent heat of fusion of the soil/ice mixture

This relationship indicated that a heat flux of approximately 200 to 600 ly/day was required to sustain typical rates of ablation that had been observed in the field. A comparison of these values with synoptic estimates of net radiation indicated a substantial disparity. There appeared to be an unaccountable source of heat involved in the ablation process. Kerfoot (1969) and McRoberts (1973) also noted that bimodal flows did not favor any particular aspect and that maximum retreat did not always occur on slopes with the most southerly aspect.

The questions concerning the high rate of ablation, the indifference to aspect, and the unique shape of the headscarp of bimodal flows remained unanswered. A complete analysis of the heat balance at the surface of exposed melting permafrost was considered necessary to properly explain the observed phenomena and to provide a rational basis for the design of remedial measures.

1.2 Scope of Thesis

Transportation facilities constructed across permafrost terrain necessitate the cutting of slopes in frozen soils that are not stable in the thawed state. A field reconnaissance was undertaken in order to appraise the behavior of existing road cuts. Chapter II outlines the nature of this reconnaissance, summarizes the findings, and contains the conclusions of the survey. The details of this study along with a variety of illustrated examples are contained in Appendix A.

One of the common forms of natural instability involves a surface movement or detachment failure of surficial material on reasonably planar surfaces. These flow dominated movements are evident not

only on natural slopes but on low angle back slope cuts as well. The necessity for some means of positive stabilization of these failures or incipient failures is apparent. Chapter III identifies the important variables involved in this problem and proposes a procedure to remedy this type of instability.

If rational design procedures are to be utilized to prevent excessive degradation of cut slopes or to control naturally occurring bimodal flows it is essential to establish the energetics of exposed melting permafrost. Chapter IV outlines the heat balance theory for a sloping surface of exposed permafrost and postulates the presence of substantial sources of heat other than net radiation. The theory was verified by field experiments which were performed at a large complex landslide on the Mackenzie River near Fort Simpson, N.W.T. The details of the field program and the interpretation of the results appear in Chapter V of this text. The results substantiate the theory and provide the basis for control of thawing of exposed permafrost.

Design and construction procedures for cut slopes are reviewed and a variety of methods for backslope preservation are presented in Chapter VI.

The final chapter contains the concluding remarks and suggests the form of ongoing research related to this aspect of surface transportation facilities in the Arctic.

CHAPTER II

BEHAVIOR OF EXISTING CUTS IN PERMAFROST

2.1 Objectives

Transportation facilities constructed across permafrost terrain often require cuts of varying size to maintain acceptable geometric standards. Exposure of these open cuts to thawing temperatures invariably cause degradation of the permafrost and subsequent deterioration of the backslopes. The magnitude and frequency of this deterioration was previously without documentation with the exception of the work of Smith and Berg (1972) on the Trans-Alaskan Pipeline System Haul Road.

General interrelationships regarding geological history, landform, type of material, and ground ice patterns had been emerging (Mackay and Black, 1973; Hughes, 1974 and others). Furthermore, there had been a mounting log of evidence (McRoberts and Morgenstern, 1973) to indicate that the frequency and scale of natural slope instability increased rapidly in areas containing fine grained ice rich soils. Although slope instability occasionally occurred in the till materials it was not generally characterized by continuing permafrost degradation. It was also evident that the amount and type of ground ice present in the frozen sediments played a major role in the extent and nature of the observed instability.

With these concepts in mind, a field reconnaissance program was undertaken to assess the current state-of-the-art regarding the behavior and development of design concepts pertaining to cut slopes in frozen soils.

The objectives were to establish (whenever possible):

- i) the geological, climatic, permafrost and geographical setting;
- ii) the soil and ice stratigraphy;
- iii) the original cross-section geometry; and,
- iv) the existing cross-section geometry.

This information should provide a basis for at least some tentative conclusions regarding the behavior and predicted behavior of cut slopes in arctic and sub-arctic regions under various geographic, climatic, and geologic conditions.

Economic considerations coupled with efficiency and convenience indicated that a small self-contained mobile home, towing a utility trailer, would provide the most versatile means of surface transport. The utility trailer contained a variety of equipment and support items deemed essential for the field work.

2.2 Route

During the course of the reconnaissance approximately 5,500 miles were travelled in 25 days and during that time many dozens of cuts on various highway locations in British Columbia, the Yukon Territory, the Northwest Territories and Alaska were examined, measured and photographed.

The details of these observations are contained in Appendix A while summaries and conclusions appear in the following pages. The information is presented under the sub-headings of Alaska Highway, Dempster Highway, Trans-Alaska Pipeline System Haul Road, and the Copper River Basin. It was felt that the locations could most logically be categorized according to specific projects rather than by territorial or physiographic boundaries. The main sub-divisions will,

therefore, appear in the order in which they were encountered (with minor exceptions).

The major part of the route location is shown in Figure (2-1). The field party started in Edmonton, Alberta on July 4, 1973 and travelled north through Grande Prairie to Dawson Creek, B.C. and then to Whitehorse in the Yukon Territory via the Alaska Highway. Travel continued north through the Yukon to Dawson City and up the Dempster Highway to its terminus at Mile 178 (1973). The route crossed the Canada-United States border at Poker Creek west of Dawson City, rejoined the Alaska Highway at Tetlin Junction and continued west to Fairbanks, Alaska. Activities in Alaska dealt primarily with the Trans-Alaska Pipeline System Haul Road, which originates near Livengood, extending fifty-five miles north west to the Yukon River. The Copper River Basin, in south eastern Alaska, was examined by travelling the loop from Fairbanks to Anchorage, east to the Copper River near Glenallen and then north to Tok Junction, and returning to Whitehorse from there.

The north end of the Mackenzie and Dempster Highways were inspected by travelling to Inuvik from Whitehorse by commercial airline and then by helicopter to Arctic Red River, Fort McPherson and the Richardson Mountains.

The field party then returned to Whitehorse from Inuvik and arrived back in Edmonton on July 29, 1973.

2.3 Alaska Highway Mile 222 (from Dawson Creek, B.C.) $57^{\circ}58'$ N latitude; $122^{\circ}46'$ W longitude

2.3.1 Summary

Concerns in this region regarding the instability of back slope cuts caused by permafrost degradation are slight due to the sporadic occurrence of permafrost (Figure (2-2)). North facing

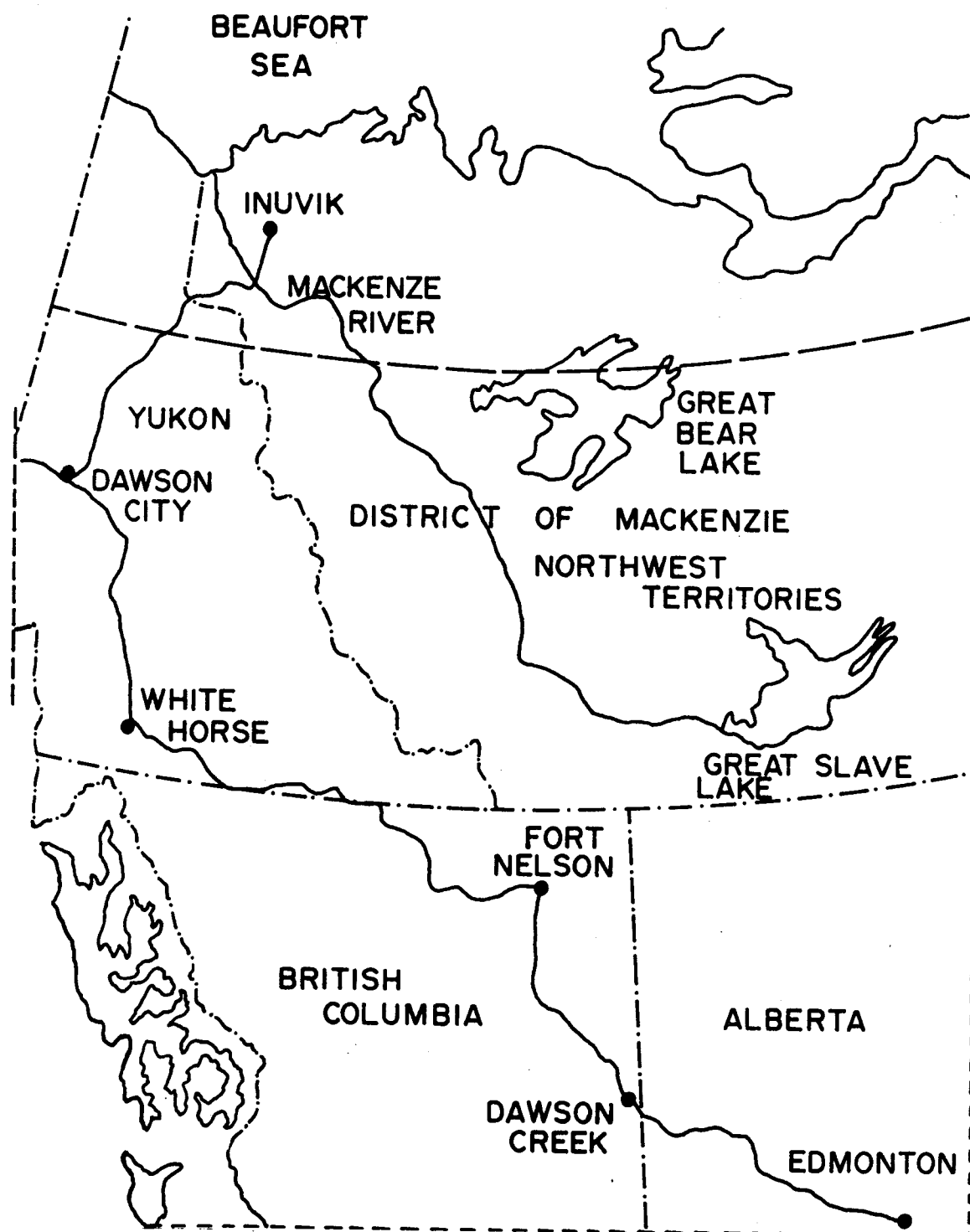


Fig. 2-1 Transportation Facilities - 1972 Northwestern Canada

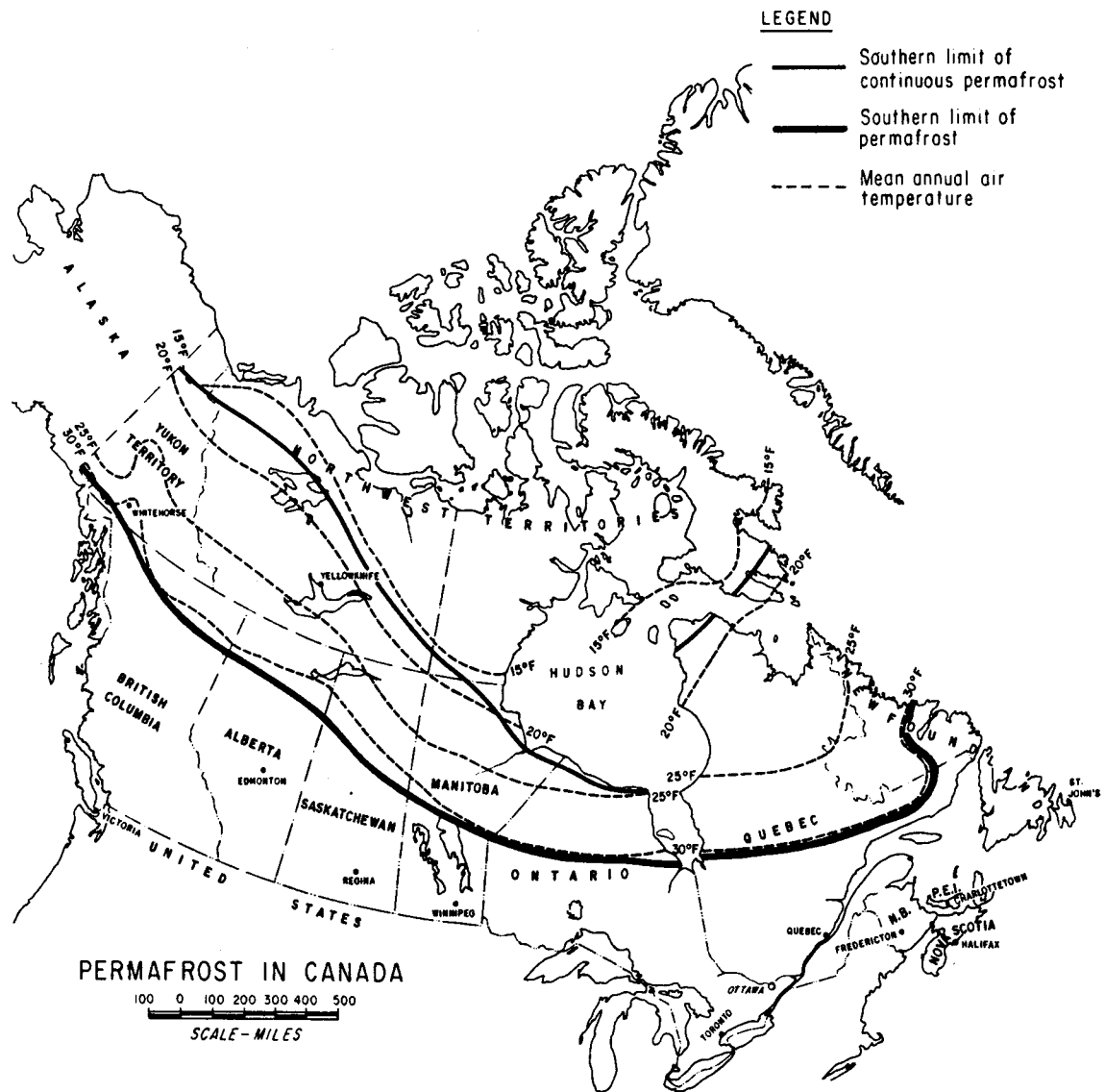


Fig. 2-2 Permafrost in Canada (After Brown, 1967)

slopes covered with heavy stands of black spruce and alder are usually avoided as are low, poorly drained areas. Encounters with permafrost are, therefore, often unexpected and as a result may lead to some particularly troublesome construction situations.

At Mile 222, a highway cut 20 to 25 ft. deep was required to maintain alignment in a reconstruction project. Very wet, fine grained partially frozen material was encountered in the fall of 1972. Cold weather, wet soil, and freezing weather conditions prompted a postponement of construction activities until spring. The material did not melt, drain, and stabilize during the following spring and summer as expected and a continuing problem of back slope instability and a wet subgrade were preventing further construction activity.

The observers felt that if the excavation had been completed and subgrade back fill consisting of select borrow had been installed, then little difficulty other than ditch maintenance would have resulted. It appeared that excavation by dragline and trucks was required to remove the saturated material from the centerline of the roadway. Subsequent back filling with free draining select borrow would provide a stable working base from which to perform ditch maintenance and the remainder of the required excavation.

2.4 Dempster Highway

2.4.1 Location and Background

The Dempster Highway follows an old overland route between the water drainage system of the Yukon and Mackenzie Rivers beginning at Dawson City, Yukon Territory $64^{\circ}04'$ N lat., $139^{\circ}26'$ W long. via Fort McPherson $67^{\circ}26'$ N lat., $135^{\circ}58'$ W long. to Arctic Red River $67^{\circ}27'$ N lat., $134^{\circ}44'$ W long. The location is shown in Figure 2-3.

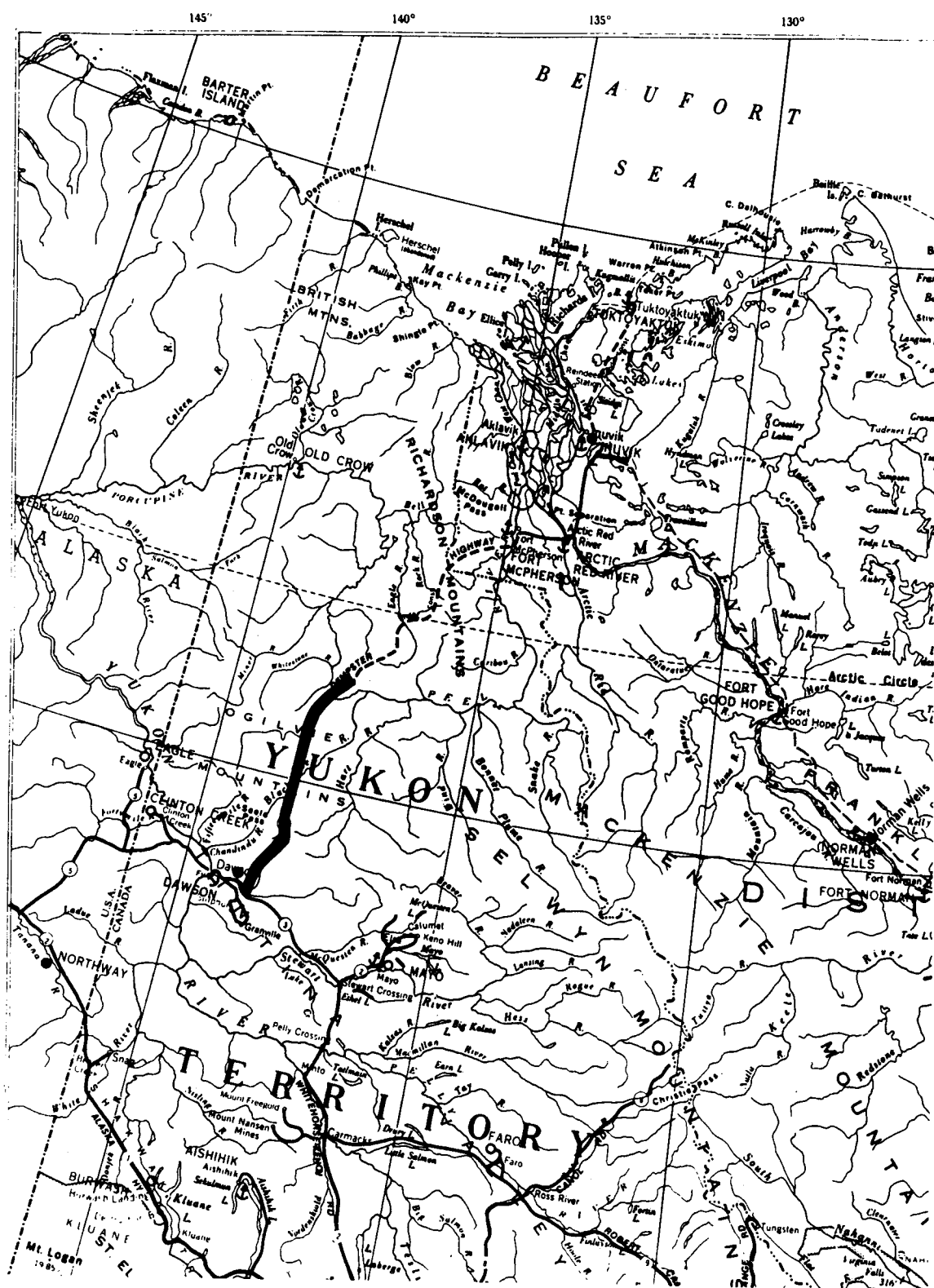


Fig. 2-3 Location of the Dempster Highway; Dawson City, Yukon Territory to Arctic Red River, N.W.T.

Construction of this highway began in 1959 and consisted largely of improving, grading and maintaining an existing tote road. Subsequently, more money was appropriated to the project with the aim of connecting Dawson City on the Yukon River to Fort McPherson on the Peel River and subsequently, the settlement of Arctic River at the confluence of the Mackenzie and Arctic Red Rivers.

The highway lies primarily within the Northern Plateau and mountain area of the Interior System of the Canadian Cordillera. Figure 2-4 indicates the different physiographic units traversed by this transportation facility.

2.4.2 Mile 0 - Mile 80

The first 45 miles of this section of highway is located along the North Klondike River and the remaining portion along the East Blackstone River. Much of this area has been glaciated and there is an abundance of sub-grade material comprised of glacial sediments along the lower portion of the route. Weathered shales and sandstones occasionally outcrop and are used extensively as surfacing materials.

Permafrost is more or less continuous and consequently the borrow pits formed in the active layer are large and shallow. Thermal subsidence of the road is common and has substantially lowered the grade line. As a result, continued maintenance has been required to sustain the road bed.

Road cuts along this eighty mile section of road were not considered significant. They were small (less than ten ft.) and were stable in all cases.

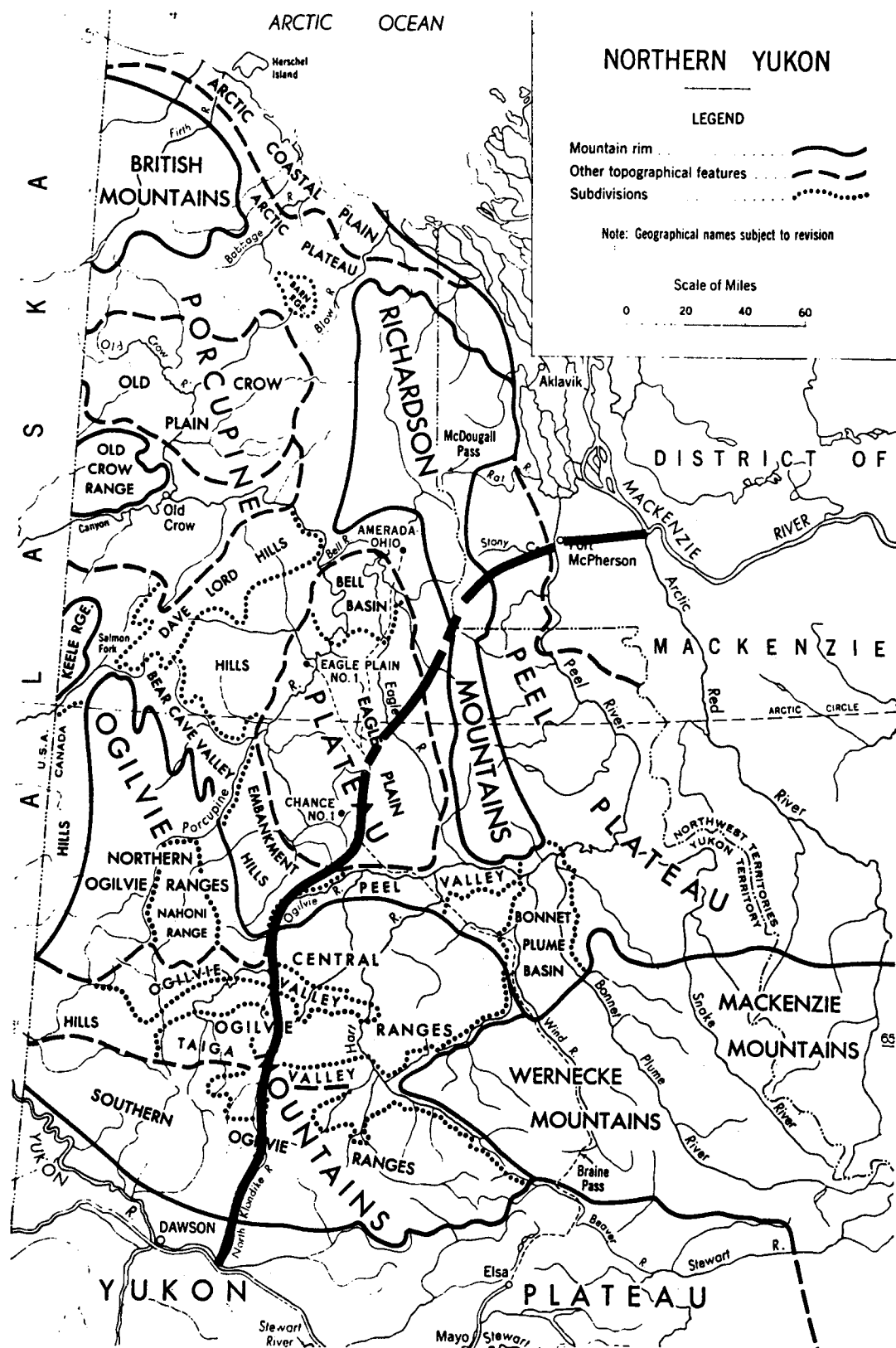


Fig. 2-4 Physiographic Regions of the Yukon Territory (Bostock, 1961)

2.4.3 Mile 80 - Mile 154

The location of this section of road is shown in Figure 2-5. The highway departs from the Blackstone River at Mile 96 and parallels Big Creek, a tributary of the Ogilvie River, to Mile 123 and from there follows the Ogilvie River to Mile 154.

The highway now lies within the unglaciated portion of the Yukon Territory and surficial deposits consist of talus covered slopes, alluvial fan deposits and active and inactive flood plain deposits. Muskeg is abundant in this area and unusually thick deposits of re-worked organic matter often cover the coarse gravel of the inactive flood plains. Pediment slopes consisting of frozen colluvium and alluvial silts interspersed with rock detritus and organic matter are frequent along the flanks of the valley.

This lower sixteen mile section of sub-grade shows substantial improvement in alignment and design standards. Back slope cuts are rare, as a major portion of the road is constructed from fill material obtained from the East Blackstone River and Big Creek. The following 20 miles flank the valley walls of Big Creek and the proximity of the river bed has often forced the location onto the sides of the valley. Twenty to thirty foot cuts in colluvial silt and weathered shale are not uncommon. Construction problems and ditch blockage resulted from the melting of ice wedges and frozen soil encountered in the cuts. Small bimodal flows occurred at some locations.

Extensive disturbance was noted on an abandoned tote road located on an alluvial silt or slope wash side hill at Mile 114 directly across the valley from the present highway location. The original activity was estimated to be eight to ten years old. Large craters have formed due to thermal subsidence caused by the subsurface melting of

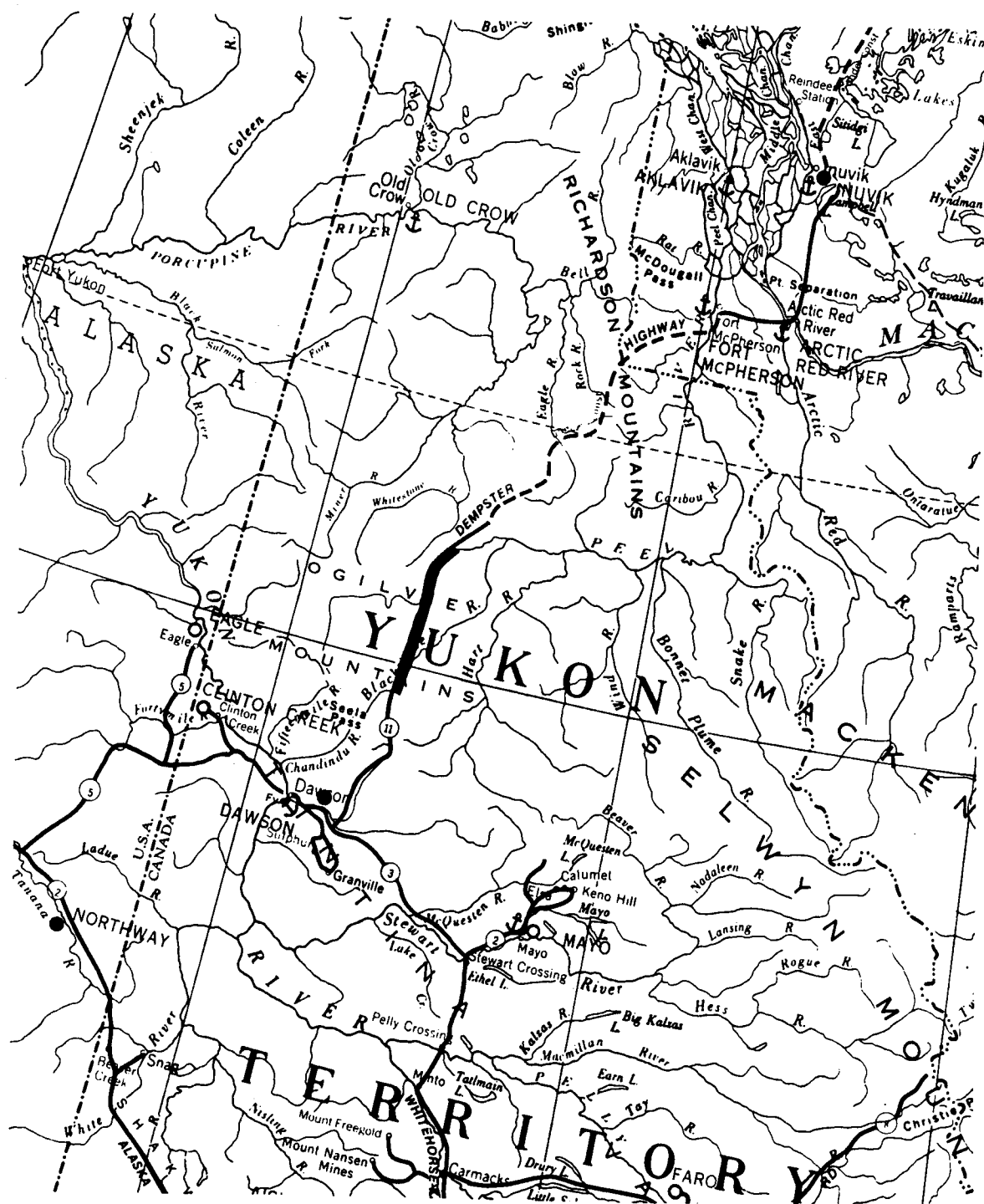


Fig. 2-5 Location of Mile 90 to Mile 180 of the Dempster Highway

large tabular masses of ice.

A significant and troublesome cut occurred at Mile 154 adjacent to the Ogilvie River. A bimodal flow eventually developed with a head scarp thirty feet high. Large ice wedges were exposed in a silt-weathered shale-soil mixture. The melted soil and ice caused a serious impediment to drainage and concern to maintenance personnel. After one complete thaw season, gravel was used to fill the crater formed by the loss of material and thus return the slope to its original dimensions. This remedial measure appears to have adequately prevented further degradation of the slope.

The performance of cuts along this section of highway has generally been good to excellent with little more than ditch clearing required to maintain adequate drainage.

2.4.4 Mile 154 - Mile 178

The Dempster Highway departs from the Ogilvie River and ascends the valley flank to the Eagle Plains. Unglaciaded surficial deposits comprise the subgrade construction materials and consists of discontinuous felsenmeer and/or colluvium over bedrock. Extensive deposits of organic matter are common along the lower reaches of this section. The sandstone bedrock is more resistant to weathering and therefore forms the tops of ridges and escarpments. The shales, on the other hand, are softer and weaker and form smoother and more gentle slopes.

Large side hill cuts and steep grades were required to attain the ascent out of the Ogilvie River Valley to the plain above. However, since the roadbed was excavated into ice free sandstone and shale bedrock, no problem was encountered with stability. Excavation of a number of small cuts was performed without major difficulty. By

loosening the frozen soil with a ripper tooth on a large crawler tractor and rapidly excavating with conventional earth moving equipment, it was found possible to construct cuts without encountering excessively wet and muddy working conditions. Occasional encounters with residual ice rich fine grained soils caused construction delays and increased costs. However, the back slopes were not found to exhibit alarming instability.

An excellent opportunity exists to compare the difference and assess the behavior and quality of subgrade constructed in late fall and early summer along this section of road. Subgrade constructed in the spring and early summer tends to undergo substantial differential settlement and cracking as melting proceeds into the active layer during the remainder of the summer. On the other hand, subgrade that was constructed in late summer and fall tends to be more stable and exhibit less differential settlement. This behavior can be attributed to the fact that much of the settlement due to conventional consolidation occurs during the construction period rather than subsequent to the completion of grading.

Mile 178 was the construction terminus on the Yukon portion of the Dempster Highway as of July, 1973. A further 56.5 miles of road is presently being constructed to the Eagle River. No inspection of this road has been made and therefore comment is beyond the scope of this thesis. Preliminary design and location reports indicated that the location would follow summits of the ridges whenever possible and borrow material was to consist almost exclusively of weathered sandstone and shale bedrock except where limited quantities of sand and gravel were available from the Eagle River or other lesser streams convenient to the right of way.

2.4.5 Fort McPherson to Arctic Red River

Mile 330 to Mile 365

This section of highway connecting the settlements of Fort MacPherson and Arctic Red River was completed during the summer of 1973. Hummocky or dead ice moraine represent the basic land form which is comprised of deposits of unsorted glacial drift occasionally draped with sorted fine grained sediments that may be water modified or reworked till. Large areas are covered with silt and organic material.

Engineering design problems involved the stability of thawed soils, embankment design and drainage structures. High moisture contents in the upper till precluded its use as a construction material and ripped sandy shales were used almost exclusively as a sub-grade material.

Excavation was generally avoided except for a large cut that was developed in a knoll at Mile 343 in order to supply borrow material for the adjacent sections. However, the material proved to have excessively high water contents and was completely unstable when thawed. Much of this material was wasted in adjacent spoil areas.

During and after completion of the cut, the back slopes exhibited reasonably serious degradation. However, the extent of the retreat was apparently limited to the areal extent of the ice. It appears that the retreat and instability of the back slopes ceased when the excess ice had melted and the water had drained away.

This is the most significant cut on the Dempster Highway and the length and width of the excavation rather than its depth make it an outstanding feature on the landscape. At the time of inspection,

rimental results.

2.4.6 Mile 178 - Mile 330

A brief helicopter reconnaissance was made of the proposed location of the section of the Dempster Highway between Fort McPherson and south to Mile 178.

Several naturally occurring bimodal flow slides were noted in the Richardson Mountains near the Yukon-Northwest Territories border. Some of these flow slides have run their course or have become dormant while others are currently active. Sediments encountered at those sites consist of significant quantities of ice rich fine grained deposits. None of these slides were in close proximity to the proposed right of way.

2.5 Mackenzie Highway (Inuvik to Arctic Red River)

Two sections of the north end of the Mackenzie Highway received a cursory inspection for the presence of back slope instability. No cuts of significance were encountered in the northernmost Inuvik section. However, the north approach to the Mackenzie River warrants a short discussion as it was the only situation where measures were taken to prevent back slope degradation rather than control it.

A forty foot deep cut had exposed 15 to 20 ft. of ice-rich fine grained sediments overlying interbedded shale and sandstone bedrock. As the excavation proceeded, the ice content of the overburden increased with distance from the river bank. To prevent subsequent degradation, the slope was benched at the bedrock level and the ice-rich fine grained sediments in the upper portion of the slope were

dressed with 10 ft. of crushed shale. The slope appeared to be functioning as anticipated at the time of inspection.

2.6 Alaska Reconnaissance

2.6.1 General

Prior to 1973, the roads in Alaska had been built in the discontinuous permafrost zone except for minor activity on the Arctic Coast. The designers, for the most part, were able to choose their locations judiciously and thus avoid cuts where ice-rich fine grained soils were suspected. Even so, requirements of the oil industry have created a need for road locations that do not allow the designer as much latitude in the choice of route. The Trans-Alaska Pipeline System (TAPS) Haul Road is a typical example of such a problem.

The TAPS Haul Road begins at Livengood some sixty miles northwest of Fairbanks and extends fifty-five miles beyond to the Yukon River (1973). This road has since been completed north to Prudhoe Bay on the Arctic Coast and provides facilities for ground surface transportation of all supplies and personnel required in the construction of the Alyeska Pipeline.

The great difficulty associated with the routing of this road was that it, of necessity, crossed the grain of the country. Its origin and destination required the route to climb south facing slopes and descend north facing slopes (Figure 2-6).

2.6.2 TAPS Haul Road

The southernmost section of the TAPS Haul Road, built in 1969-70, crosses broad undulating divides and flat-topped spurs of the Yukon-Tanana Upland and descends to the Yukon River Lowland which exhibits gently rolling topography with maximum relief in the order

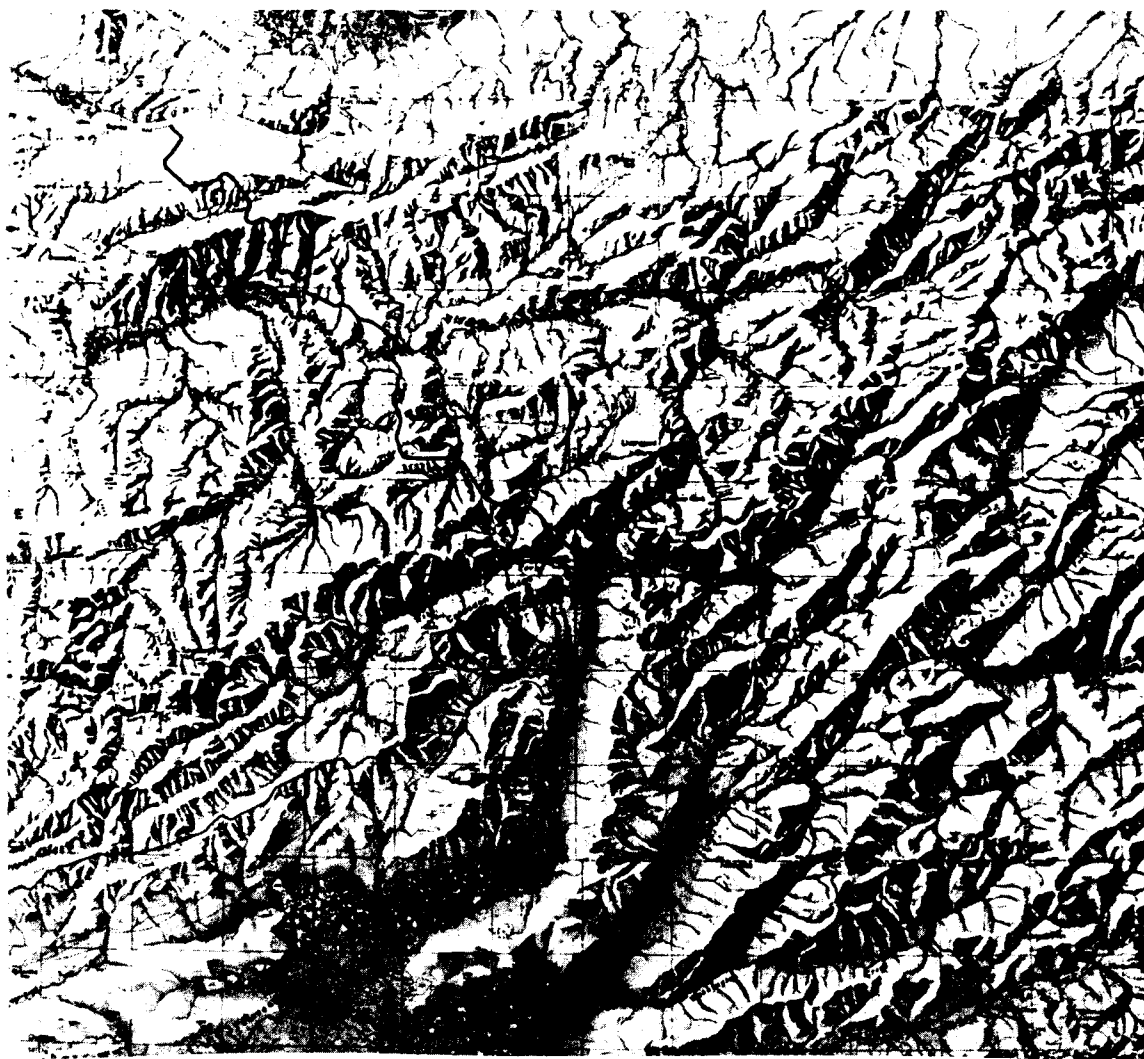


Fig. 2-6 TAPS Haul Road; Livengood to the Yukon River, Alaska
(Road crosses northeast-southwest trending ridges at
right angles)

of 1,000 to 1,500 feet. This entire fifty-five mile section lies within the discontinuous permafrost zone (Ferrians et al, 1969). The unglaciated surficial deposits consist of reworked aeolian silt, colluvial and alluvial silt, sand and rock fragments, dune sand, and alluvial sand and gravel and exhibits an active layer depth that varies from 18 in. to 10 ft. below the surface. These surficial sediments are unconsolidated, usually frozen, and are often very rich in ice. Ice forms include wedges, lenses, and interstitial ice.

The TAPS Haul Road has provided the first real opportunity to observe and record the performance of a significant number of road cuts in ice-rich fine grained soils. The road has many substantial cuts on north facing slopes that exposed what was termed "massive ice". Certainly the ice did appear massive in that cuts in the order of 20 ft. had 12 ft. or more of ice exposed in the section. However, the tabular extent of these ice exposures was not and has not been established.

Many of these cuts were excavated with vertical or near vertical faces with the thought that prior to any self-healing, the cuts would have to melt back to a vertical scarp. It was anticipated that the upper mantle of soil and organic mat would then slough down over the melting ice and soil and provide sufficient insulation to stabilize the slope. Vegetation would then re-establish itself preventing erosion and any further fouling of the ditches.

Inspection of these cuts in the summer of 1973 indicated that the back slopes had essentially stabilized. Many slope angles were very steep (35° to 40°) and the present conditions probably do not represent ultimate stable slope angles for most of the colluvial silt encountered along the route. The relatively free-draining nature

of the silt deposits, the extensive re-vegetation program, and probably the initial vertical cross section have all contributed to rapid stabilization. More important, however, may be that the ground ice occurs in the form of wedges of limited extent and that the back slopes stabilized when the exposed ice wedges melted and allowed the remaining soil to slough down forming a quasi stable slope from material with moderately low moisture contents. Summaries of the soil classification for the TAPS Haul Road appear in Table 2-1.

2.6.3 Copper River Basin

The Copper River Basin is located in southeastern Alaska in the discontinuous permafrost zone. This region has been subjected to extensive glaciation and pro-glacial lakes were common during the retreat of the ice. As a consequence, major deposits of glacio-lacustrine silts and clays, fluvial silt and sand, sand and gravel, colluvium, and organic soil comprise the surficial materials. Ground ice forms and amounts are extremely variable. Ice wedges, massive tabular bodies, and interstitial ice are common. Natural water contents often exceed the liquid limit (EISTAPS, 1972).

Instability of large cuts and fills is common in this region. Slopes are designed to ensure stability in the thawed but essentially undrained case, with no excess pore water pressure considered due to thaw consolidation.

Several cuts were observed at various locations in the area. The back slopes did not exhibit any serious distress due to permafrost degradation. Many slopes along the valley wall undergo significant movements. Most of these failures are semi-rotational or block-type movements and are not necessarily related to changes in permafrost conditions.

2.7 Conclusions

The observations made during the field reconnaissance program are summarized in Table 2-2 and indicate that slope behavior varies widely in the areas that were investigated. It is also apparent that at least limited instability may be encountered in cuts in all regions which contain fine-grained, ice-rich sediments. There appear to be a number of factors which contribute to the amount of instability.

These are:

- (1) geological history (primarily glacial);
- (2) landform and soil type;
- (3) ice content of sediments;
- (4) nature or type of ground ice;
- (5) geometric cross-section of the back slopes.

All of these factors are inter-related and are listed in approximate order of importance.

The determination of the geological history along with the recognition of associated landforms will provide a sound basis for the preliminary design and predicted behavior of highway back slopes. Although local exceptions may exist, it appears that the greatest risk of precipitating unstable conditions arises in areas that contain significant deposits of stratified drift in the form of pro-glacial, lacustrine silts, and clays. These deposits generally contain large amounts of segregated ground ice in the form of lenses varying in thickness from a few tenths of an inch to massive sheets many feet thick (Mackay and Black, 1973).

The areal extent of these lacustrine deposits is often quite significant, varying from a few hundred feet to a number of miles. Thus, a flow slide initiated in such an extensive deposit is not likely to

terminate due to a lack of material. When these soils are thawed, large amounts of meltwater coupled with low permeabilities provide an ideal condition for the generation and maintenance of large excess pore water pressures. The thawed soil is very weak and flows at very low angles (McRoberts and Morgenstern, 1973). It is unlikely that vertical cuts would provide any great degree of stabilizing influence unless they were less than ten feet in height. Under these conditions, the intact organic cover may be able to provide a retarding effect on the rate of thaw and the subsequent generation of excess pore water pressures.

The effectiveness of the organic mat is directly related to its continuity. Tearing or ripping of the cover under self-weight can be reduced by removing the larger vegetation and in some cases reinforcing the mat with wire mesh fastened to the tree stumps.

The reconnaissance did not encounter highway or right-of-way locations in regions of extensive glacio-lacustrine deposits with the exception of the Copper River Basin in Alaska. This latter area did not exhibit the bi-modal flow slides characteristic of the Mackenzie Valley (McRoberts and Morgenstern, 1973). Although it would appear that both areas were subjected to similar glacial histories, there is a distinct difference in the ice contents of the sediments. The reasons for this deserve further study.

Conventional slope analyses using thawed, undrained strength parameters appear to provide acceptable margins of stability for most highway cuts in this region. However, there seems little doubt that route locations encountering extensive areas of pro-glacial lake basin sediments are exposed to the hazards of backslope instability. Great care must therefore be taken to avoid cuts in these regions whenever possible.

The other major classification of glacial sediments is that of unstratified drift. Till plains formed from basal or lodgement till and hummocky or dead ice moraine composed of ablation till are the two most common landforms.

Ground ice conditions in the till plains are usually not particularly severe. The ice occurs as thin subhorizontal segregated lenses. The top layer of this landform may occasionally contain significant ice lenses just below the active layer due to aggrading permafrost conditions (Hughes, 1974). These ground ice deposits usually occur within three to six feet below the surface and should, therefore, not create any sustained construction hazard. It should also be noted that this terrain has rather low relief and cuts will be uncommon.

Hummocky or dead ice moraine is common in the northern part of the Mackenzie Valley and appears sporadically along the Alaska Highway and the lower and upper portions of the Dempster Highway. This terrain unit is highly irregular and may contain lenses of silt, sand, and gravel as was witnessed at Mile 222 on the Alaska Highway and at Mile 343 on the Dempster Highway. Complex hydrologic, geologic, and topographic conditions prior to deposition of the sediments and aggradation of permafrost have produced equally complex and irregular patterns of ground ice. These forms may consist of lenses of varying thickness, wedges, and occasionally significant amounts of interstitial ice (ibid). However, it must be emphasized that these ground ice forms are usually of finite dimensions and that flow slides initiated in these sediments will be of limited (and often acceptable) extent.

Good construction practice involving wide ditches, low rock revetments, occasionally combined with minor amounts of backslope

reshaping and revegetation should provide an acceptable measure of stability and pleasing appearance.

The unglaciated regions of the Yukon and Alaska contain a variety of classic landforms consistent with the geological history and periglacial conditions. The soils are generally formed from weathered sandstones and shales and consist of colluvial and alluvial silts, sands, and gravels. Occasional deposits of medium to highly plastic residual clays are encountered in the central and northern Yukon. The ground ice conditions are again very irregular in all these deposits and occur in a variety of forms. Ice wedges and lenses of variable thickness are the most common type encountered (Kachadoorian, 1971).

The relatively high permeability of these materials coupled with low interstitial ice contents provide conditions for moderately fast stabilization under thawing conditions. Flow slides initiated in this material, with these particular ground ice conditions, will normally stabilize after two or three seasons of thaw (Davies, 1973).^{*} Again, good construction practice should reduce the time required for stabilization and the amount of slope retreat that may be expected. Wide ditches are recommended to provide reasonable space for sloughing material. Rock revetments appear to play a significant role in retaining the soil at the toe of the backslope while drainage proceeds. Vertical cuts may be desirable in areas that contain soil and ice conditions as previously described in that they tend to expose or intersect fewer ice wedges. This aspect combined with the steep quasi-stable angles developed by the soil between and above the ice provide

* Personal communication.

encouragement for the designer in the use of steep slopes. However, it must be noted that generalization is not possible with the current state of knowledge and that steep cuts will not be desirable everywhere. There is no evidence and little rationale to suggest that vertical slopes will perform satisfactorily in ice-rich glacio-lacustrine sediments except under conditions previously outlined.

The occurrence of instability of natural slopes is undoubtedly the best indicator available to assess or predict potential instability of cut slopes. If areas do not exhibit natural instability due to permafrost degradation then it is unlikely that cutting of a slope will cause serious and extensive instability in the form of flow slides.

The only reliable method encountered for preventing rather than controlling flow slides was that utilized on the Mackenzie Highway at the approach cut to the Mackenzie River near the settlement of Arctic Red River. A thick layer of crushed rock was used to dress the exposed slope before degradation of the permafrost occurred.

Procedures to prevent melting of the permafrost in colder regions are well known and are relatively simple in comparison with preventing permafrost degradation in the discontinuous zone (Lachenbruch, 1957).

The experience with cut slopes in permafrost reviewed here, albeit limited, indicates that the behavior of cuts need not be a serious impediment to the routing of transportation arteries across permafrost.

TABLE 2-1
SUMMARY OF SOIL DATA

LOCATION	SOIL TYPE	LIQUID LIMIT %	PLASTIC LIMIT %	NATURAL WATER CONTENT %	SPECIFIC GRAVITY	SAND AND SILT GRAVEL %	CLAY %
Alaska Highway Mile 222	Silt			23		30	10
Alaska Highway Mile 222	Silty-clay	50	19			10	40
Dempster Highway Mile 108	Silt					20	5
Dempster Highway Mile 114	Silt	27		25	2.71	10	10
Dempster Highway Mile 153	Silt					20	5
Dempster Highway Mile 174		54	25			40	60
Dempster Highway Mile 175		45	23	30-40		5	60
Dempster Highway Mile 175		48	24	30-40		5	50
Bi-modal Flow Richardson Mts.	Till	36	22	Dry	2.70	30	30
Bi-modal Flow Richardson Mts.	Alluvium	39	24	38	2.72	15	32
TAPS Haul Road Mile 19.6	Silt	25				0	8
TAPS Haul Road Mile 23.4	Silt					10	7
TAPS Haul Road Mile 54.4	Silt	24				0	9
Dempster Highway Mile 343	Upper till	26	18			25	20
Dempster Highway Mile 343	Lower till	23	15			30	30

TABLE 2-2

SUMMARY OF CUTS

LOCATION	HEIGHT (Feet)	INITIAL SLOPE (Degrees)	CURRENT SLOPE (Degrees)	SOIL TYPE	COMMENTS
Alaska Highway Mile 222	20-25	26.5	Varies from near vertical to 6° frontal lobe.	Till with lenses of silt and silty clay.	The slope had retreated approximately 15 feet at the time of inspection and gave no indication of stabilizing.
Dempster Highway Mile 96	8-10	26.5	21	Till-relatively fine-grained with low ice content.	Slope is stable.
Mile 107.6	30	34	32	Colluvial silt and weathered shale with low ice content.	Organic mat tearing loose; slope is stable.
Mile 108.9	35	34	12 to 35	Colluvial silt, some weathered shale. Large ice lenses.	Slope has stabilized with small amounts of ditch maintenance.
Mile 114 Tote Road	Instability of natural slope		9 to 11	Alluvial silt and slope wash. High ice content.	Caused by locating tote road on 50 side hill. Disturbance approximately 6 years old and continu- ing to stabilize.
Mile 120.7	Less than 10	26.5	12	Ice-rich organic alluvial and/or colluvial silts.	Slope presently quite stable. Some ditch clearing required to maintain drainage.

TABLE 2-2 (Continued)

LOCATION	HEIGHT (Feet)	INITIAL SLOPE (Degrees)	CURRENT SLOPE (Degrees)	SOIL TYPE	COMMENTS
Trans-Alaska Pipeline System Haul Road Mile 2	40	26.5	26.5	Weathered sandstone bedrock.	Slope is stable and revegetation is well established.
Mile 14	10 to 25	26.5	Backscarps at 35 to 45; lobes at 7 to 10.	Colluvial silt and massive ice.	Trees were removed by hand and the moss has draped itself over the retreating face. The slope is essentially stable.
Mile 19.6	15 to 20	34	20	Colluvial silt with large ice lenses and wedges.	Crushed rock revetments were used to retain the sloughed material.
Mile 20.3 to Mile 20.5	20 to 40	76	35 to 45	Colluvial silt with large ice lenses and wedges.	This section was referred to as the "ice tunnel". Vegetation is well established.
Mile 22.9	15 to 20	76	Varies from 17 to 40	4 to 6 feet of org- anic matter over silt and ice.	Boreholes indicated massive ice in excess of 32 feet. Slope degraded 75 feet in localized areas.

TABLE 2-2 (Continued)

LOCATION	HEIGHT (Feet)	INITIAL SLOPE (Degrees)	CURRENT SLOPE (Degrees)	SOIL TYPE	COMMENTS
Mile 153	40	40 to 45	Angle of repose of coarse gravel	80% silt; 20% shale; no interstitial ice. Large lenses or wedges exposed.	Backslope retreated until a 35 foot vertical section was formed. Gravel placed on face to control melting. Slope appears stable.
Mile 168	Less than 10	34	11	Sandy silt with angular weathered rock. Ice-rich.	Backslope has retreated 20 to 25 feet. Appears to be stabilizing under present conditions.
Mile 175	8 to 10	34	40 to 50	Silt and silty clay with shale fragments.	Activity due to melt- ing of large ice lense, slope has retreated 25 feet at time of inspec- tion.
Mile 343	35	34	17	Silty clay till; ice lenses up to 4 feet in thick- ness.	Cut is 1/2 mile long. Backslopes are essen- tially stable; some ditch clearing and back- slope reshaping has been done.
Mackenzie Highway Mile 894	45	34 on upper slope to 45 on lower slope	45	Upper 25 feet is ice- rich and fine-grained Lower 20 feet is bedrock.	Upper 25 feet was benched and dressed with 10 foot thick layer crushed shale slope is completely stable.

CHAPTER III

STABILIZATION OF PLANAR LANDSLIDES IN PERMAFROST

3.1 Introduction

Flow dominated land slides in periglacial regions have been documented by numerous researchers (Capps, 1919; Eakin, 1919; Sigafos and Hopkins, 1952; and others). Skin flows or planar landslides involving the detachment of vegetation and thawed soil from the underlying frozen soil are abundant in the Mackenzie Valley and have been described by Hardy and Morrison (1972), Hughes (1972), Issacs and Code (1972), Mackay and Mathews (1973), and McRoberts and Morgenstern (1973).

Since skin flows are common, a method of stabilizing them or inhibiting their occurrence is of interest.

A technique for the analysis of thawing slopes of infinite extent has been developed which incorporates pore water pressure components due to steady state seepage as well as those resulting from self weight and surcharge loading during thaw consolidation. Insulation used in conjunction with a surcharge load reduces the rate of thaw, decreases the induced pore water pressures and may effectively stabilize the slope.

3.2 Thaw-Consolidation Pore Water Pressures

Excess pore pressures in thawing soils may be predicted from the theory given by Morgenstern and Nixon (1971). The magnitude of these water pressures at a horizontal thaw front in a homogeneous single layer soil due to self weight and surcharge loading are given by the following equations:

$$U_Y' = \gamma' X(t) \frac{1}{1 + \frac{1}{2R^2}} \quad - - - [3.1]$$

$$U_{p_0} = \frac{(P_0 - \sigma_0') \operatorname{erf}(R)}{\operatorname{erf}(R) + \frac{e^{-R^2}}{\sqrt{\pi R}}} \quad - - - [3.2]$$

where $\gamma' =$ effective unit weight of the soil

$X(t) =$ depth of the thaw front, predicted by

$$X(t) = \alpha \sqrt{t} \quad (\text{Carslaw \& Jaeger, 1947}) \quad - - - [3.3]$$

where $\alpha = \sqrt{\frac{2K_u Ts}{L}} \quad (\text{Stefan, 1891}) \quad - - - [3.4]$

$K_u =$ thermal conductivity of the unfrozen soil;

$T_s =$ surface step temperature;

$L =$ latent heat of fusion of the soil/ice mixture;

$t =$ time

$$R = \frac{\alpha}{2\sqrt{C_v}} \quad (\text{thaw consolidation ratio}) \quad - - - [3.5]$$

$\operatorname{erf} () =$ error function

$P_0 =$ surcharge load

$\sigma_0' =$ residual effective stress (assumed to be zero at shallow depths in ice rich fine grained soils). The solution for equations [3.1] and [3.2] have been given in graphical form by Morgenstern and Nixon (1971).

The depth of thaw in a two layer medium is given by Nixon and McRoberts (1973):

$$X(t) = \sqrt{\left(\frac{K_2}{K_1} H\right)^2 + \frac{2K_2 Ts(t - t_0)}{L_2}} - \left(\frac{K_2}{K_1} H\right) \quad - - - [3.6]$$

where $X(t)$ = depth to the thaw front measured from the interface of the two layers.

K_1 = thermal conductivity of the upper layer

K_2 = thermal conductivity of the lower layer

H = thickness of the upper layer

t = length of the thawing season

$t_0 = \frac{H^2 L_1}{2K_1 T_s}$; (time to thaw layer 1)

L_2 = latent heat of fusion of the soil/ice mixture in the lower layer.

$$L(1,2) = \gamma_t (W - W_u) L' \quad - - - [3.7]$$

where γ_t = total unit weight of the soil

W = water content of the soil

W_u = unfrozen water content of the soil expressed as a ratio of gms. of water to gms. of dry soil

L' = latent heat of fusion of ice (79.6 cal/gm.)

If the upper layer consists of an insulating material or incompressible surcharge loading, a measure of the pore pressure in the soil below the insulation may be determined by computing $X(t)$ from equation [3.6], substituting into equation [3.3] and obtaining an equivalent α_e . R can then be evaluated from equation [3.5] and the pore pressures evaluated for this modified rate of thaw.

The above procedure is not strictly correct because the thaw depth as computed from equation [3.6] will in general not be linear with the square root of time. Figure 3.1 indicates the manner in which the thaw depth varies with time for a typical problem. It is apparent that this technique will slightly underestimate the thaw-

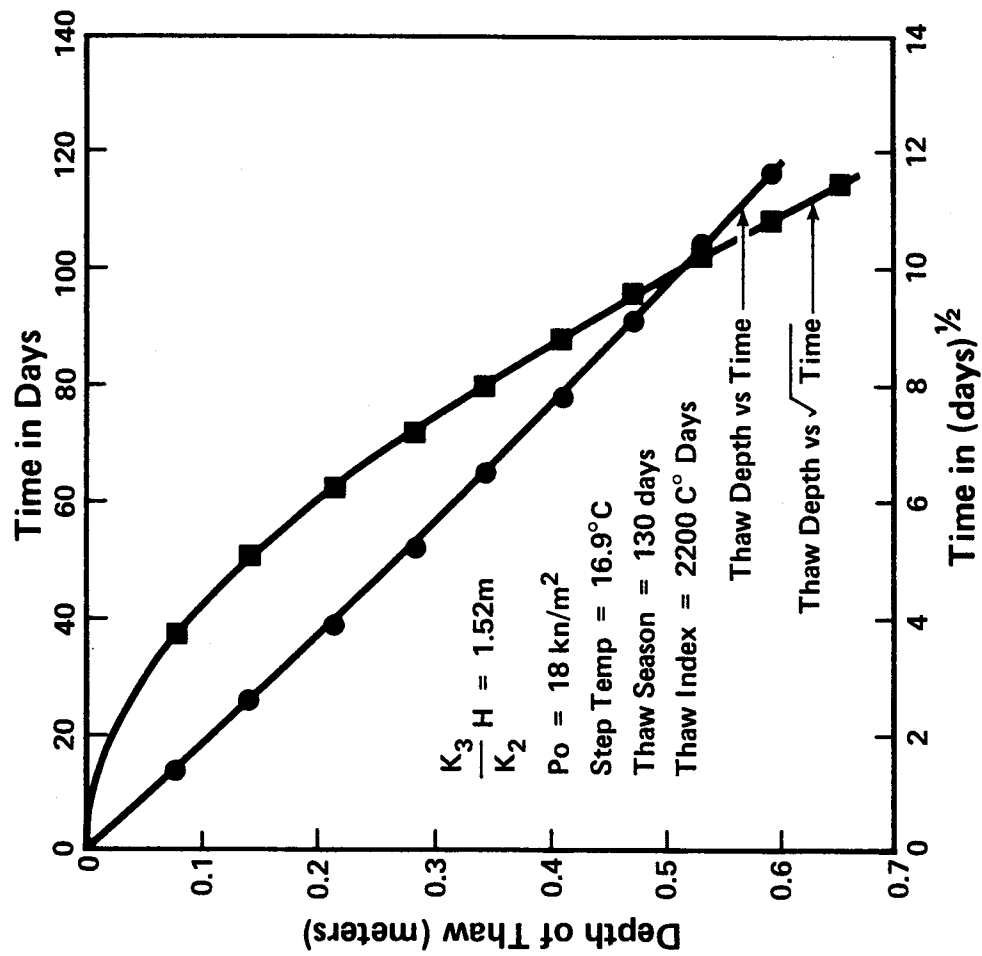


Fig. 3.1 Thaw Depth vs Time and Thaw Depth vs $\sqrt{\text{Time}}$ for an Insulated Thawing Slope

consolidation pore pressures generated in this particular two layer medium. A better estimate of these water pressures can be made either by numerical techniques or by modelling the thaw rate from:

$$X(t) = B(t)^n \quad (\text{Nixon and Morgenstern, 1973}) \quad - - - [3.8].$$

The thaw depth must be calculated for various times from equation [3.6] and a suitable value of n determined for equation [3.8]. Graphical procedures may then be used to properly evaluate the pore pressures at the thaw front at different periods of time (ibid).

3.3 Stability Analysis of Infinite Thawing Slopes

The pore pressure term in the stability analysis of an infinite slope with surcharge loading will be composed of:

- 1) Pore pressure due to steady state seepage.
- 2) Thaw-consolidation pore water pressure due to self weight.
- 3) Thaw-consolidation pore water pressure due to surcharge loading.

These three components may be evaluated separately as shown in Figure 3.2 and then added numerically to obtain the total pore water pressure acting at the thaw front. This procedure is similar to that of McRoberts (1972), and McRoberts and Morgenstern (1974).

The condition for steady state seepage is shown in Figure 3.2(a). This is a well known solution and the pore pressure term is:

$$U_s = X(t) \cos i \gamma_w \quad - - - [3.9(a)]$$

Figure 3.2(b) indicates the condition for the pore pressure due to self weight generated from one dimensional thaw-consolidation. This magnitude is expressed by:

$$U_{\gamma} = \gamma_3 X(t) \cos i \frac{1}{1 + \frac{1}{2R^2}} \quad - - - [3.9(b)]$$

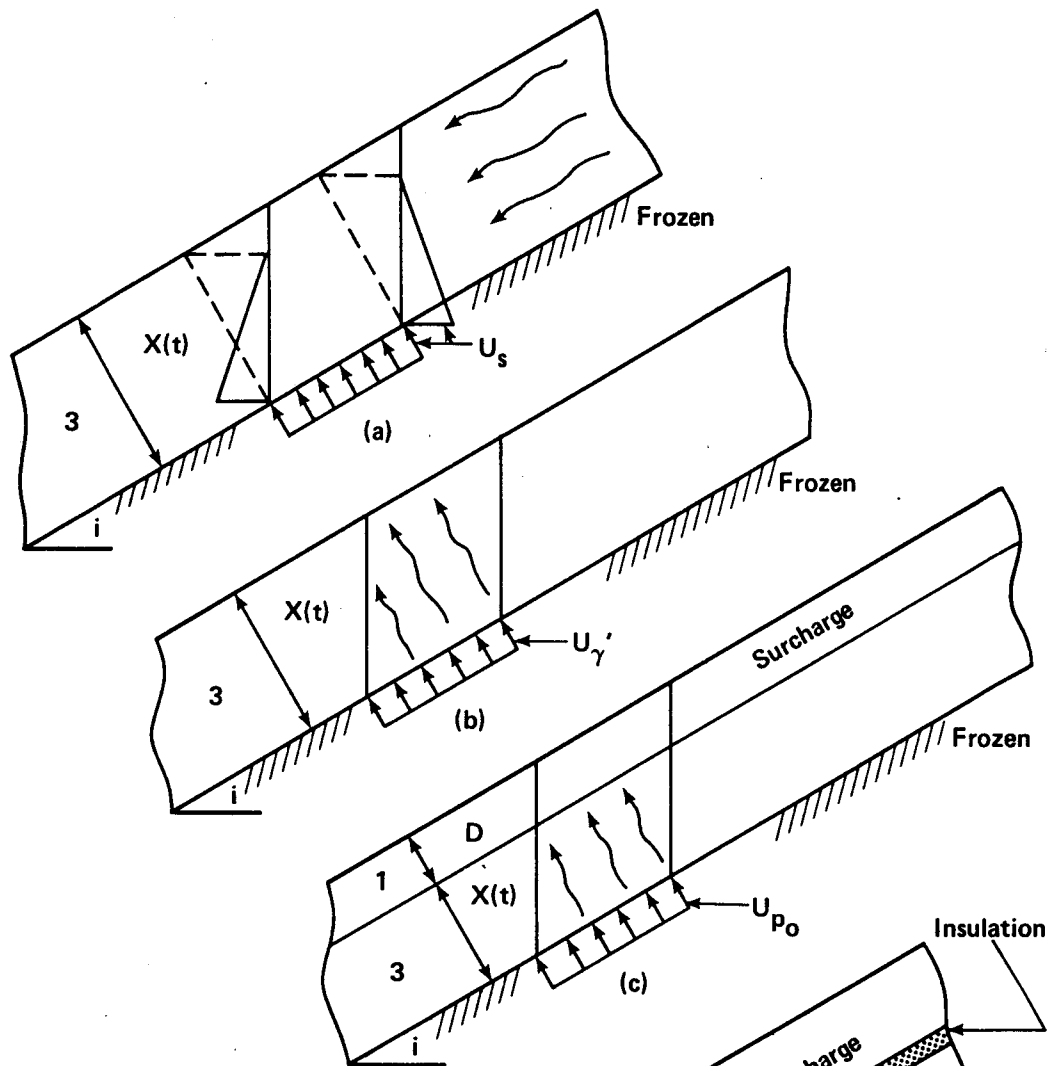


Fig. 3.2 Pore Pressure at the Thaw Front of a Thawing Infinite Slope

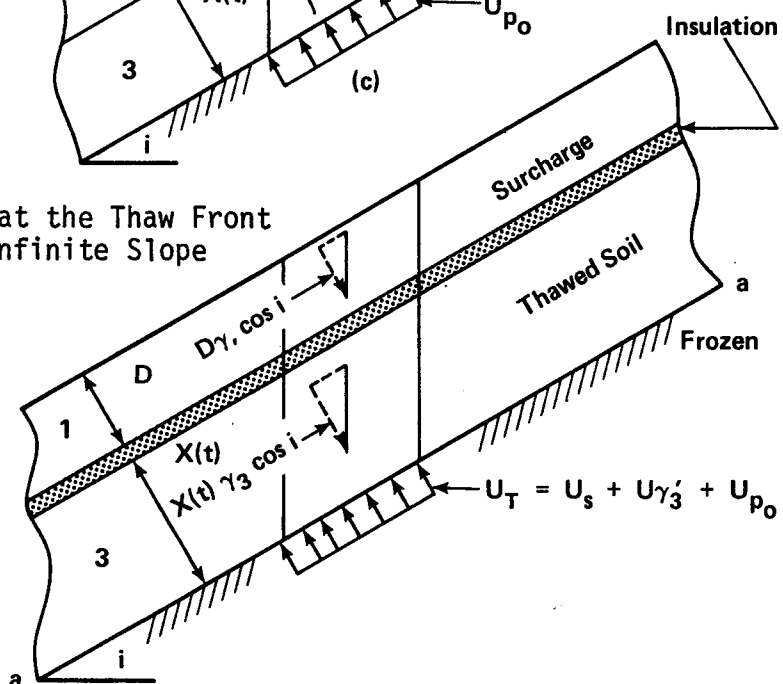


Fig. 3.3 Balance of Forces on a Thawing Infinite Slope

where $\gamma_3' X(t) \cos i$ is the normal stress on the thaw plane produced by the effective unit weight of the thawed soil. The pore pressure due to the surcharge is shown in Figure 3.2(c) and is given by:

$$U_{P_0} = \frac{P_0 \cos i \operatorname{erf}(R)}{\operatorname{erf}(R) + \frac{e^{-R^2}}{\sqrt{\pi} R}} \quad - - - [3.9(c)]$$

where $P_0 \cos i$ is the normal pressure exerted by the surcharge on the thaw plane.

If $R' = \frac{1}{1 + \frac{1}{2R^2}}$ and

$$R'' = \frac{\operatorname{erf}(R)}{\operatorname{erf}(R) + \frac{e^{-R^2}}{\sqrt{\pi} R}} \quad \text{then}$$

$$U_T = X(t) \cos i \gamma_\omega + \gamma_3' X(t) \cos i R' + P_0 \cos i R'' \quad - - - [3.9(d)]$$

R' and R'' may be evaluated from Figure 3.4 and 3.5 respectively. A statical balance of forces applied at the thaw front as indicated by section a-a in Figure 3.3 results in a factor of safety:

$$F = \frac{\{D\gamma_1 (1 - R'') + \gamma_3' X(t) (1 - R')\}}{D\gamma_1 + \gamma_3 X(t)} \frac{\tan \phi'}{\tan i} \quad - - - [3.10]$$

where γ_1 and γ_3 = total unit weights of the surcharge and the thawed soil respectively.

γ_3' = effective unit weight of the thawed soil.

i = angle of inclination of the slope.

If the depth or unit weight of the surcharge is zero, the equation becomes:

$$F = \frac{\gamma_3'}{\gamma_3} (1 - R') \frac{\tan \phi'}{\tan i} \quad - - - [3.11]$$

which is in agreement with McRoberts (1972) and McRoberts and Morgen-

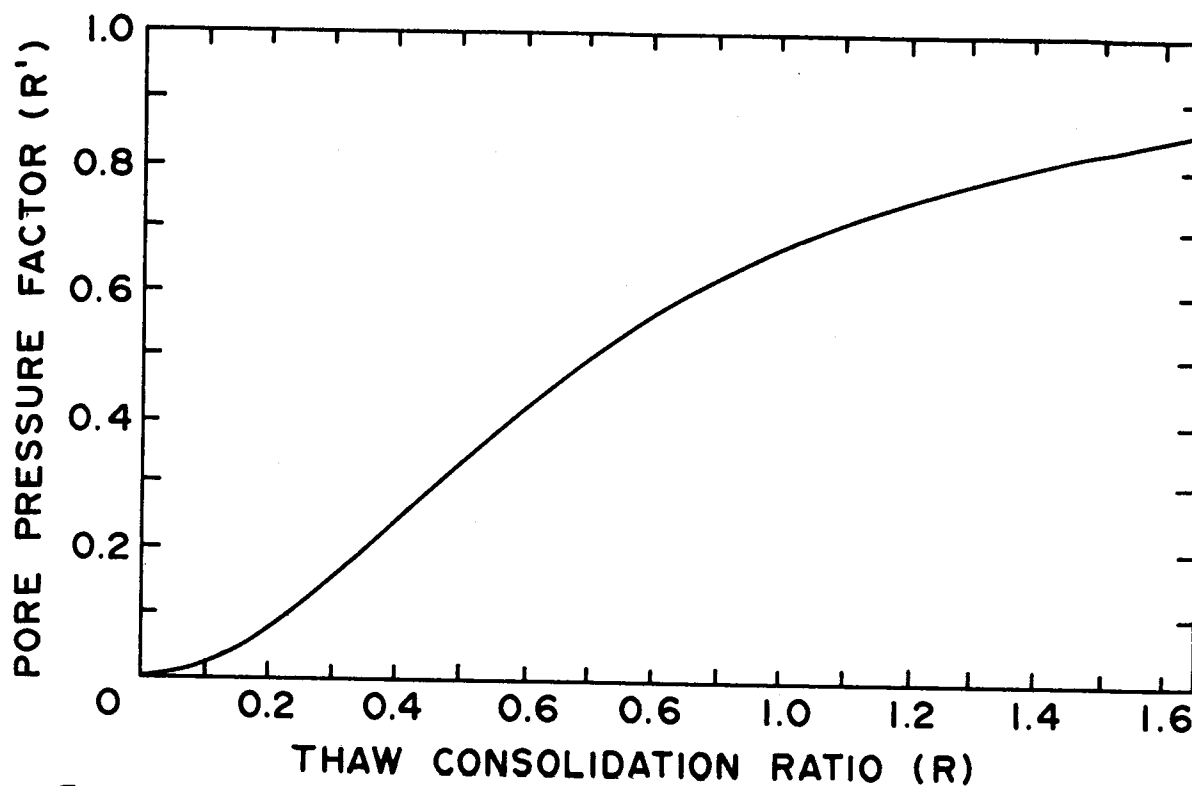


Fig. 3.4 Pore Pressure Factor (R') (self weight only) for Different Thaw Consolidation Ratios (R). After Morgenstern & Nixon (1971).

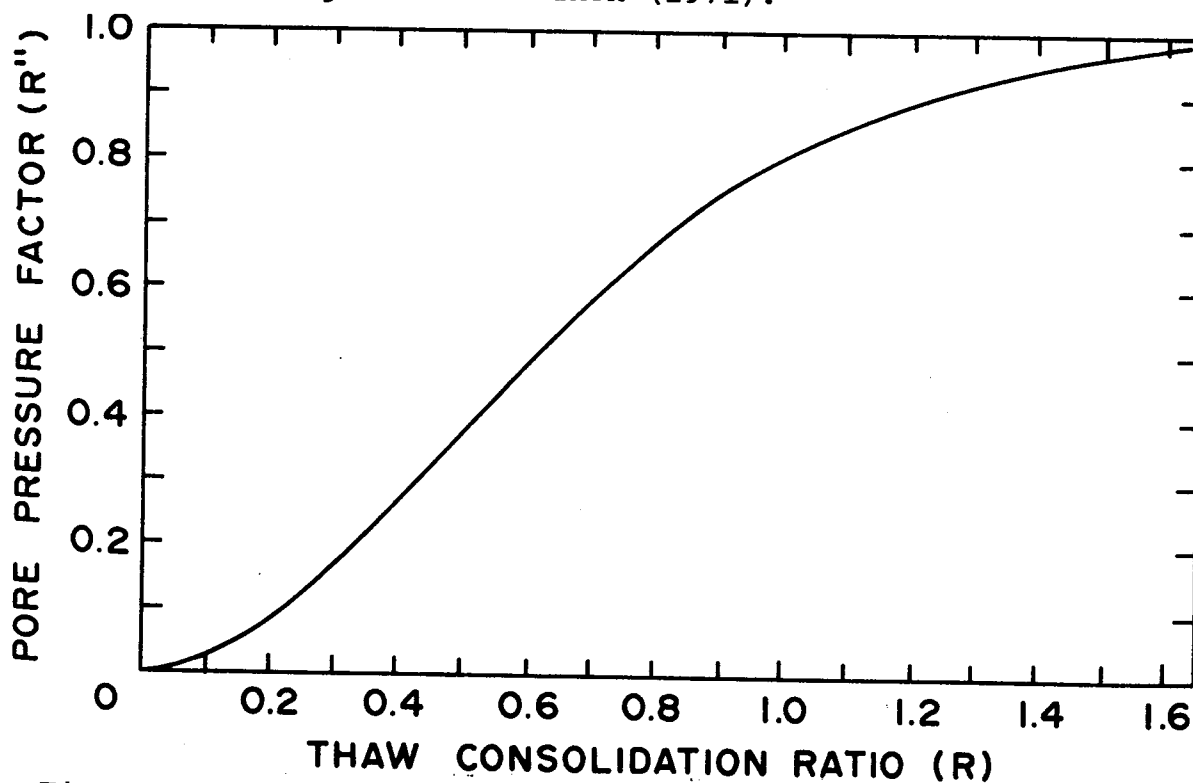


Fig. 3.5 Pore Pressure Factor (R'') (surcharge only) for Different Thaw Consolidation Ratios (R). After Morgenstern & Nixon (1971).

stern (1974). Equation [3.10] produces an approximate and slightly unconservative solution because the procedure underestimates the pore water pressures and therefore overestimates the factor of safety.

If the rate of thaw is plotted as in Figure 3.1 and modelled from equation [3.8], R' and R'' as obtained from Nixon and Morgenstern (1973) will be larger and the factor of safety will be proportionately smaller. The relative magnitude of these safety factors will be compared later.

3.4 Numerical Procedure For Design

The need for a numerical procedure to analyze the stability of a thawing slope covered with insulation and surcharge load is based on the lack of a suitable analytical method to evaluate pore water pressures for rates of thaw that are not proportional to the square root of time. A program was developed to compute the depth of thaw from equation [3.6] and uses a Crank-Nicholson finite difference procedure to solve the equation of consolidation subject to the boundary conditions at the thaw line (Nixon, 1973). The factor of safety is computed from:

$$F = \left[\frac{D\gamma_1 + \gamma_3 X(t) - U(N)/\cos i}{D\gamma_1 + \gamma_3 X(t)} \right] \frac{\tan \phi'}{\tan i} \quad - - - [3.12]$$

where $U(N)$ is the pore pressure due to thaw consolidation and surcharge loading acting at the thaw front, and the other terms are as defined previously. This equation is identical to equation [3.10], except for the pore pressure term ($U(N)$).

The input parameters are:

- 1) thermal conductivities of layers 1, 2 and 3
(cal/C⁰ cm sec) (Kersten, 1949 and Table 3.1);

TABLE 3-1

PHYSICAL AND THERMAL PROPERTIES OF
VARIOUS INSULATING MATERIALS

Material	Moisture Content %	Density gm/cc	Specific Heat cal/gm °C	Thermal Conductivity cal/°C cm sec
1) *Styrofoam HI	Dry	0.052	0.28	7.9×10^{-5}
2) *Polyurethane	Dry	0.03 to 0.08	0.28	5.5×10^{-5}
3) *Fibreglass	Dry	0.048	0.16	8.2×10^{-5}
2) *Woodchips	37	0.26	0.33	3×10^{-4}
3) *Sawdust or shavings	Dry	0.19	0.33	1.6×10^{-4}
4) *Peat	Varies with water content			

- 1)* Dow Chemical (1972)
 2)* Smith, Berg and Muller (1973)
 3)* ASHRAE (1963)
 4)* Dept. of Army (1966)

- 2) trial thickness of insulation (m);
- 3) the equivalent step temperature ($^{\circ}\text{C}$);
- 4) the length of the thawing season (days);
- 5) the coefficient of consolidation of the parent material (cm^2/sec);
- 6) the grid spacing in the parent material (a suitable depth increment is ≈ 0.040 m);
- 7) the thickness and unit weight of the surcharge respectively (m and kN/m^3);
- 8) the specific gravity of the soil solids in the parent material;
- 9) the total and unfrozen water contents of the parent material (expressed as a ratio of gms of water/gms of dry soil);
- 10) the effective angle of internal friction of the parent material;
- 11) the angle of the slope with the horizontal ($^{\circ}$); and,
- 12) the number of times output is desired over the length of the thaw season.

The output information consists of elapsed time, the depth of thaw, the pore pressure depth increment profile, the effective normal and shearing stress at the thaw front, and the factor of safety against failure.

If pore pressures and corresponding factors of safety are to be computed throughout the thaw season, then an equivalent surface step temperature must be used in equation [3.6]. This temperature is a function of the air thawing index (Thompson, 1963), a surface index factor (N) (Dept. of U.S. Army, 1966), and the length of the thaw

season (Burns, 1973).

$$\text{Thus } T_s = \frac{ATI \times N}{\text{Length of thaw season}} \quad - - - [3.13]$$

On the other hand, if pore pressures and factor of safety are desired only at the end of the thaw season when the thaw depth is at its maximum value and the factor of safety is at its minimum value, then only the surface thawing index need be used in equation [3.6].

The surface thawing index is the product of the surface temperature T_s and the total length of the thaw season. Generally, the time (t_0) required to thaw through the gravel surcharge will not be significant and may, therefore, be ignored. This simplifies the computations and provides a more conservative answer. The number of days that are chosen to represent the length of the thaw season is not particularly critical, for it is the product of the length of the thaw season and the step temperature which governs the maximum depth of thaw and is, therefore, of interest in the final analysis. It is, however, conservative to choose a slightly shorter thaw season and a correspondingly larger step temperature. Under these conditions larger pore pressures are generated in the early stages of the thaw season and therefore accentuate any critical condition that may occur at that time.

The actual temperature boundary conditions are approximated more closely by a sinusoidal variation rather than a surface step temperature. It is of interest to note that this former temperature variation will produce larger rates of thaw and therefore larger pore water pressures in mid-season than does an equivalent step temperature boundary condition (Nixon and McRoberts, 1973). At late stages in the thaw season the velocity of the thaw front is

reduced and eventually goes to zero when the thaw depth reaches its maximum value. Although the factor of safety of the slope decreases with increasing thaw depth, it is unlikely that the increase in the velocity of the thaw front at mid-season combined with a relatively shallow depth of thaw would seriously decrease the factor of safety at that time. On the other hand, the reduction in the velocity of the thaw front at the end of the thaw season diminishes the severity of the condition of decreasing factor of safety with increases in depth of thaw.

Estimates of thermal conductivity for the surcharge (K_1) and in situ material (K_3) may be obtained from Kersten (1949). These values must be multiplied by 4.13×10^{-3} to change the units to cal/cm $^{\circ}$ C sec. Table 3.1 lists the thermal conductivities (K_2) of various insulation materials that may be used. The surcharge material will provide some small but significant insulative value. The U.S. Army and Air Force (1966) suggest that one layer of material may be converted to an equivalent thickness of another from the ratio of their diffusivities. If the simple Stefan solution is employed to calculate the rate of thaw, then the ratio of the conductivities may provide a reasonable and conservative evaluation of the insulating effect of the sand/gravel surcharge. It should also be noted that the latent heat effects of the surcharge and insulation have been omitted from the computations. This term acts to retard the rate of thaw through these upper layers and therefore essentially reduces the length of the thaw season. On the other hand, the large water contents associated with significant magnitudes of latent heat increase the thermal conductivity of these materials and reduce their insulating

value. It was, therefore, considered preferable to neglect the latent heat effects of the upper layers and assume that the time to thaw through these upper two layers (to) in equation [3.6] be equal to zero.

Values of the coefficient of consolidation (C_v) may vary from 1×10^{-2} to 5×10^{-2} cm^2/sec . for materials encountered in the active layer at a number of sites in the Mackenzie Valley (Roggensack, 1975).^{*} Test results also indicate that C_v will decrease with depth to values in the order of 3×10^{-3} cm^2/sec . when tested at pressures equal to or greater than the effective overburden. The minimum value that may be encountered will not likely be less than 5×10^{-4} cm^2/sec . (ibid). However, when cuts are made in this material, the soil will be thawing under low normal stresses and the tendency for consolidation will be minimal. The values of C_v quoted for the active layer are therefore considered to be appropriate for the majority of the situations encountered in this region of the Arctic.

Values of ϕ' will vary from 20 to 24 degrees for the predominantly illitic clays found in this region (ibid). The effective cohesion intercept has been considered as zero for the purposes of computation.

3.5 Design Charts

A series of design charts have been prepared for use in determining the appropriate thicknesses of insulation and surcharge that may be required to stabilize thawing slopes in frozen soils (Figures 3.6 to 3.17). These charts establish the relationship between the factor of safety of a thawing slope and the factor of

^{*} Personal communication

safety of the same unfrozen slope with steady state seepage pore pressures only. The ratio $F_{\text{thaw}}/F_{\text{seepage}}$ is plotted against the coefficient of consolidation. Four curves appear on each plot indicating conditions for surcharge loads varying from 0 to 18.0 kN/m^2 (0 to 375 psf).

Three surface thawing indices, (1,500; 2,500 and 3,500 $^{\circ}\text{C}$ days) were chosen to embrace thawing conditions extending from the latitudes of Fort Simpson to the Beaufort Sea. Four water contents varying from 20 to 50% span the range likely to be encountered for most problems. The ratio of K_3/K_2 H indicates the effective insulation thickness. The three values of 0, 1.52 m (5.0 ft.) and 3.05 m (10.0 ft.) provide the necessary range for typical conditions.

The factor of safety varies with time, decreasing with increasing time and thaw depth. Therefore, only the minimum values that correspond to the maximum thaw depths have been considered.

The total unit weight of the surcharge was taken as 19.6 kN/m^3 (125 pcf) with a water content of 12% and a thermal conductivity (K_1) of $0.0065 \text{ cal/}^{\circ}\text{C cm. sec.}$ The permafrost was assumed to be saturated and the soil grains to have a specific gravity of 2.70. Thaw depths were computed using unfrozen thermal conductivities (K_3) that vary with water content according to Kersten (1949). The unfrozen water content was assumed to be zero.

3.6 Example Problem

The information for the example problem regarding soil, insulation, climate, and desired factor of safety appears in Table 3-2. The solution is obtained by referring to Figures 3-6 to 3-17.

Trial I determines the thaw depth and the F ratio for the

TABLE 3-2

SOIL, INSULATION AND CLIMATE INFORMATION FOR EXAMPLE PROBLEM

SOIL PROPERTIES	INSULATION PROPERTIES	CLIMATE	F_1 (SEEPAGE) $\frac{\gamma_3}{\gamma_3} \frac{\tan \phi'}{\tan i}$	F_R
$W = 35\%$	wood chips:	Air thawing Index: 1260 C° days (Thompson, 1963)	0.89	$\frac{1.3}{0.89} = 1.46$
$W_u = 0$	$K_2 = 0.003 \text{ cal/}^\circ\text{C cm sec}$			
$C_v = 0.002 \text{ cm}^2/\text{s}$	Styrofoam:	Surface Thawing Index Factor: 1.75 (U.S. Dept of Army, 1966)		
$\phi' = 22^\circ$	$K_2 = 0.000079 \text{ cal/}^\circ\text{C cm sec}$			
$K_3 = 0.003 \text{ cal/}^\circ\text{C cm sec}$		Surface Thawing Index: 1260 x 1.75 = 2200 C° days		
Slope Angle = 12°				

* Assume F (Thaw) required = 1.3

slope after disturbance, but without insulation or surcharge. The results are obtained by linear interpolation between soil water contents of 30 and 40% and surface thawing indices of 1,500 and 2,500 $^{\circ}\text{C}$ days.

Trial II determines the thaw depth and F ratio for a $\frac{K_3}{K_2} H$ ratio of 1.52 m (5.0 ft.) and a surcharge load of 18.0 kN/m^2 (375 psf) (1 m of surcharge) for the same water content and surface thawing index. An F ratio of 1.47 was obtained for this combination of insulation and surcharge.

Trial III produces results for a $\frac{K_3}{K_2} H$ value of 2.3 m (7.5 ft.) and a surcharge load of 12 kN/m^2 (250 psf) (≈ 0.6 m of sand/gravel). An adequate F ratio is obtained with this combination of surcharge and insulation.

Linear interpolation for thaw depth between thawing indices produces negligible error. However, linear interpolation between $\frac{K_3}{K_2} H$ values of 0 and 1.52 m causes a maximum of 8% overestimation of the thaw depth. Overestimation of thaw depth between $\frac{K_3}{K_2} H$ values of 1.52 m and 5.05 m is not significant.

Both Trial II and Trial III solutions are viable but it is probable that Trial II would be more economical depending on the relative availability of surcharge and insulating materials. However, the thaw depth in Trial II is approximately 20% greater than in Trial III. This may be a distinct disadvantage if the lower material is significantly inferior to the surficial deposits. Trial II would require approximately 15 cm. (6 in.) of woodchips along with 1 m (3 ft.) of sand/gravel surcharge. If styrofoam board were used approx-

imately 4 cm. (≈ 1.51 in.) would provide the same $\frac{K_3}{K_2} H$ value.

If the same problem is solved by direct hand computations, the thaw depth is computed from equation [3.3]. The modified thickness of insulation is determined from:

$$HE = H + \frac{K_2}{K_1} \text{DEP} \quad - - - [3.14]$$

where H = thickness of insulation

DEP = thickness of sand/gravel surcharge

K_1 and K_2 are the thermal conductivities of the surcharge and insulation respectively. α_e is determined from equation [3.3], R from equation [3.5], R' and R'' from Figures 3.3 and 3.4 and F from equation [3.10]. The results are shown in Table 3-3.

Figure 3-1 illustrates the manner in which the thaw depth varies with time for the combination of insulation and surcharge represented by Trial II. The thaw depth is almost linear with time, indicating a reasonable value of n (in equation [3.8]) equal to 1. R' and R'' may be evaluated from Nixon and Morgenstern (1973) and F computed from equation [3.10]. The results appear in Table 3-4.

A comparison of the values for factor of safety in this example indicate a slight variance in the magnitude depending on the method chosen for evaluation. The maximum value of the difference in this example is less than 10%. Since it is impossible to predict the various soil and climatic parameters required for the solution within this tolerance, it may be concluded that all methods produce acceptable values for design. The design charts are favoured in a choice of methods because of their convenience. The numerical procedure provides a more exact solution and generates data throughout

TABLE 3-3

THAW DEPTH AND INSULATION AND SURCHARGE REQUIREMENTS FOR EXAMPLE PROBLEM

Surface Thawing Index Co Days	Water Content %	$K_3 \frac{H}{K_2}$ (m)	Po (kN/m ²)	Thaw Depth (m)	F _R
TRIAL I					
1500	30	0	0	1.57	0.64
1500	40	↓	↓	1.33	0.71
1500	35	↓	↓	1.45	0.68
2500	30	↓	↓	2.03	0.54
2500	40	↓	↓	1.71	0.63
2500	35	↓	↓	1.87	0.59
2200	35	0	0	1.74	0.62
TRIAL II					
1500	30	1.52	18	0.53	1.50
1500	40	↓	↓	0.38	1.77
1500	35	↓	↓	0.45	1.63
2500	30	↓	↓	0.82	1.25
2500	40	↓	↓	0.61	1.54
2500	35	↓	↓	0.71	1.40
2200	35	1.52	18	0.64	1.47
TRIAL III					
1500	30	1.52	12	0.57	1.37
1500	40	↓	↓	0.42	1.63
1500	35	↓	↓	0.49	1.50
2500	30	↓	↓	0.94	1.13
2500	40	↓	↓	0.71	1.39
2500	35	↓	↓	0.82	1.26
2200	35	1.52	↓	0.72	1.33
1500	30	3.05	↓	0.34	1.60
1500	40	↓	↓	0.25	1.84
1500	35	↓	↓	0.30	1.72
2500	30	↓	↓	0.58	1.39
2500	40	↓	↓	0.40	1.66
2500	35	↓	↓	0.49	1.53
2200	35	3.05	↓	0.43	1.59
2200	35	2.3	12	0.59	1.46

TABLE 3-4

COMPARISON OF FACTORS OF SAFETY BY DIFFERENT METHODS OF COMPUTATION

FOR $K_3 H = 1.52 \text{ m}$ $P_o = 18 \text{ kN/m}^2$ (TRIAL II)
 $\frac{K_2}{K_2}$

$X(t) \propto \sqrt{\text{Time}}$ Equation (3-10)	$X(t) \propto \text{Time}$ Equation (3-8)	Design Charts	Numerical Methods
Max. Thaw Depth 0.649 m (2.13 ft)	Max. Thaw Depth 0.649 m (2.13 ft)	Max. Thaw Depth 0.64 m (2.10 ft)	Max. Thaw Depth 0.649 m (2.13 ft)
$\alpha_e = 0.0194 \text{ cm/sec}^{1/2}$	$\alpha_e = 0.0194 \text{ cm/sec}^{1/2}$	$F = 1.31$	$F = 1.28$
$R = 0.217$	$R' = 0.14$		
$R' = 0.086$	$R'' = 0.16$		
$R'' = 0.090$	$F = 1.28$		
$F = 1.36$			

the complete thaw season. The choice between the latter two methods will, therefore, depend upon the extent of the information required in the design project.

3.7 Recommendations For Installation

Since there is little documented experience regarding the actual performance of such installations, the following section is not intended to provide a detailed contract specification, but rather to highlight some of the more important aspects of the topic. Each site will demand innovative methods depending upon location, geographical setting, accessibility and a host of other logistic problems.

The ideal time for installation of the stabilizing materials would be in late winter or early spring when the permafrost is at its minimum temperature. It is intended that the placement of the insulation precede that of the surcharge. It may, however, be necessary to dress the slope with a layer of sand and gravel to provide a uniform surface for the insulation.

It is imperative that adequate drainage be provided directly above the permafrost to prevent the possibility of impeding the dissipation of excess pore water pressures. This may be most readily achieved by placing a four to six inch granular inverted filter or perforated plastic drainage pipe embedded in a herringbone pattern within a layer of sand immediately adjacent to the base material.

Insulation in the form of styrofoam board, wood chips, sawdust or planer shavings would then be placed over this drainage facility. Some consideration might be given to prevent these insulating materials

from absorbing excessive surface run-off and thus increasing their thermal conductivities. Styrofoam board will absorb 0.25% water by volume (Dow Chemical, 1972) and this small amount of moisture retention will not measurably affect the thermal characteristics of this material. Similar data is not available for foamed in place polyurethane but it is reasonable to assume that its water retention characteristics would be somewhat greater than the extruded styrofoam board. Increases in thermal conductivity with increasing water content in planer shavings and wood chips are also not known. However, these materials may be protected with an overlay of polyethylene plastic that would help to prevent substantial increases in water content. Surface runoff should be diverted by construction of small diversion dykes above the slope rather than by ditching.

The surcharge material, consisting of a sand/gravel mixture capable of sustaining plant growth forms the upper layer of the stabilizing components. This material must be end dumped and worked down the slope using all reasonable care to prevent disturbance of the underlying materials. It is necessary to ensure that this material is sufficiently resistant to erosion to maintain it in place prior to re-establishing vegetation on the slope.

Re-vegetation procedures should take place subsequent to the final trimming of the slope. It would be desirable to apply the seed in the form of hydro seed at the beginning of the growing season. The choice of plant species should be made in accordance with the results of on-going research experiments being conducted in the arctic and sub-arctic regions.

3.8 Longterm Performance

The most critical conditions regarding pore water pressures and stability will not necessarily occur during the first season of thaw. During this period of time, the soil will be consolidating under the imposed surcharge load and the water content will be reduced accordingly. Freeze back in the fall will not occur until movement of the thaw front has ceased and the pore water pressure has essentially dissipated. Therefore, there does not appear to be any danger of impeded drainage due to freeze back from the surface. During the second season of operation the $\frac{K_3}{K_2} H$ ratio will be increased because of the increased thermal conductivity of the soil due to the decrease in water content. However, this increase is not large enough to limit the melting to the same level during the first year. As a consequence, the thaw line will be penetrating the material below the maximum thaw depth of the preceding year, resulting in a smaller factor of safety. The magnitude of the decrease is less than 10% for the extreme condition, where the water content is reduced from 50 to 20%. These changes in factor of safety from one season to another are generally not considered to be significant. However, the designer may wish to choose a slightly larger initial value for the factor of safety in view of the foregoing. Increased thaw depth during subsequent years will not be significant. As vegetation is developed on the slope the surface heat balance will change and the surface will experience cooler temperatures, resulting in a decreased thaw depth and increased stability.

3.9 Choice of Insulation

A number of different insulating materials have been listed

in Table 3-1 for consideration. The final choice of material for each location will be made on the basis of availability of the material, the ease of placement and ultimately, the cost in place. A detailed economic analysis is beyond the scope of this presentation and the following discussion is only meant to provide guide lines for the designer in his choice of material.

Styrofoam board is readily available in southern Canada and may be shipped by rail f.o.b. Hay River, N.W.T. for approximately 17 cents per board foot (1974 quotation). This material is easy to place but requires a significant amount of unskilled hand labour. It has a low value of thermal conductivity, low water retention characteristics and a high compressive strength. It is not biodegradable, which may or may not be an advantage.

Polyurethane (foamed in place) has insulative qualities similar to those of styrofoam. It requires a high level of expertise and sophisticated equipment for placement. As a comparative cost, this option has been quoted (Edmonton, 1974) at 25 cents per board foot for material and \$1.00 per square foot for placement. Mobile equipment is available for transport into remote regions.

Large quantities of planer shavings are available at points as far north as High Level, Alberta. Small quantities may be available from local saw mills in the southern part of the Yukon and Northwest Territories. The cost of this material is very low. On the other hand, transportation costs may be very high. Placement is simple, requiring combined machine and hand operations. Plastic sheeting should be used to encapsulate the shavings and prevent excessive increases in the water content. This insulating material may undergo a substantial

amount of compaction under the influence of the surcharge load. Some reduction in insulative quality will undoubtedly result. Placing 50-75% of the surcharge below the shavings would help to alleviate this problem. Planer shavings and sawdust are biodegradable which may be a desirable aspect.

Woodchips, as used in the example, appear to possess considerable merit as an acceptable form of insulation. They would be manufactured near or on site with a commercial wood chipper using trees cleared from the right of way. However, careful assessment must be made of the quantity of trees available for this purpose. For example, a 100 foot wide right of way might require 9 in. of wood chips for insulation. One hundred lineal feet of this right of way would require $7,500 \text{ ft}^3$. At 17 pcf, 12,750 lbs. of wood chips are required. Assuming green spruce or poplar weighs approximately 40 pcf, then $3,200 \text{ ft}^3$ of wood are required. If a cord of wood has a porosity of 20%, then the volume of solids per cord of wood is approximately 100 ft^3 . Therefore, 32 cords of wood per 10,000 sq. feet of area are required. This is a substantial amount of wood and forestry personnel should be consulted regarding estimates of the availability of these quantities in the areas where they are required.

Environmental restrictions will generally make the on-site mining of peat moss impractical. If the material is gathered locally, it must be dried to obtain a suitable moisture content and correspondingly low coefficient of thermal conductivity. Transporting processed peat moss from southern Canada to northern regions is generally considered to be impractical when compared with artificial insulation materials. It, therefore, seems reasonable to conclude that wood chips, planer shavings or styrofoam board are the three prime contenders in the choice of insulation.

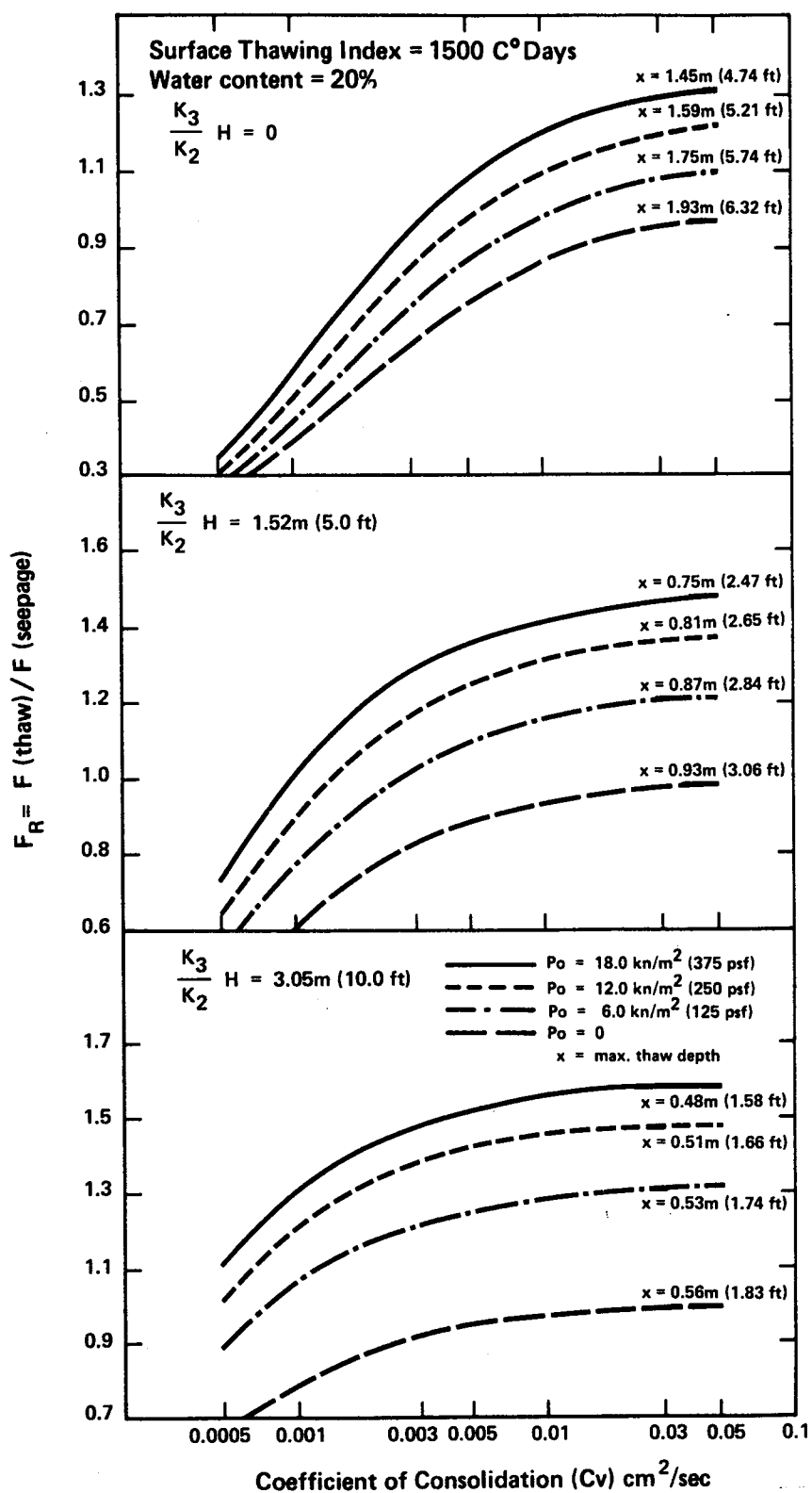


Fig. 3.6 Design Chart for Stabilization of Planar Landslides

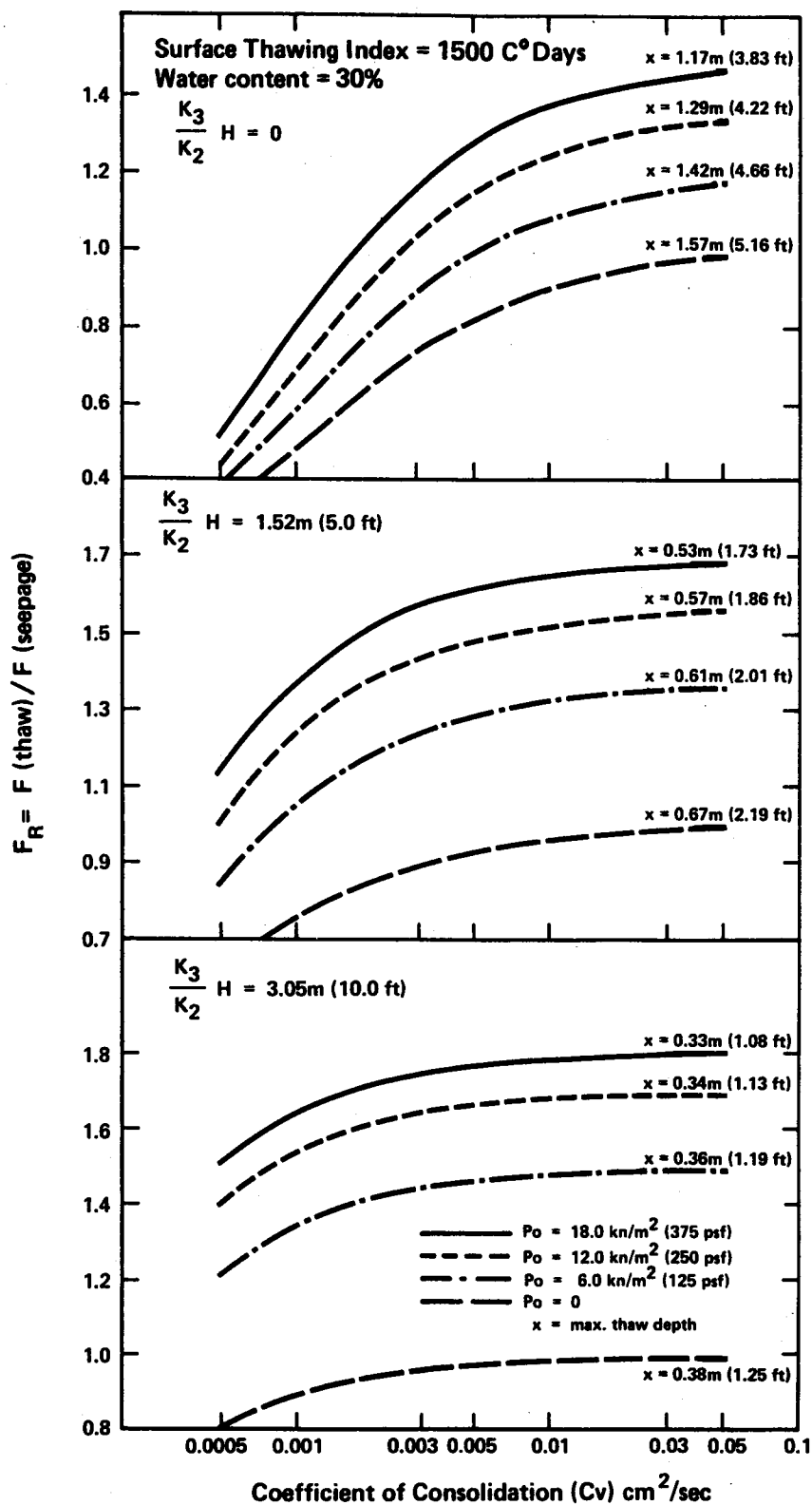


Fig. 3.7 Design Charts for Stabilization of Planar Landslides

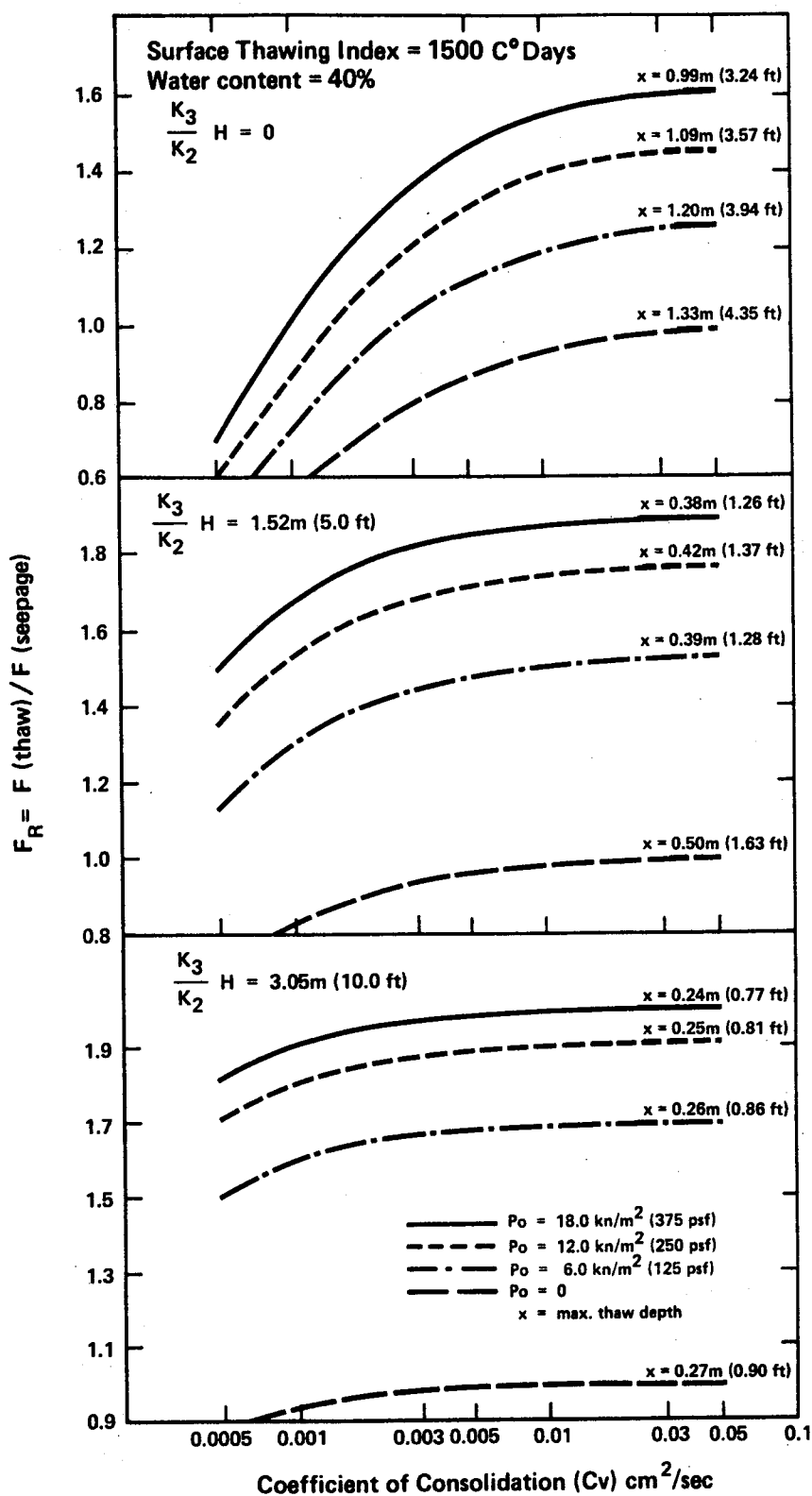


Fig. 3.8 Design Charts for Stabilization of Planar Landslides

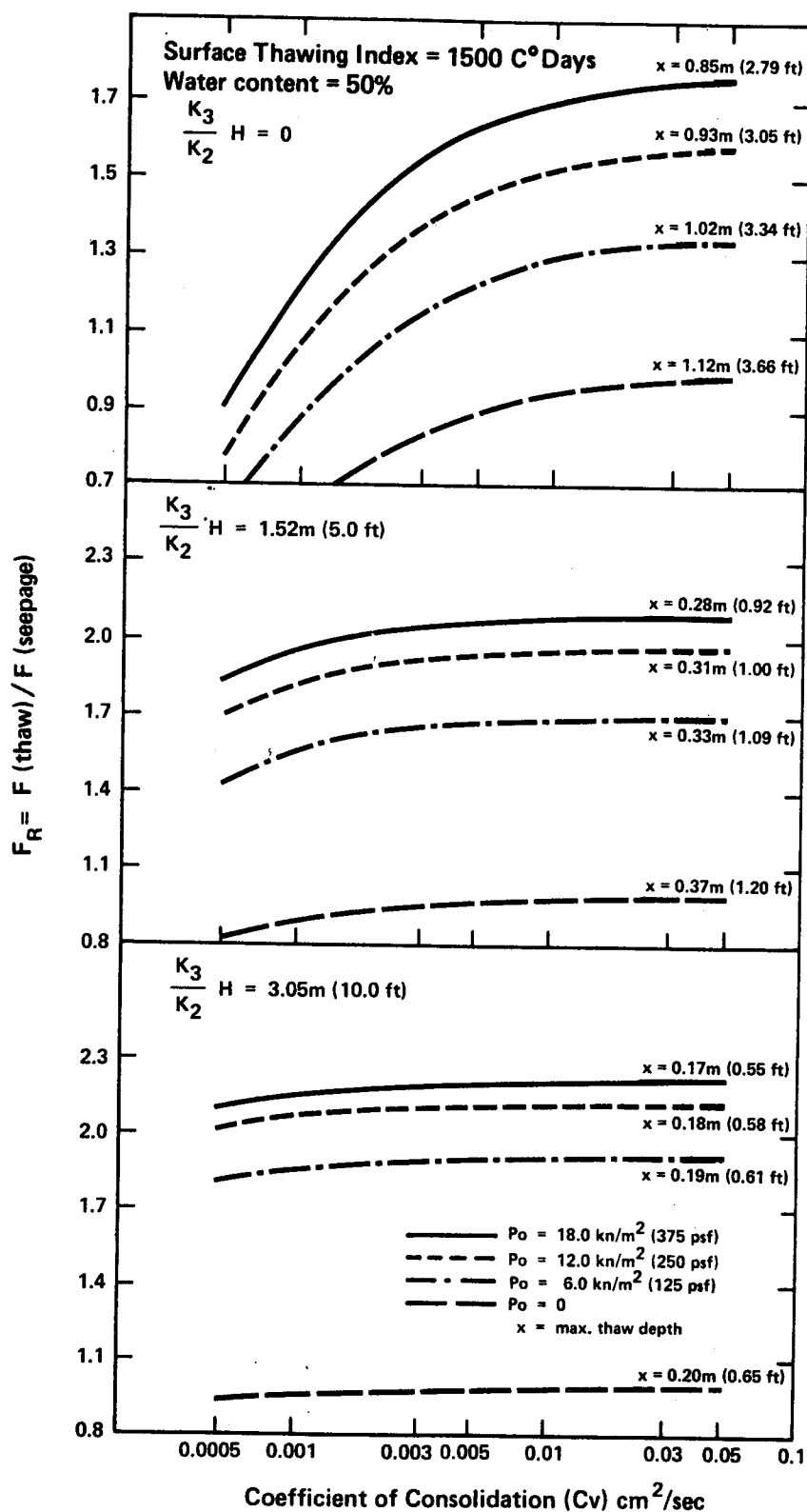


Fig. 3.9 Design Charts for Stabilization of Planar Landslides

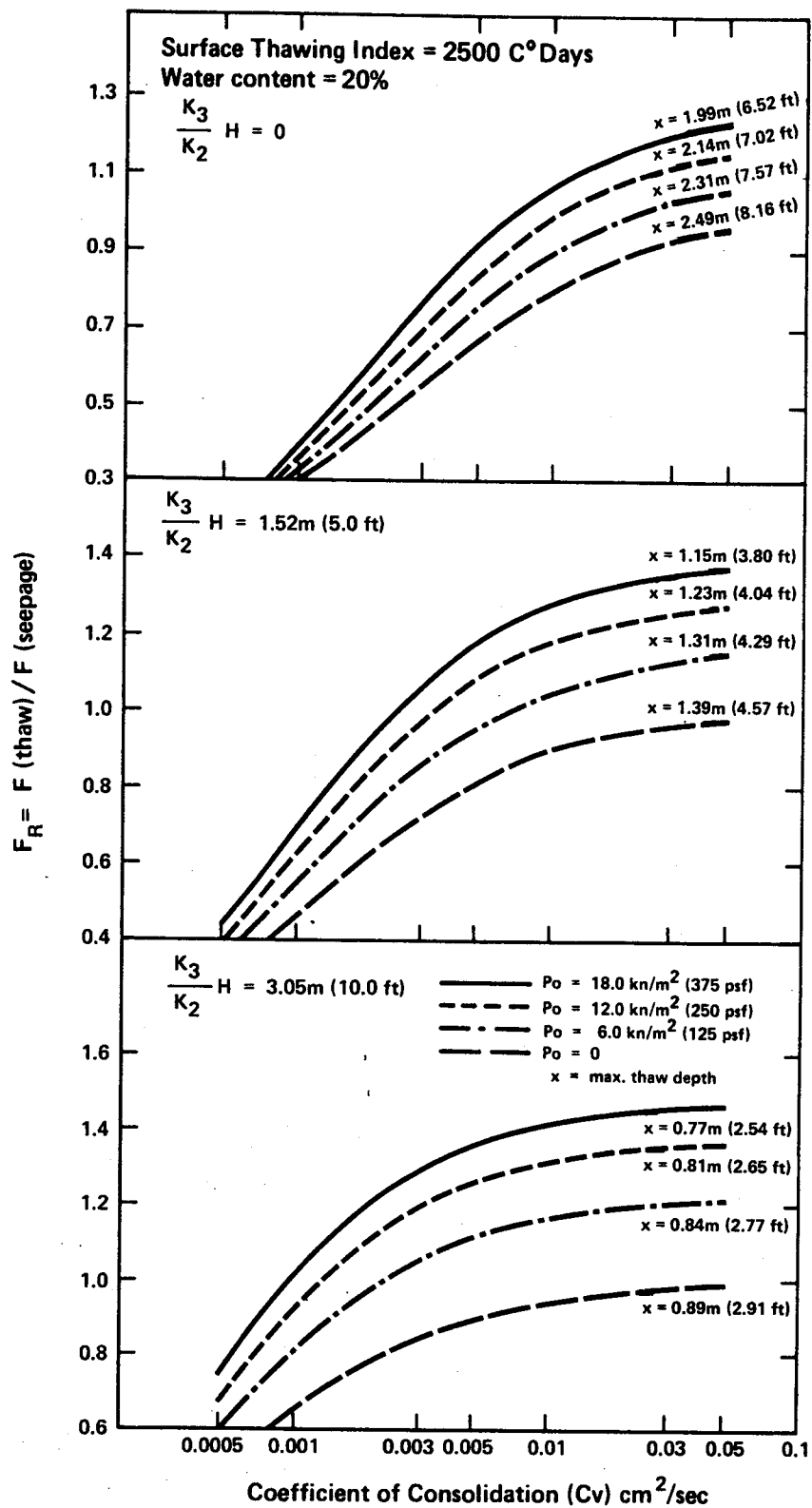


Fig. 3.10 Design Charts for Stabilization of Planar Landslides

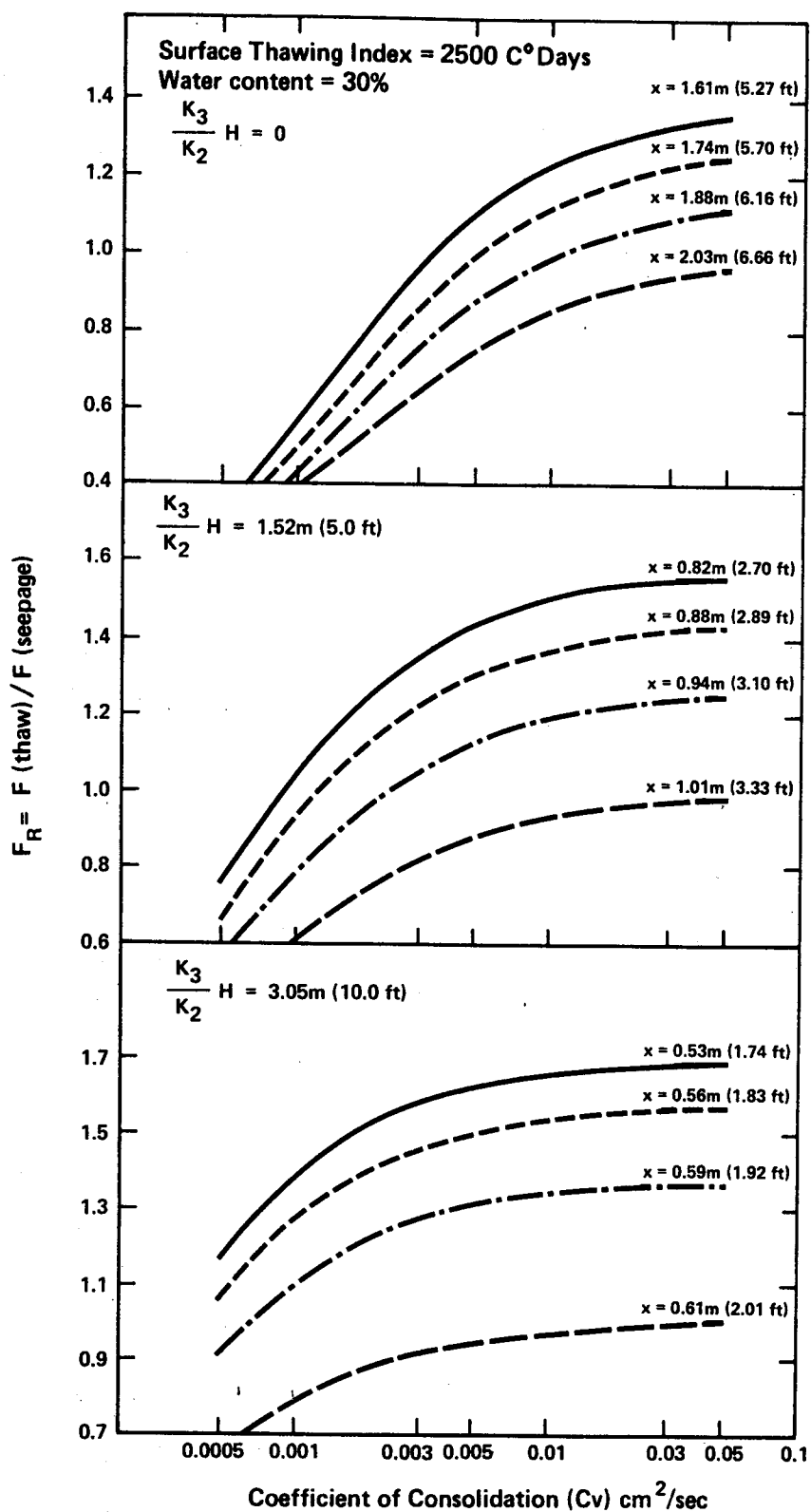


Fig. 3.11 Design Charts for Stabilization of Planar Landslides

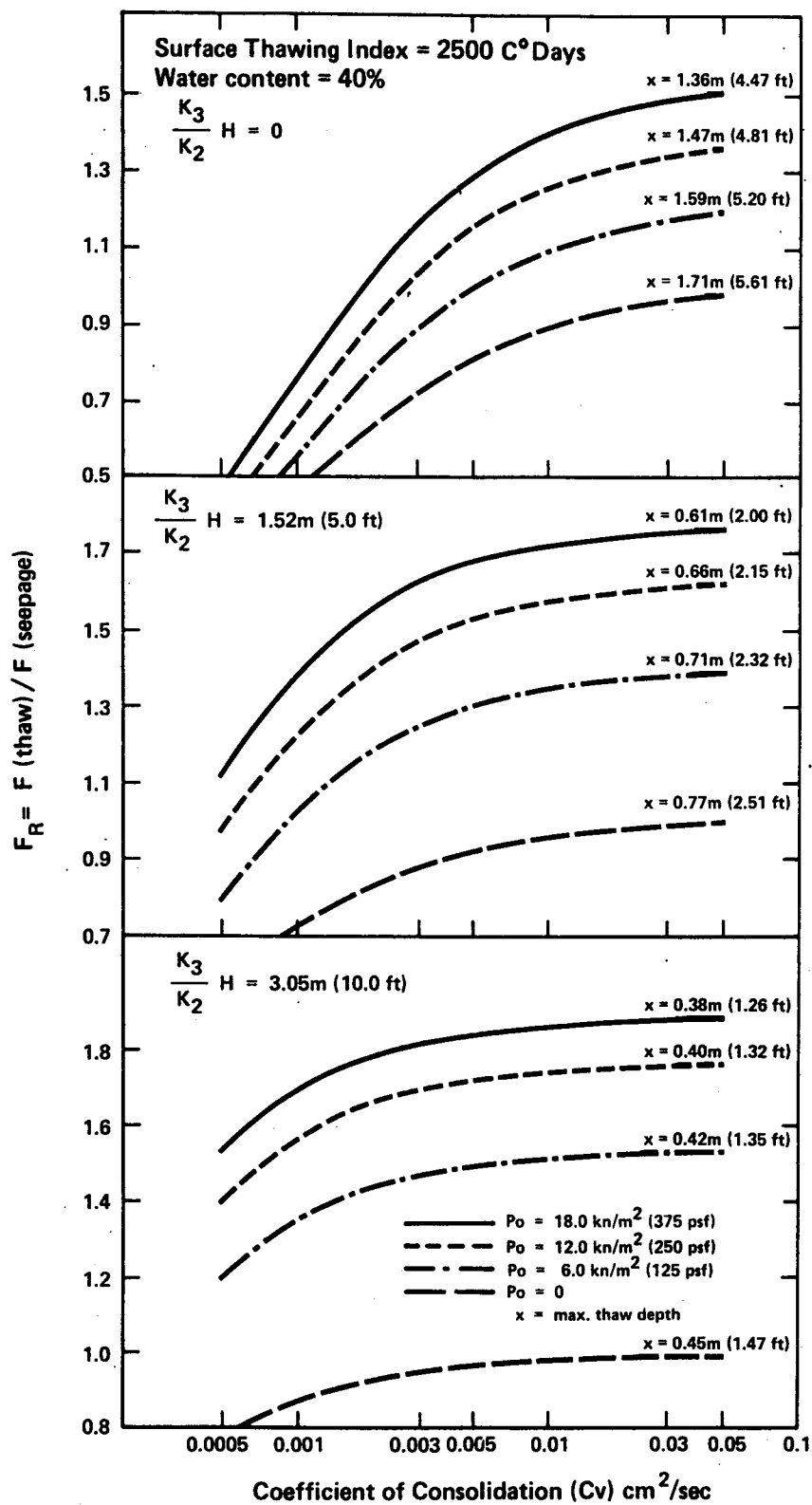


Fig. 3.12 Design Charts for Stabilization of Planar Landslides

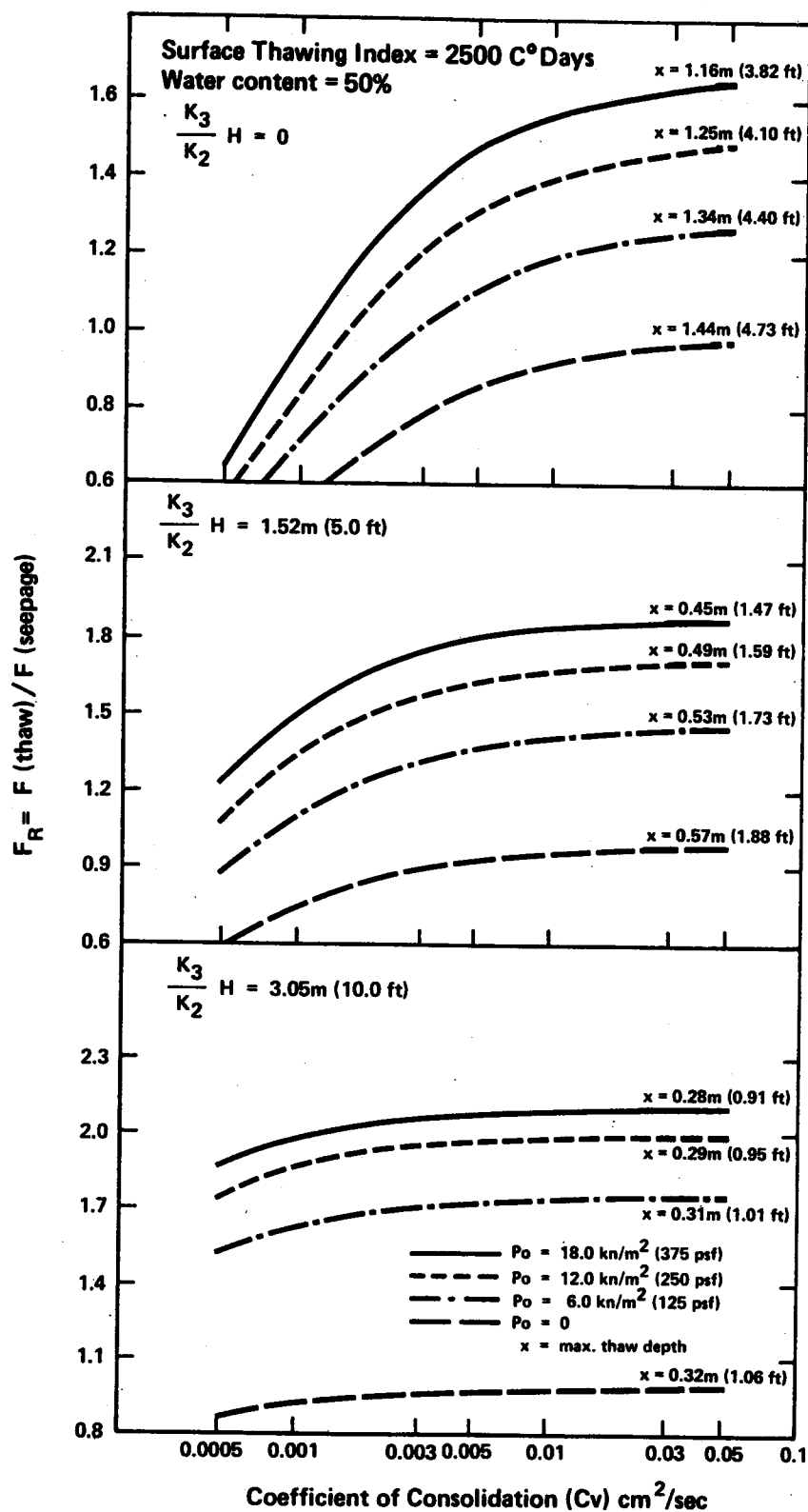


Fig. 3.13 Design Charts for Stabilization of Planar Landslides

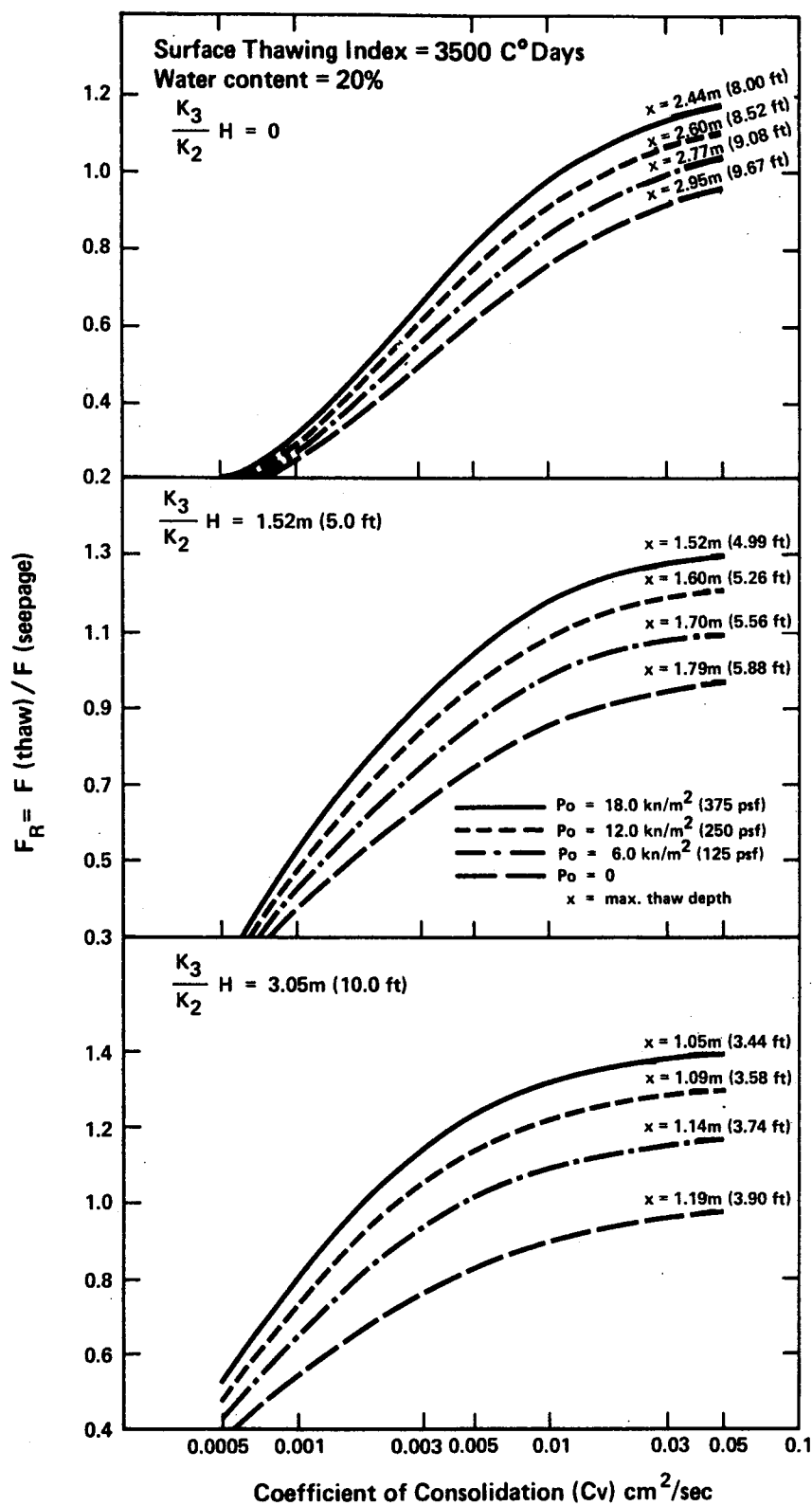


Fig. 3.14 Design Charts for Stabilization of Planar Landslides

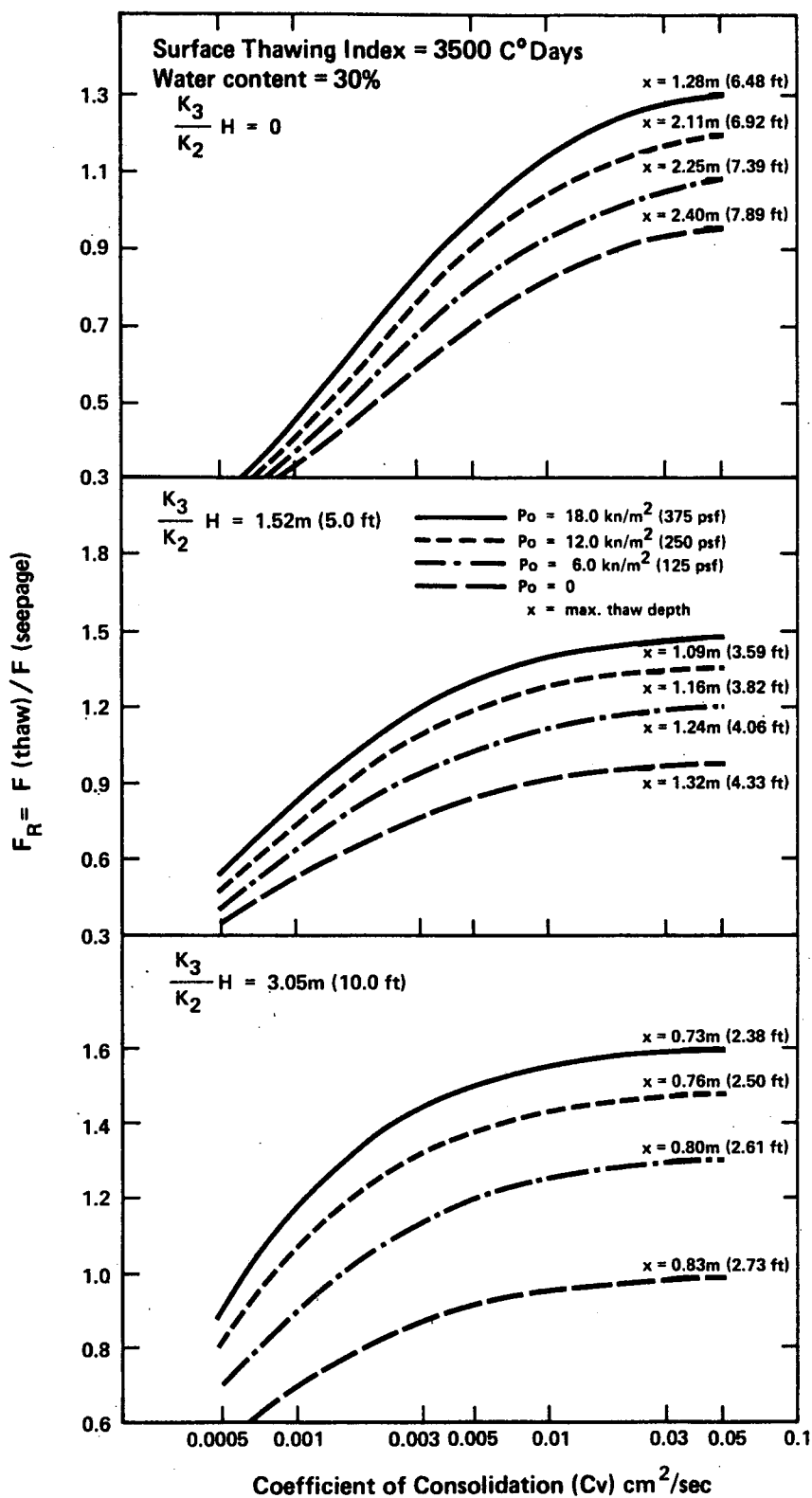


Fig. 3.15 Design Charts for Stabilization of Planar Landslides

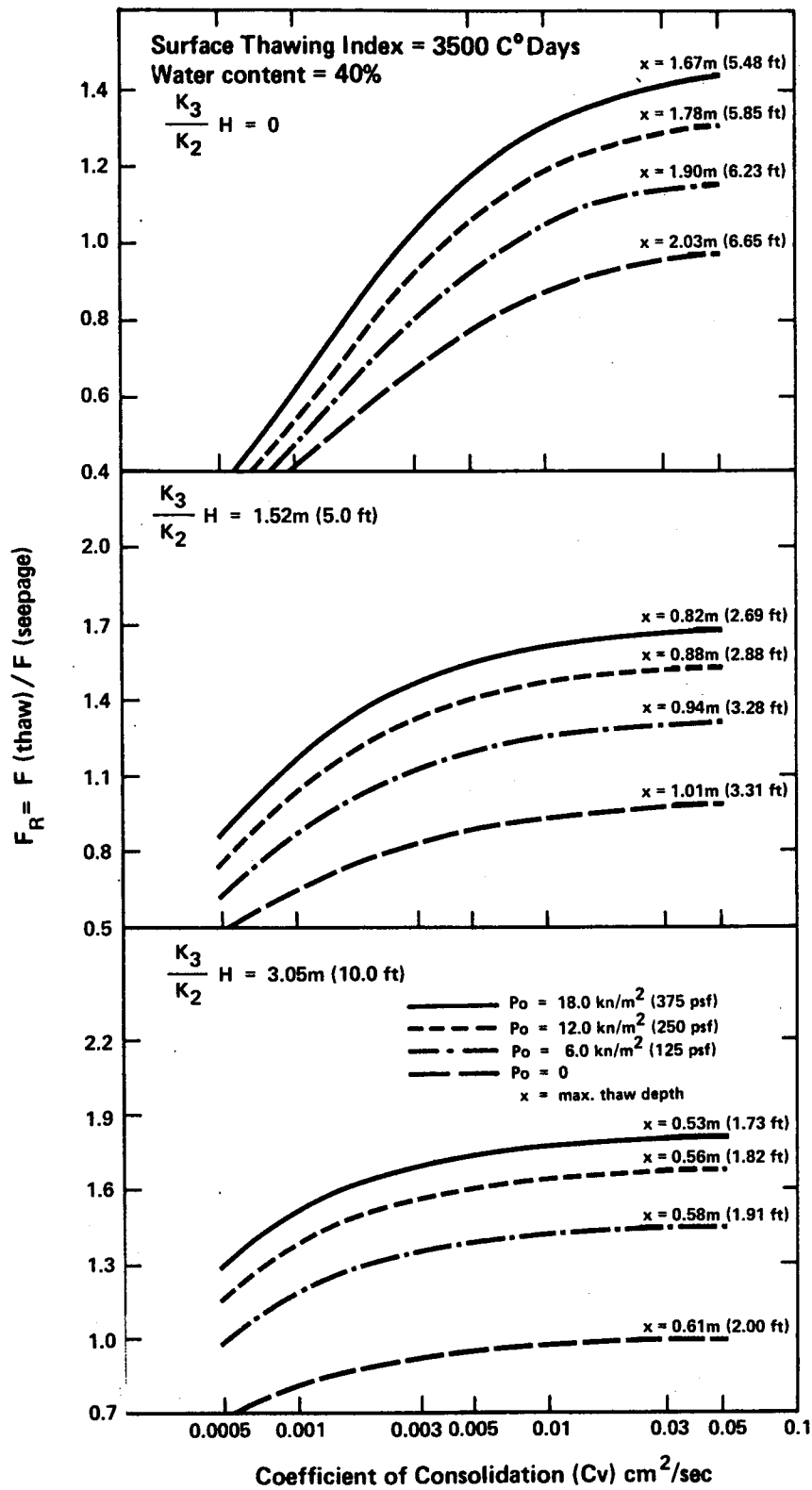


Fig. 3.16 Design Charts for Stabilization of Planar Landslides

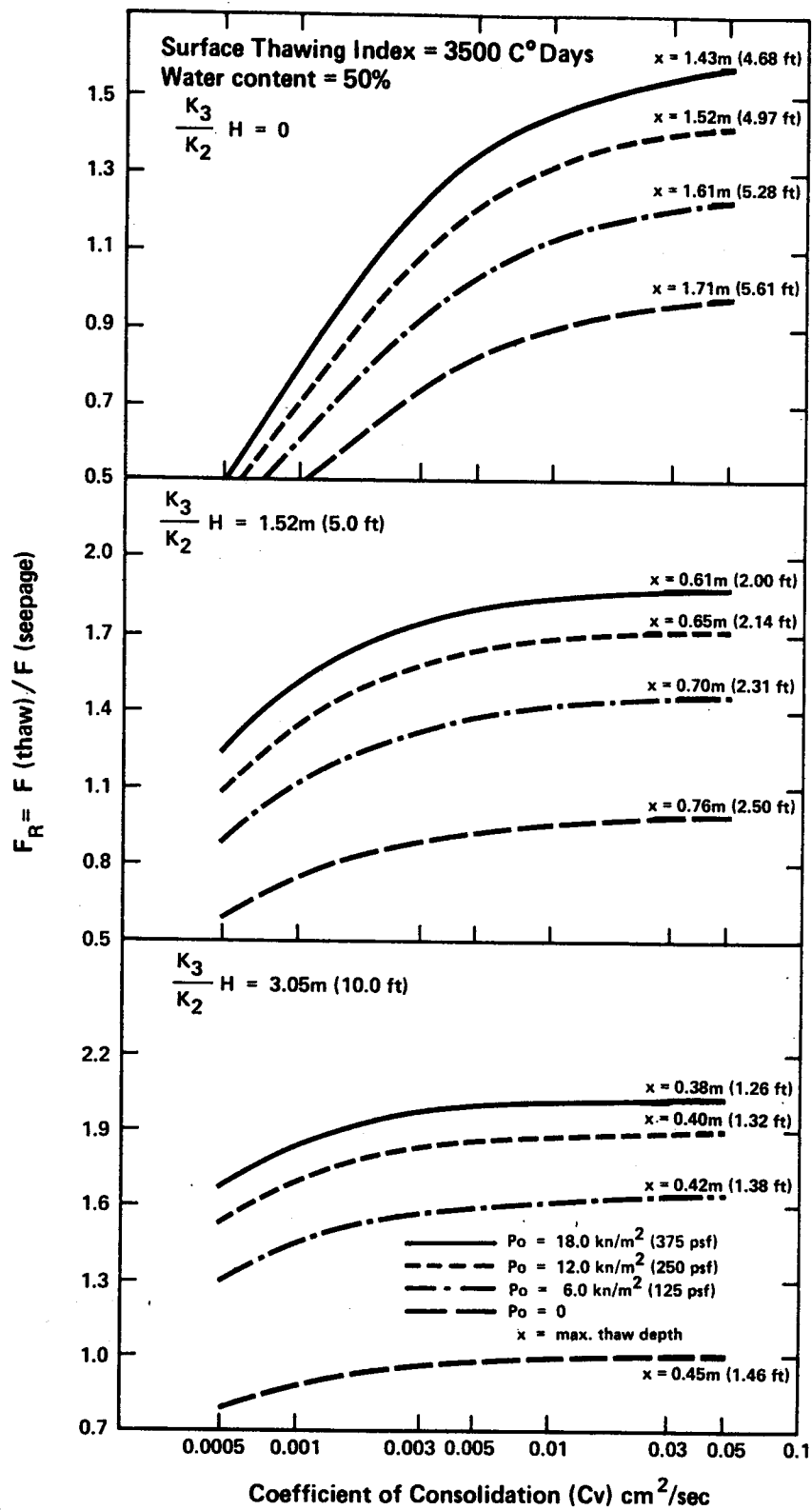


Fig. 3.17 Design Charts for Stabilization of Planar Landslides

CHAPTER IV

THE ENERGY BALANCE

4.1 Basic Concepts

The energy balance at the surface of the earth may be expressed in terms of a mathematical equation:

$$q_{DS} + q_{dS} + q_{RS} + q_{LU} + q_{LD} + q_L + q_H + q_p + q_G = 0 \quad - - - [4.1]$$

The symbol q represents energy per unit of area per unit of time and has units of gm. cal/cm² min. or simply ly/min. The subscript refers to the source of this energy. The equation is written with all terms positive. If the direction of energy flow is toward the surface of the ground, the sign will be positive and if energy flow is directed away from the surface, the sign will be negative. This convention also applies to heat flow below the surface. In equation [4.1]:

- q_{DS} = direct beam short wave energy from the sun.
- q_{dS} = diffuse short wave energy from the sky.
- q_{RS} = short wave radiation reflected by the earth's surface.
- q_{LD} = long wave radiation directed downward from the atmosphere to the ground.
- q_{LU} = long wave radiation emitted by the ground surface.
- q_L = the transfer of energy to or from the surface through the latent heat of vaporization or condensation.
- q_H = the transfer of energy by sensible heat to or from the surface by turbulent or convective processes.
- q_p = the gain or loss of energy through the addition of sensible heat due to precipitation on the surface.

q_G = the transfer of energy to or from the surface through the ground.

4.2 Radiative Components on a Horizontal Surface

4.2.1 General

All bodies radiate thermal energy, the intensity and spectral distribution of which is a function of the temperature and emissivity of the body.

A "black body" is a body or object that completely absorbs all radiation (at all angles) incident upon its surface. It is also a perfect emitter at all wave lengths. The emissivity (ϵ) of a body is the ratio of the emissive power (E) of a body at absolute temperature (T) to the emissive power of a black body (E_b) at the same absolute temperature (T). Thus,

$$\epsilon = E/E_b \quad - - - [4.2]$$

Radiation is characterized according to wave length (λ) usually measured in microns (μ). The spectral distribution ranges from some small, but finite value ($.10\mu$) to wave lengths in excess of 50μ .

Planck (1959) used quantum theory to derive the hemispherical emissive power of a black body.

$$E_{b\lambda} = \frac{C_1}{\lambda^5 (e^{C_2/\lambda T} - 1)} \quad - - - [4.3]$$

where C_1 and C_2 are constants and $E_{b\lambda}$ is the emissive power at wave length λ and absolute temperature (T) expressed in $^{\circ}K$. Figure 4.1 indicates the manner in which black bodies emit energy at different temperatures and wave lengths. It also shows that the maximum energy emitted by a black body occurs at some unique wave length

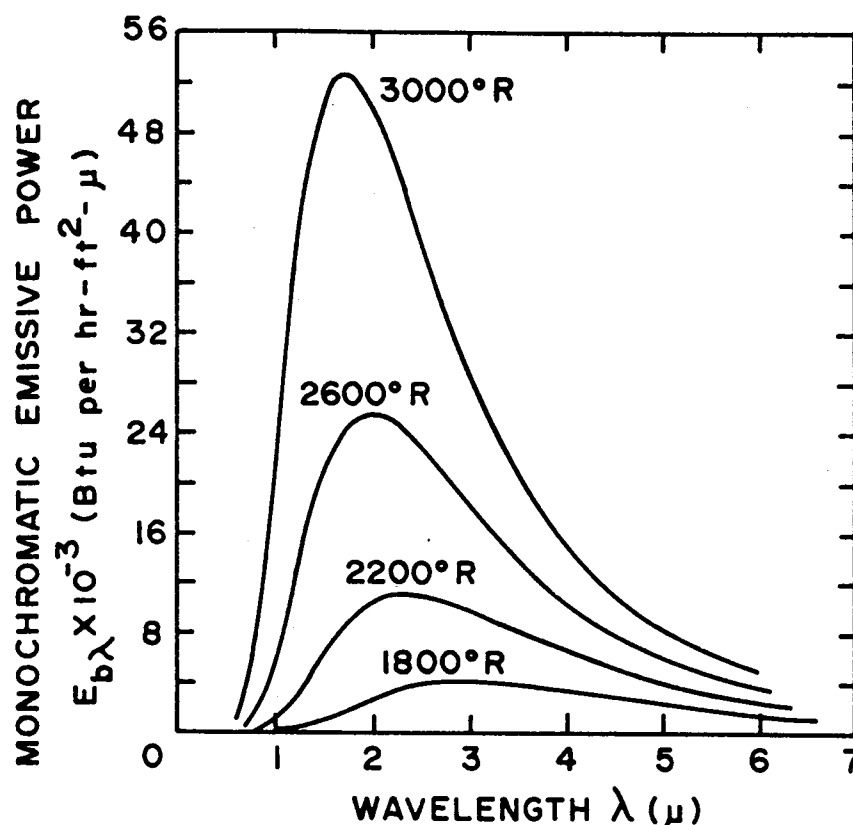


Fig. 4.1 Monochromatic Emissive Power for Several Temperatures vs Wavelength (After Wiebelt (1966))

associated with some unique temperature. If equation [4.3] is differentiated partially with respect to wave length and set equal to zero, the equation $\lambda_{\max} T = \text{constant}$ emerges where λ_{\max} is the wave length corresponding to the maximum emissive power (Wien, 1894). The Wien's Displacement Law indicates that the peak intensity of emitted radiation occurs at a wave length which is inversely proportional to the absolute temperature. It is evident that so called "hot bodies" radiate maximum amounts of energy at short wave lengths and cooler bodies radiate at longer wave lengths. The sun, at approximately $6,000^{\circ} \text{K}$, has its peak emissive power in the 0.47 to 0.49 μ range, whereas the earth at approximately 300°K emits at a peak intensity of 11 to 12 μ. It is of interest to note that 45% of the emitted energy in the solar spectrum falls within the visible range of 0.4 to 0.74 μ (Sellers, 1965). Short wave radiation is generally

considered to be all that radiation less than 4μ in length.

The Planck equation for emissive power in monochromatic wave lengths may be recast and integrated over all wave lengths to form the Stefan-Boltzman equation.

$$E = \sigma T^4 \quad - - - [4.4]$$

This equation describes the energy emitted by a black body in all wave lengths at absolute temperature (T) and where the Stefan-Boltzman constant (σ) equals $8.26 \times 10^{-11} \text{ ly/min. } ^\circ\text{K}^4$. If the emissivity (ϵ) is included, then the equation describes the manner in which bodies other than black bodies emit radiation.

4.2.2 Direct Beam Clear Sky Solar Radiation

As solar radiation passes through the atmosphere it is selectively scattered and/or absorbed by gases and impurities in the air. Ozone absorbs all the energy at wave lengths less than 0.3μ and selectively up to 0.35μ . Water vapour effectively prevents solar radiation longer than 4.0μ from reaching the ground. It selectively transmits in the 11 to 13μ range and this accounts for the significant influence of long wave radiation.

Carbon dioxide is the only other gas in the atmosphere that absorbs radiation. It will, however, absorb only in two narrow bands. The first band occurs between 0.29 and 4.0μ and the second between 12 and 16μ (Simpson, 1929).

Actual depletion of a direct ray of radiation is a function of the composition and thickness of the medium through which it passes. The quantity of direct beam radiation (on a plane normal to the beam) reaching the earth's surface is commonly expressed by Beer's Law.

$$q_{DSN} = J_0 e^{-\beta m} \quad - - - [4.5]$$

where q_{DSN} is the flux of energy transmitted to the earth by direct short wave radiation.

β = coefficient of extinction.

m = thickness of the medium traversed by the beam or commonly called the optical air mass.

This quantity m may be adequately approximated by $1/\cos z$ (where z equals the zenith angle of the sun) for angles of z less than 80 degrees. The solar constant (J_0) is defined as the intensity of solar radiation received on a unit area of a plane normal to the incident radiation at the outer limit of the earth's atmosphere with the earth at its mean distance from the sun. The magnitude of this constant varies within limits of $\pm 1.5\%$. List (1968) proposes a value of 1.94 ly/min. Occasionally adjustments are made to J_0 that take the form of J_0/r^2 where r , the radius vector of the earth, is the distance from the center of the earth to the center of the sun expressed in terms of the length of the semi-major axis of the earth's orbit (ibid). This variation in distance produces a variation in intensity of $\pm 3.5\%$.

The term $e^{-\beta}$ is alternately called the transmittance (a). This parameter is a function of scattering due to air molecules and water vapour as well as absorption of radiation by water vapour. The amount of radiation reaching a horizontal plane on the earth's surface may then be written as

$$q_{DSH} = J_0 a^m \cos z \quad - - - [4.6]$$

where z again represents the zenith angle of the sun and can readily be expressed in terms of the declination, latitude and the hour angle.

If the designer wishes to calculate or estimate the amount of direct beam radiation reaching the surface of the earth, he must in some way be able to evaluate the transmittance (a).

The classical approach to calculating direct beam radiation at the surface of the earth has been to express it as some fraction of the direct beam radiation incident upon a horizontal surface at the outer limits of the atmosphere. Thus the ratio $q_{DSH}/q_{DSHE} = a^{11}$ (and $a^{11} = a^m$) must be determined. a^{11} is defined as the atmospheric transmission coefficient. The subscript E indicates extraterrestrial. Kimball (1928) has prepared charts which allow the evaluation of a^{11} for different values of the precipitable water in the air (w) and various values of the optical air mass (m).

For example, if the amount of precipitable water is 30 mm and a low to moderately dusty atmosphere prevails, the transmission coefficient (a^{11}) for $m = 1$ is 0.63 and for $m = 5$, $a^{11} = 0.28$. Thus the length of path of the sun's rays through the atmosphere is of extreme importance in affecting the reduction of solar intensity. The reader is referred to Klein (1948) for the most lucid presentation of the technique.

The amount of precipitable water in the atmosphere is that amount of water that would be obtained from a column of air extending from the earth's surface to the top of the atmosphere. The magnitude of this parameter can be related to the moisture in the air at the surface of the earth which in turn is a function of the dew point temperature. Reitan (1963) suggests the relationship

$$\ln w = a + b (t_d) \quad - - - [4.7]$$

where w = the amount of precipitable water vapour in the air (cm).

t_d = dew point ($^{\circ}\text{C}$).

$a = 0.110$ and $b = 0.614$.

Similar equations have been suggested by Threlkeld and Jordan (1958), Brooks (1959), Stephenson (1967), and ASHRAE (1967). The amount of precipitable water may be adjusted for elevation when sites are in excess of 2,000 feet above sea level (Klein, 1948, Threlkeld and Jordan, 1958).

Direct evaluation of the precipitable water may be omitted if published values of the apparent extinction coefficient (β) are available (ASHRAE, 1967, Sadler, 1970). The precipitable water and scattering are considered as a monthly average and the values have been determined experimentally and tabulated for each month of the year.

The accuracy of computed values of clear sky radiation is reasonably good for most unindustrialized areas of the world. However, the value of such computations is not always evident in most micro-meteorological problems. Cloud cover has a profound effect on direct beam radiation and must be considered in most practical problems.

4.2.3 Diffuse Clear Sky Radiation

A significant part of the direct solar radiation which has been scattered and diffusely reflected in the atmosphere by molecules of air, water vapour and dust arrives at the earth's surface unchanged in wave length. This portion of short wave radiation is known as diffuse radiation and is in excess of the direct beam radiation.

Kimball (1935) has suggested that -- "about half the radiation lost from the incoming rays through scattering and diffuse reflection is finally received at the ground as diffuse radiation from the sky". The total depletion by atmospheric scattering and diffuse reflection

can be expressed as:

$$s = 1 - a^1 \quad - - - [4.8]$$

where a^1 is the transmission coefficient after scattering by air and water molecules. It differs from the previous transmission coefficient a^{11} in that it does not include water vapour absorption. Thus for a given amount of precipitable water in the atmosphere a value for a^1 may be obtained from Figure 4.2 and a scattering coefficient calculated from equation [4.8]. The quantity of short wave diffuse radiation incident upon a horizontal surface may be estimated as:

$$q_{ds} = J_0 \cos z S (0.5) \quad - - - [4.9]$$

Typical values of S range from 0.11 to 0.20. These values agree reasonably well with Stephenson (1967).

A technique devised by Lui and Jordan (1960) to estimate diffuse radiation appears to have significant merit. They suggest the equation:

$$\tau_d = 0.2710 - 0.2939\tau_D \quad - - - [4.10]$$

where $\tau_d = q_{dSH}/q_{DSHE}$ and

$$\tau_D = q_{DSH}/q_{DSHE}.$$

If a value of total short wave radiation is available the equation may be written as:

$$\tau_d = 0.3840 - 0.4160\tau_T \quad - - - [4.11]$$

where $\tau_T = (q_{DSH} + q_{dSH})/q_{DSHE}.$

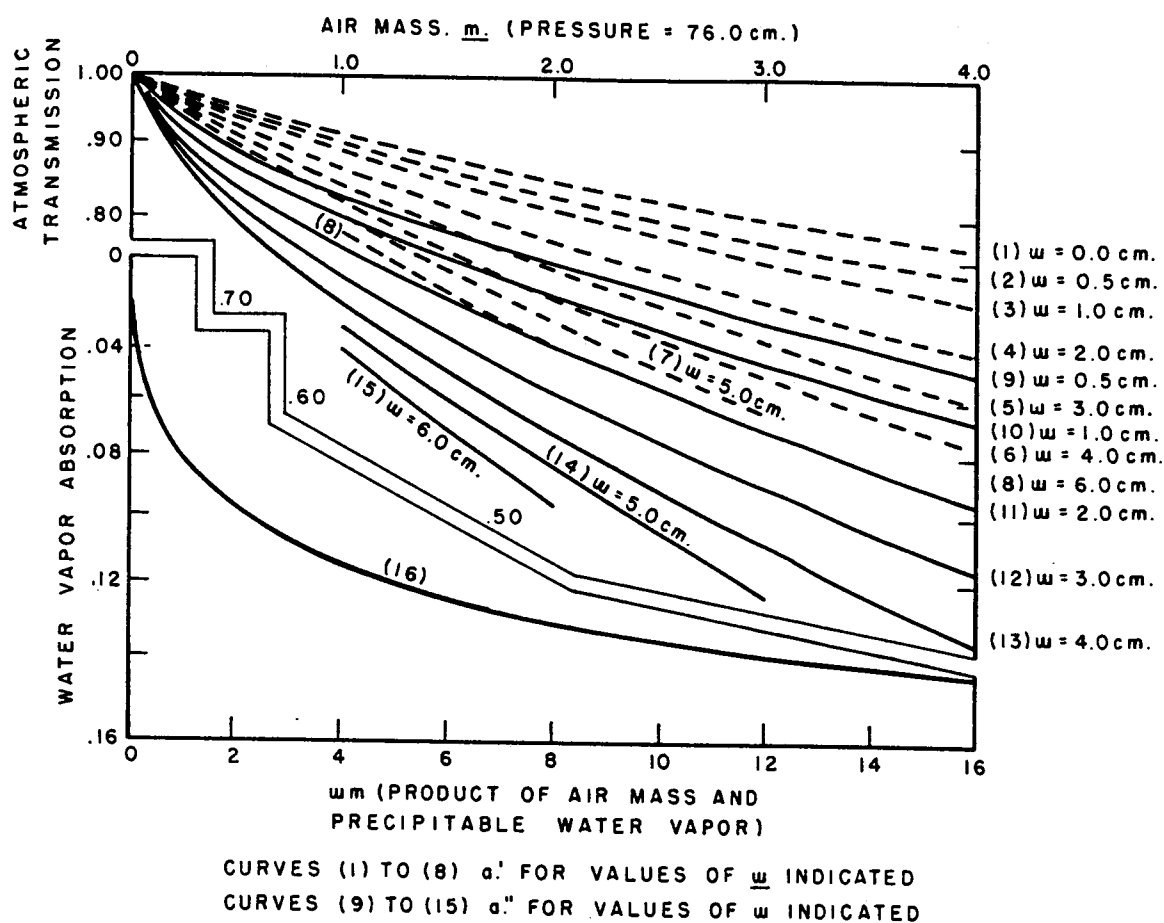


Fig. 4.2 Atmospheric Transmission Chart (After Kimball 1928)

A better procedure, also by Lui and Jordan (1960), is to use Figures 4.3 and 4.4 which relate the ratio

$$K_T = (Q_{DSH} + Q_{dSH})/Q_{DSHE} \quad \text{to} \quad Q_{dSH}/(Q_{DSH} + Q_{dSH}) \quad \text{where } Q$$

represents monthly average daily totals and the subscripts are as before. It is assumed that $(Q_{DSH} + Q_{dSH})$ is available from measurements. With this information the diffuse component can readily be estimated on an average monthly daily basis.

Partitioning of diffuse and direct radiation may also be accomplished by relating the ratio of direct beam to total radiation relative to the sun's zenith distance (List, 1968).

London (1957) also provides a chart relating the ratio of direct to diffuse radiation for various latitudes and months of the year (Figure 4-5). The advantage gained in using London's chart is that it considers the effect of latitude. It is, however, interesting to note that Figure 4.4 shows no significant difference in results from latitudes ranging from 42° to 60° N.

4.2.4 The Effect of Clouds

All discussion to this point has referred to clear sky radiation only, except for the treatment of diffuse radiation by Lui and Jordan (1960). By using the proper transmittance with adjustments made for dust particles reasonable values of clear sky direct beam radiation are readily obtainable from one or more of the previous references. However, by far the largest variation in the portion of solar radiation transmitted to the earth through the atmosphere is caused by cloud cover.

Different relationships involving estimated cloud cover have

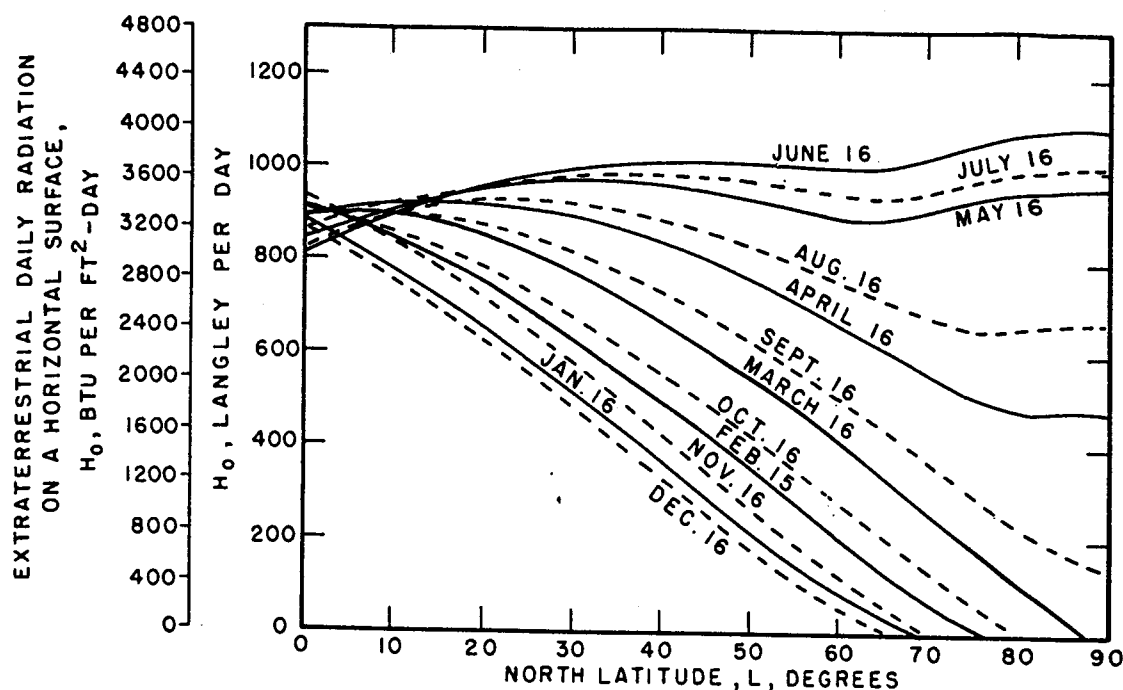


Fig. 4.3 Extraterrestrial Daily Radiation Received on a Horizontal Surface (After Lui and Jordan, 1960)

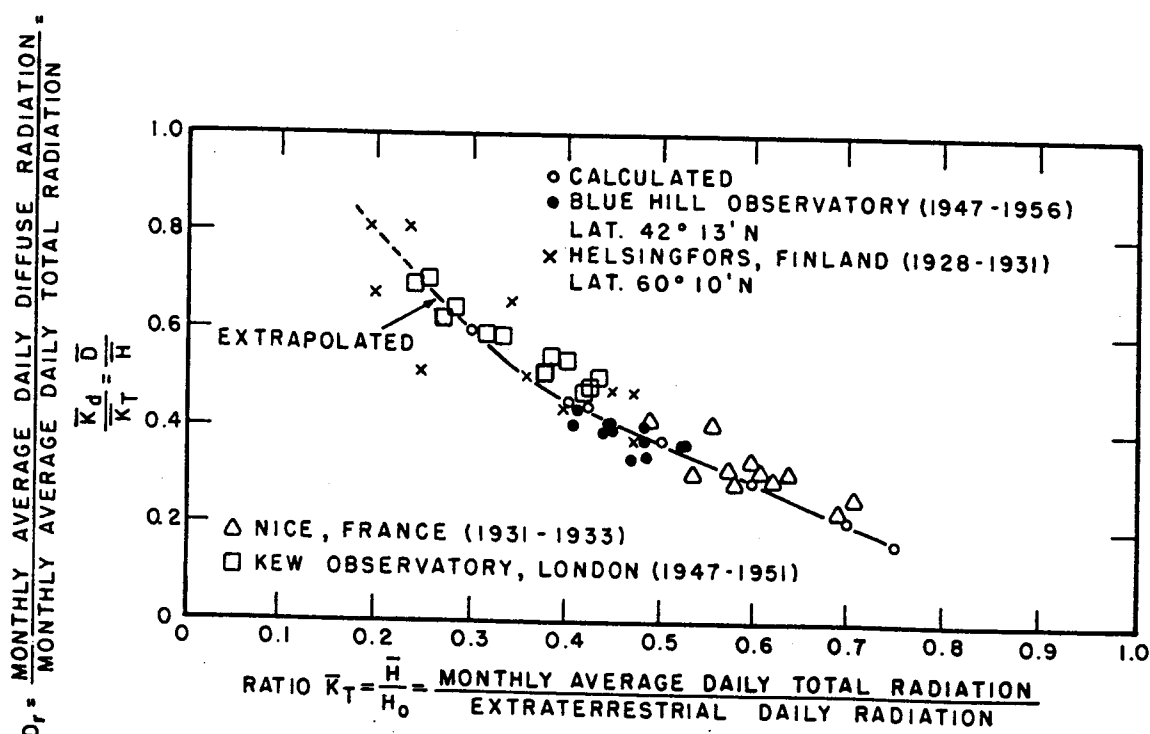


Fig. 4.4 The Ratio of the Monthly Ave. Daily Diffuse Radiation to the Monthly Ave. Daily Total Radiation as a Function of the Cloudiness Index K_T (After Lui & Jordan, 1960)

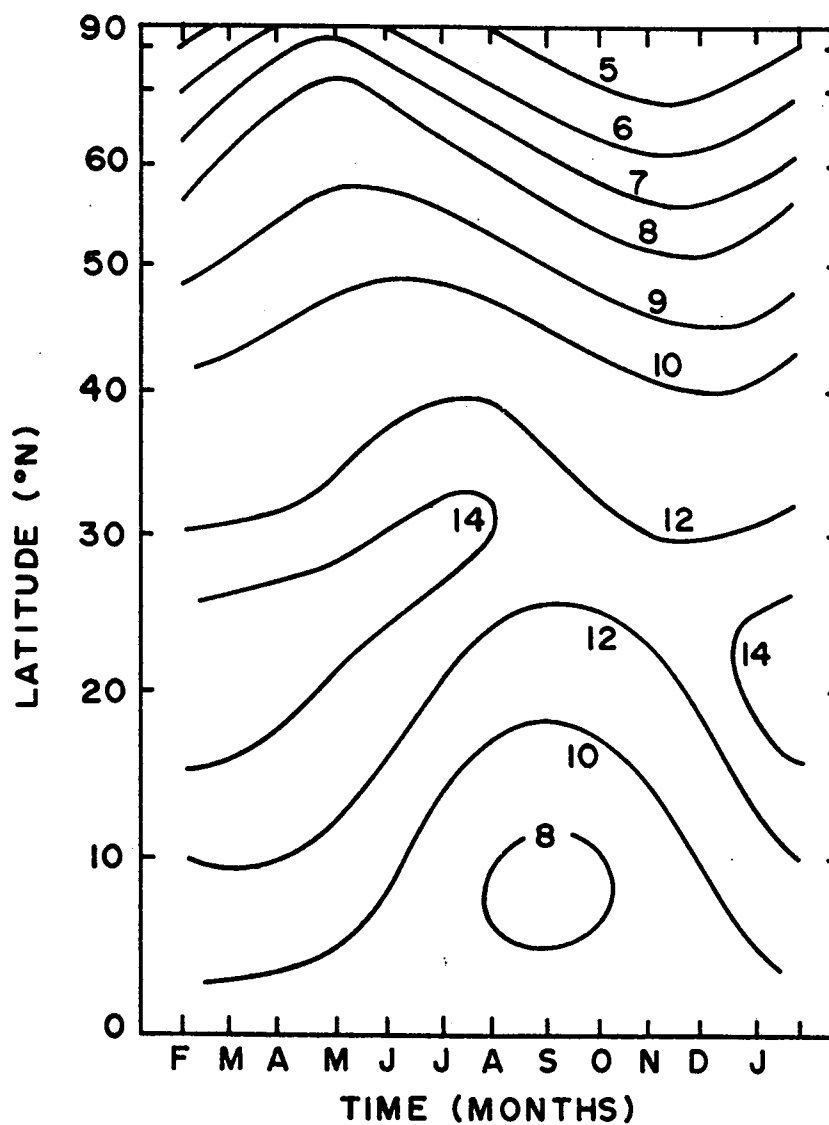


Fig. 4.5 Ratio of Direct to Diffuse Radiation Received at the Ground Surface (%) After London (1957)

been suggested by various authors. Difficulties arise with these methods because of variations in the height, type and distribution of the clouds. The subjective nature of such estimates tend to detract from this approach.

Kimball (1928) suggested:

$$q_{STHA}/q_{STHC} = a + b(1-n) \quad - - - [4.12]$$

where q_{STHA} = actual total short wave radiation.

q_{STHC} = clear sky short wave radiation.

a and b are constants and n is the cloud cover in tenths.

Quadratic functions of n have been suggested by Mateer (1955).

Budyko (1956) suggests:

$$q_{STHA}/q_{STHC} = 1 - (1-k)n \quad - - - [4.13]$$

where k depends on latitude, climatic region and season of the year.

The reader is referred to Sverdrup (1942), Newman (1954), and Haurwitz (1948) for more details on cloud cover in relation to total radiation.

The other approach commonly used is an equation expressing the actual radiation to total radiation as a function of sunshine.

The general form of these relationships are:

$$q_{STHA}/q_{STHC} = a + b.S \quad - - - [4.14]$$

(List, 1966).

where a and b are empirical constants

S = ratio of actual hours of sunshine to the total possible hours of sunshine.

Typical values of a and b are 0.35 and 0.61 respectively. Additional details regarding similar equations may be obtained from Fritz and

MacDonald (1949), Hamon et al (1954), Vowinckel and Orvig (1962) and others.

4.2.5 Summary of Short Wave Radiation

It is apparent that accurate calculations of solar radiation quantities other than clear sky values may be somewhat futile. However, weather bureaus throughout the world provide meteorological stations that record various and sometimes all of the components of short wave radiation. Summaries of radiation in Canada and the United States are contained in Monthly Radiation Summaries published by the Meteorological Service in Canada and National Summary of Climatological Data by the U.S. Weather Bureau.

However, many of the remote stations only record total short wave radiation on a horizontal surface (q_{STHA}) and it may be necessary to separate the two components when considering the amount of radiation incident upon a sloping surface.

The direction of the flow of energy associated with short wave radiation is always positive, i.e. the energy flows from the atmosphere to the ground. Typical clear sky intensities of solar radiation as the sun approaches the zenith at elevations of 2,000 ft. or less above sea level during the summer in the middle north to north latitudes are about 1.3 to 1.5 ly/min. Daily values in the same regions range from 400 to 600 ly/day in the summer months for average cloud conditions (Mateer, 1955).

4.2.6 Short Wave Radiation Reflected by The Surface of the Earth (q_{RS})

All the short wave radiation transmitted through the atmosphere is not absorbed by the surface of the earth. A significant portion may be reflected back to space, depending primarily on the

color and composition of the surface. Most of this radiation will be lost to space but part of the diffuse component may again be scattered with half of this amount again returning to the ground. Generally this portion is quite small and can usually be neglected. However, studies involving solar heat gain may include this factor (Klein, 1948).

The ratio of the amount of short wave radiation reflected by a surface to the amount incident upon it is defined as the albedo (α). Thus the albedo of a perfect reflector and a perfect absorber would be 1 and 0 respectively.

$$q_{RS}/q_{STHA} = \alpha \quad - - - [4.15]$$

Values of albedo for different surfaces are shown in Table 4-1.

Albedo is not necessarily a constant value for a given material. Changes in moisture content can change the albedo of a surface by as much as 30% (Table 4-1). Variations also occur with solar altitude and spectral changes in the radiation flux. Geiger (1961) indicates values may vary from 35 to 100% for dry sand and 7 to 100% for water, depending on the solar altitude of the sun. Spectral changes cause much less variation in albedo and are probably not significant in most instances.

4.2.7 Net Short Wave Radiation

The amount of short wave radiation absorbed by the ground or made available for heat gain of the soil is given by:

$$q_{STHA} - q_{RS} = q_{STHA} (1-\alpha) \quad - - - [4.16]$$

It is only this net amount of short wave radiation that can

TABLE 4-1
ALBEDO OF VARIOUS SURFACES

Surface	Albedo (%)	Source
Dry sand	35 - 45	Sellers (1965)
Wet sand	20 - 30	Sellers (1965)
Light sand	30 - 60	Geiger (1965)
Sandy soil	15 - 40	Geiger (1965)
Fields	12 - 30	Geiger (1965)
Woods	5 - 20	Geiger (1965)
Dark soil	7 - 10	Geiger (1965)
Water Surfaces	3 - 10	Geiger (1965)
Tundra Surfaces:		
1. Shrub	16 - 17	Haag and Bliss (1974)
2. Wet sedge	18 - 25	Haag and Bliss (1974)
3. Winter road	7 - 11	Haag and Bliss (1974)
4. Burn	10	Haag and Bliss (1974)
Boreal Forest:		
1. Forest	14	Haag and Bliss (1974)
2. Seismic line	13	Haag and Bliss (1974)
Seeding Experiment on Winter Road:		
Control	15	Haag and Bliss (1974)
Spring after use	8	Haag and Bliss (1974)
1st growing season	11.5	Haag and Bliss (1974)
2nd growing season	13.2	Haag and Bliss (1974)
3rd growing season	14.0	Haag and Bliss (1974)

be used to warm the surface, melt snow, evaporate water or be transferred as heat to the soil below.

The sign of this term is always positive as the albedo is always less than 1. The magnitude of this term varies from 20 to 85% of the incident radiation depending on the nature of the surface and the time of year.

4.2.8 Longwave Radiation Emitted by the Ground Surface

The earth is a source of terrestrial or longwave radiation. Since the temperature range is usually within 230 to 300⁰ K, the infrared spectral range is from 3 or 4 to 100 μ .

The earth's surface is assumed to be either a black body or a grey body within the spectral range quoted above. A grey body is one that emits a fixed proportion of the black body radiation in all wave lengths. Suggested values of infrared emissivity for naturally occurring materials on the earth range from 85 to 100%, with more commonly accepted values of 95 to 97% (Table 4-2).

The equation:

$$q_{LU} = \epsilon_s \sigma T_s^4 \quad - - - [4.17]$$

where ϵ_s = infrared emissivity,

T_s = surface temperature in ⁰K,

adequately describes the transfer of radiant energy from the earth to the atmosphere. The magnitude of this term ranges from 320 ly/day to 920 ly/day for temperatures of 230 and 300⁰K respectively. The sign of this component of the heat balance equation is always negative.

TABLE 4-2

INFRARED EMISSIVITIES

(Percent)

A. WATER AND SOIL SURFACES

Water -----	92-96
Snow, fresh fallen -----	82-99.5
Snow, ice granules -----	89
Ice -----	96
Soil, frozen -----	93-94
Sand, dry playa -----	84
Sand, dry light -----	89-90
Sand, wet -----	95
Gravel, coarse -----	91-92
Limestone, light gray -----	92-92
Concrete, dry -----	71-88
Ground, moist, bare -----	95-98
Ground, dry plowed -----	90

B. NATURAL SURFACES

Desert -----	90-91
Grass, high dry -----	90
Fields and shrubs -----	90
Oak woodland -----	90
Pine forest -----	90

C. VEGETATION

Alfalfa, dark green -----	95
Oak leaves -----	91-95
Leaves and plants -----	
0.8 μ -----	5-53
1.0 μ -----	5-60
2.4 μ -----	70-97
10.0 μ -----	97-98

D. MISCELLANEOUS

Paper, white -----	89-95
Glass pane -----	87-94
Bricks, red -----	92
Plaster, white -----	91
Wood, planed oak -----	90
Paint, white -----	91-95
Paint, black -----	88-95
Paint, aluminum -----	43-55
Aluminum foil -----	1-5
Iron, galvanized -----	13-28
Silver, highly polished -----	2
Skin, human -----	95

4.2.9 Longwave Radiation From the Atmosphere to the Ground

Longwave atmospheric radiation originates from gases in the air, some of which absorb and emit radiation in the far infrared range.

The amount of longwave radiation from the sky, as with short wave radiation is a function of cloud cover. Therefore, initial discussion will deal with clear sky conditions and the effect of cloud cover will be dealt with subsequently.

The temperature of the atmosphere varies within relatively narrow limits of 200 to 300⁰K and within this range the elementary gases of the atmosphere emit no radiation whatsoever. Therefore, atmospheric longwave radiation originates from water vapour, carbon dioxide and other asymmetrical molecules present in the air (Simpson, 1929).

Carbon dioxide is present in relatively large quantities throughout the atmosphere, but it absorbs only within a very narrow band of the longwave spectrum. Water vapour is therefore the most important radiating gas in the atmosphere.

Water vapour selectively absorbs energy as longwave radiation from the ground, energy from the transport of sensible heat from the ground and energy from the latent heat of condensation of water vapour. It then re-radiates this energy back to earth as longwave radiation. It, therefore, becomes important to understand the absorption characteristics of water vapour.

For certain wave lengths of the spectrum water vapour absorbs (and therefore emits) as a black body, while at other wave lengths it absorbs only a portion, and from 8.5 to 11 μ it is completely transparent (ibid). This range of the spectrum is referred to as the "atmospheric

window (Sellers, 1965). As soon as radiation within this latter band of wave lengths leaves the earth's surface, it is effectively lost as far as the atmosphere is concerned.

The problem has then resolved itself into one of estimating the amount of radiation emitted by a column of gas with varying composition, temperature and pressure. The appropriate equation would take the form of an integral summing the downward radiation from a level z_0 near the earth's surface to some level z a few thousand meters above the surface.

Elsasser (1942) has developed a method to determine the contribution of various levels of the atmosphere to the total long-wave radiation received at the earth's surface. This method is quite complex and requires upper air soundings to determine the relevant air parameters. Meyers (1966) has computerized Elsasser's technique which relieves a great deal of the tedium otherwise required in the use of the radiation charts.

The major problem associated with the computation of this term arises in the determination of the emissivity of the atmosphere at various levels. The emissivity of a column of air is a function of:

- i) the density-length product (m_v) of the water vapour.
- ii) the partial pressure of the water vapour (p_w).
- iii) the total pressure of the atmosphere (P).
- iv) the temperature of the mixture (T).

However, the emissivity varies only slightly for the range of p_w and T encountered in the atmosphere, and therefore, it may be considered to be essentially independent of these two variables. The effect of

change in total pressure is usually corrected for by increasing or decreasing m_v in the ratio of P/P_0 or $\sqrt{P/P_0}$ where P_0 is the reference pressure and P is the pressure at whatever level is being considered. The increase in emissivity due to the presence of carbon dioxide can also be considered (Elsasser, 1949, Kondratyev, 1956 and others).

Bliss (1961) has used these approaches and has reduced the required information to that of air temperature near the ground and dew point or relative humidity. The method requires the use of various charts and the reader is referred to the original publication for details.

Since the majority of atmospheric radiation originates within the first few hundred meters above the ground and since it is this region that shows the greatest variability of the factors controlling the amount of radiation, it is, therefore, reasonable to attempt to relate air temperature and vapour pressure near the surface to incoming longwave radiation.

Empirical equations relating longwave radiation from the sky to conditions prevailing near the surface are many and varied. However, for the most part, they take the form of:

$$q_{LD} = \sigma T_a^4 \{fn(\text{vapour pressure})\} \quad - - - [4.18]$$

where the term in brackets is equivalent to the average emissivity of the atmosphere.

Angstrom (1916) appears to be one of the first researchers to suggest an equation of this form. A reasonably complete listing of these equations is given by Sellers (1965). Brunt (1952) has suggested the ratio:

$$q_{LD}/\sigma T_a^4 = a + b \sqrt{e} \quad - - - [4.19]$$

where a and b are constants and e is the vapour pressure in mb at the corresponding screen air temperature (T_a).

A summary of the range of values of a and b found by various researchers is given by Goss and Brooks (1954). The value of the constant a ranges from 0.34 to 0.71 and the range of b is from 0.023 to 0.110 (Sellers, 1965). Median values are $a = 0.605$ and $b = 0.048$. Thus, the equation may be written as:

$$q_{LD} = \sigma T_a^4 (0.605 + 0.048 \sqrt{e}) \quad - - - [4.20]$$

and can be used to estimate the quantity of long wave radiation emitted by the atmosphere on a synoptic basis.

Typical values of atmospheric radiation from cloudless skies range from 400 to 600 ly/day (Dines and Dines, 1927) to as little as 320 ly/day in mid-winter in the arctic regions (Vowinckel and Orvig, 1964). The sign of this component of radiation in the heat balance equation is always positive.

The effect of clouds is always to increase long wave atmospheric radiation relative to clear sky conditions. Any cloud which is visually opaque is assumed to radiate as a black body at the temperature of the cloud base. The effect of clouds is to close "the atmospheric window". The absorption spectrum of liquid water is similar to that for water vapour, however, the magnitude of the absorption is much greater. Even relatively thin clouds contain more precipitable water than is required to allow them to radiate as black bodies.

Various equations are put forth to adjust the clear sky values to account for cloud effects (Sellers, 1965). Since the cloud

base is usually at a temperature less than the temperature of the air mass near the ground, the overall effect is to increase the downward radiation by only 15 to 25 per cent (ibid). Dines and Dines (1927) present results to indicate increases of from 20 to 40 per cent of clear sky values due to cloud cover.

Anderson and Baker (1967) provide a convenient and apparently accurate equation for estimating long wave radiation from the sky. It is presented here to illustrate an alternative method of allowing for cloud effect:

$$q_{LD} = \sigma T_a^4 - \{228.0 + 11.16 (\sqrt{e_s} - \sqrt{e_a})\} q_{STHA}/q_{STHC} \quad - - - [4.21]$$

where e_s = saturated vapour pressure at the surface air temperature;
 e_a = actual vapour pressure at the surface air temperature;
 q_{STHA} = total short wave radiation on a horizontal surface measured at the site;
 q_{STHC} = calculated or measured clear sky radiation on a horizontal surface at the site.

Thus q_{STHA}/q_{STHC} is a measure of cloud cover, haze or other impurities in the air.

It would appear that a relationship involving the short wave radiation ratio is a better and much less subjective method of accounting for the effect of clouds on downward long wave radiation.

Long wave radiation from the sky is not entirely isotropic. This is due primarily to the decrease in effective radiating atmospheric temperatures from the horizon to the zenith. It is, therefore, apparent that slopes or areas sheltered by a canopy of trees or similar obstruction will record larger fluxes of downward atmospheric radiation than will areas exposed directly to the zenith.

4.2.10 Net Long Wave Radiation

It has been established that the earth radiates as a grey body with an emissivity (ϵ_s) of less than one. Since the temperature of the lower atmosphere and earth are not remarkably different, it is valid to assume that the emittance and absorptance of the earth are equal (Kirchhoff's 3rd Law, Wiebelt, 1966). Thus

$$\epsilon_s = 1 - \alpha_L \quad - - - [4.22]$$

where $(1 - \alpha_L)$ = absorptance and

α_L = infrared reflectivity or albedo.

The net long wave is, therefore, the difference between that absorbed and that which is emitted. It may be expressed as:

$$q_{LN} = \epsilon_s q_{LD} - q_{LU} \quad - - - [4.23]$$

Brunt's (1952) empirical equation for q_{LN} is useful in illustrating the sign and magnitude of this component of the heat balance.

$$q_{LN} = \epsilon_s \sigma \{ T_a^4 (a + b\sqrt{e}) - T_s^4 \} \quad - - - [4.24]$$

where ϵ_s = emissivity of the surface,

T_a = air temperature of the surface $^{\circ}\text{K}$
(usually measured at screen height),

T_s = surface temperature $^{\circ}\text{K}$,

e = vapour pressure of the air at screen height
in mb.

If the air temperature is considered to be approximately equal to the surface temperature, then the equation may be written as:

$$q_{LN} = \epsilon_s \sigma T_a^4 (a + b\sqrt{e} - 1) \quad - - - [4.25]$$

For average summer conditions in the middle north latitudes, the following conditions are applicable:

$$\epsilon_s = 0.95$$

$$a = 0.605$$

$$b = 0.048$$

$$\sigma = 0.826 \times 10^{-10} \text{ ly/min } ^\circ K^4$$

$$(11.9 \times 10^{-8} \text{ ly/day } ^\circ K^4)$$

$$T_a \approx T_s = 20^\circ C = 293^\circ K$$

For this air temperature and a $5^\circ C$ wet bulb depression the vapour pressure (e) = 20 mb. The term $a+b\sqrt{e}$ may be considered to be the average emissivity of the atmosphere (ϵ_a). Thus

$$\epsilon_a = a+b\sqrt{e}$$

$$= 0.82$$

Hence, for average conditions

$$q_{LN} = -0.104 \text{ ly/min}$$

$$= -150 \text{ ly/day}$$

Therefore, under these average conditions there is a net loss of approximately 6 ly/hr from the earth to the atmosphere.

Although there is some diurnal and seasonal variation in net long wave radiation losses from clear skies with peaks occurring in the summer months, the average losses are usually tempered to some extent by increased vapour pressure and cloudiness.

A somewhat similar approach (but less fundamental) may be taken for evaluating the net long wave radiation balance using concepts and data provided by London (1957) and Vowinkel and Orvig (1964).

The latter authors suggest that the ratio

$q_{LDa}/q_{LU} = G_s$, where q_{LDa} = the component of atmospheric downward long wave radiation caused by absorption in the atmosphere of radiation from the ground (i.e. "the green house effect").

q_{LU} = long wave radiation from the earth's surface.

$G_a = q_{LDa}/q_{LD}$, where G_a represents the ratio of the component of atmospheric downward long wave radiation caused by absorption in the atmosphere of radiation from the ground to the total downward long wave atmospheric radiation. Combining the two equations produces:

$$G_s/G_a = q_{LD}/q_{LU} \quad - - - [4.26]$$

Substituting in equation [4.23] gives:

$$q_{LN} = -q_{LU} + \epsilon_s \frac{G_s}{G_a} q_{LU} \quad - - - [4.27]$$

and substituting equation [4.17] results in:

$$q_{LN} = \epsilon_s \sigma T_s^4 \left(\frac{G_s}{G_a} \epsilon_s - 1 \right) \quad - - - [4.28]$$

If $T_s = T_a$ the equation reverts to [4.25]

and $\frac{G_s}{G_a} \epsilon_s$ is equivalent to the average emissivity of the atmosphere.

Average summer and winter values of $\frac{G_s}{G_a} \epsilon_s$ (for $\epsilon_s = 0.95$) using London's data are 0.86 and 0.83 respectively.

If $T_s = T_a = 20^\circ\text{C}$ as in the previous example, then,

$$q_{LN} = -117 \text{ ly/day.}$$

This value is significantly greater than that computed from equation [4.25]. An appropriate synoptic estimate of q_{LN} probably lies somewhere between these two estimates.

Although this latter method appears suitable to evaluate net long wave radiation on a long term or general basis, it gives the inexperienced researcher in radiative heat transfer very little feeling for the fundamentals of the problem. It is for this reason that the author prefers the more basic concepts of emissivity and its variation with changes in atmospheric pressure and water vapour concentration. It is important to review the nature of the above argument. It is the concept rather than actual values of net long wave radiation that are in question. There may be cases when the latter equation provides, what appear to be, better estimates of the magnitude of this component in the heat balance equation.

The so called "green house effect" is a term used by many researchers to describe the phenomenon of water vapour and carbon dioxide absorption and emission characteristics. There is no doubt that a real greenhouse substantially modifies the heat balance in comparison to the natural surroundings. However, the reasons for this serendipitous discovery are only weakly related to long wave radiation. Kondratyev (1965) provides a detailed description and presents field data to show that the glass covering in an average greenhouse has a detrimental or negative effect on the radiation balance during the day and only a slight beneficial effect at night. The real benefit of the covering is that it effectively prevents heat loss by turbulent or convective transfer processes and also heat losses by evaporation are substantially reduced. Obviously the former process is not modified in any way by water vapour, carbon dioxide or cloud cover and

the latter process (evaporation) varies somewhat with changes in relative humidity.

It is for these reasons that the author is opposed to using misleading if not incorrect terminology to describe the fundamental physics of long wave radiation exchange between the earth and the atmosphere.

The foregoing treatment of net long wave radiation is adequate for an assessment of this component of the heat budget on a general basis. However, it is of interest to review the equations with regard to specific situations.

An interesting condition often develops over cold surfaces such as snow packs, glaciers and probably ablating head scarps of bimodal flows in permafrost during the spring and summer months, especially under cloudy conditions.

It has been shown that ϵ_s of such a surface is essentially equal to unity (O'Neill, 1973). It was previously stated that a cloud mass is assumed to emit black body radiation at the temperature of the cloud base. The net long wave radiation exchange for such a condition is:

$$q_{LN} = \sigma(T_c^4 - T_s^4) \quad - - - [4.29]$$

where T_c = temperature of the cloud base in $^{\circ}\text{K}$. It, therefore, becomes apparent that the net long wave radiation becomes zero or positive for cloud temperature of 0°C or greater. This reversal in sign of heat flux has even been noted when ground temperatures are substantially above zero (Muller, 1967). These occurrences would be much more frequent when colder surface temperatures prevail (Streten and Wendler, 1968). Partial cloud cover will obviously contribute

to decreasing the loss of long wave radiation to the sky and various equations have been cited in an attempt to evaluate this effect (Sellers, 1965).

The foregoing treatment illustrates that applying synoptic estimates of net long wave fluxes to specific situations may often cause substantial errors in the estimation of these values. Net long wave radiation fluxes for conditions previously described are likely to be in the order of minus 40 ly/day to plus 6 ly/day (Streten and Wendler, 1968) rather than minus 100 to 150 ly/day as computed from synoptic data.

4.3 Radiative Components on a Sloping Surface

4.3.1 General

Topographic influences on both short and long wave radiation should be considered in evaluating the microclimate of a specific site. These influences are the most significant for the direct beam short wave component.

The equation used to describe the radiation balance on sloping surfaces may be written as follows:

$$q_{NS} = q_{DSS} + q_{dSS} + q_{RSS} + q_{RS} + q_{LDS} + q_{LDR} \\ + q_{LUR} + q_{LUS} \quad - - - [4.30]$$

where q_{NS} = net radiation balance on a sloping surface.

q_{DSS} = short wave direct beam component (+).

q_{dSS} = short wave diffuse component (+).

q_{RSS} = short wave component of radiation reflected to the surface by surrounding surfaces (+).

q_{RS} = short wave component of radiation reflected by

the slope (-).

q_{LDS} = downward long wave component of radiation falling on the slope (+).

q_{LDR} = downward long wave component reflected to the surface by surrounding surfaces (+).

q_{LUR} = upward component of long wave radiation reflected onto the slope by surrounding surfaces (+).

q_{LUS} = upward component of long wave radiation emitted by the surface (-).

4.3.2 Direct Beam Radiation (q_{DSS})

The ideal method for evaluating the direct beam component of short wave radiation from clear skies on to a sloping surface oriented in any direction appears to have been first formulated by Ohmura (1968) and Garnier and Ohmura (1968). It consists of taking the dot or scalar product of two unit vectors, one parallel to the sun's rays and the other normal to the slope. The result is then combined with the flux density of radiation normal to the sun's ray.

The foregoing may be summarized as follows:

$$q_{DSS} = J_0 a^m (\overline{S}u' \cdot \overline{S}L \cos \Lambda) \quad - - - [4.31]$$

where q_{DSS} = flux density of direct beam radiation on the slope.

$\overline{S}L$ = unit vector normal to the slope.

$\overline{S}u'$ = unit vector parallel to the sun's rays.

Λ = angle formed between the two vectors.

The remaining terms have been previously defined.

The amount of direct beam radiation upon a slope over a finite period of time equals:

$$Q_{DSS} = J_0 \int_{H_1}^{H_2} a^m (|\bar{S}u'| \quad | \quad |\bar{S}L| \cos \Lambda) dH \quad - - - [4.32]$$

where H = hour angle measured from solar noon.

The equation is evaluated by expressing the unit vectors in terms of their direction cosines. The equation is then evaluated and summed over twenty minute time intervals. The details of this procedure are provided by Ohmura (1968) and Garnier and Ohmura (1968).

The treatment, thus far, has considered conditions involving an unobstructed sky line. In many cases topographic obstructions prevent the sun's rays from falling directly upon the ground and the site remains in shadow for a major part of the day especially during period of time of low sun angles. This aspect of the problem is readily handled by comparing the altitude of the obstruction with the altitude of the sun at the appropriate azimuth during the twenty minute time interval of computation. A variety of equations will determine the azimuth of the sun in terms of the local co-ordinates, the simplest of which is:

$$\sin a = \sin H \cos \delta \csc z \quad (\text{Hosmer \& Robbins, 1958})$$

- - - [4.33]

where a = azimuth of the sun (measured positively through east).

H = hour angle of the sun.

δ = angle of declination of the sun.

z = zenith angle of the sun.

The altitude and azimuth of the obstruction must be determined by physical measurements or estimates at each particular site.

Another and possibly superior alternative is to calculate

the length of the shadow cast by the obstructing object and then to check whether the site lies within that shadow.

The length of shadow cast by an object on a horizontal surface may be easily calculated from the equation:

$$L = H \tan z \sin (A-B) \quad - - - [4.34]$$

where L = length of shadow.

H = height of the obstruction.

z = zenith angle of the sun.

A and B are the azimuths of the sun and obstruction respectively.

No similar simple expression exists for the calculation of shadow length on sloping ground. An equation has been developed to compute this variable. It is contained in Appendix C.

In summary, the amount of direct beam radiation incident upon a sloping surface is a function of:

- i) latitude of the site
- ii) declination of the sun
- iii) strike and dip of the slope
- iv) orientation and height of obstruction
- v) transmittance of the air

The exact declination of the sun at different times of the year may be determined from one of the common ephemerides used for celestial observations. However, for most meteorological computations it is adequate to calculate the declination of the sun by describing its variation as a function of a sine curve.

$$\delta = A_0 \sin \frac{2\pi}{365} t \quad - - - [4.35]$$

where δ = declination of the sun

A_0 = amplitude of the sine curve (23.5°)

$\frac{2\pi}{365}$ = period of the function

t = time in days starting from March 21 (vernal equinox)

The orientation of the slope is given by the azimuth and zenith angle of the normal to the slope. The azimuth is measured positively from the north through east.

The obstruction is described by the height, the azimuth of the beginning and the termination, and the azimuth of a projection along the base.

The transmissivity of the atmosphere may be estimated by vapour pressure data and the direct beam radiation may be corrected for cloud cover as previously outlined. The optical air mass m is adequately described as $1/\cos z$ for zenith angles of 80° or less. Published values (List, 1968) must be used for zenith angles greater than 80° .

A simple and acceptable alternative to the procedure outlined above is to relate the actual normal direct short wave radiation on the slope to the actual direct short wave radiation on a horizontal surface.

$$q_{\text{DSHA}} = q_{\text{DSNA}} \cos z$$

$$q_{\text{DSS}} = q_{\text{DSNA}} \cos \Lambda$$

$$q_{\text{DSS}} = q_{\text{DSHA}} \cos \Lambda / \cos z \quad - - - [4.36]$$

where q_{DSS} is the direct short wave radiation on the sloping surface

q_{DSHA} = actual direct beam short wave radiation on a horizontal surface

z = zenith angle of the sun

$\cos \Lambda$ = cos of the angle between the sun's rays and the unit normal to the slope.

This is a complex function of latitude, declination, slope orientation and hour angle. The equation for Λ is listed in Appendix C.

Since the value $\cos \Lambda / \cos z$ is a function of time, it becomes a matter of judgement for each problem as to what time increment is to be used to obtain an average value for this ratio. The problem was handled by evaluating $\cos \Lambda$ and $\cos z$ over 20 min. time periods and plotting these values as ordinates versus time on a daily basis. The ratio of the areas under the curves represents the average daily ratio of $\cos \Lambda / \cos z$. Sky line obstructions and shadows can be handled in the same manner.

4.3.3 Diffuse Radiation (q_{dSS})

The amount of diffuse or scattered short wave radiation from the sky incident upon a sloping surface may be estimated by relating it to the amount falling on a horizontal surface. Kondratyev (1965) has suggested that:

$$q_{\text{dSS}} = q_{\text{dSH}} \cos^2 a/2 \quad - - - [4.37]$$

where q_{dSS} = diffuse short wave radiation on the sloping surface

q_{dSH} = diffuse short wave radiation on a horizontal surface

a = inclination of slope from the horizontal

This simple equation assumes that the diffuse component of short

wave radiation is isotropic. Such an assumption is not rigorously correct. The intensity increases with zenith distance for clear sky conditions and decreases with zenith distance for cloudy conditions (Dines and Dines, 1927). The intensity of diffuse radiation is also related to the position of the sun. It increases toward the sun and decreases away from the sun. Thus, the correct equation to describe the flux density of diffuse radiation on a sloping surface would be a function of the direction of the unit normal of the slope relative to the zenith and to the sun.

Stephenson (1965), using data from Threlkeld (1962) formulated an equation to account for the anisotropy of diffuse radiation on vertical surfaces. The empirical relationship is:

$$q_{dSV} = q_{dSH} V_f \quad - - - [4.38]$$

where $V_f = (0.55 \text{ to } 0.437 \cos \theta + 0.313 \cos^2 \theta)$ and

θ = angle formed between the rays of the sun and the unit normal to the wall.

If $102^\circ < \theta < 259^\circ$, $V_f = 0.45$; otherwise $V_f = 0.55 + 0.437 \cos \theta + 0.313 \cos^2 \theta$. For the condition of $\theta = 0$, $V_f = 1.3$ and

$$q_{dSV} = q_{dSH} (1.3) \quad - - - [4.39]$$

This expression indicates that at certain periods during the day a vertical surface whose unit normal coincides with the rays of the sun will receive a maximum of 30% more diffuse radiation than a horizontal surface. This observation may be applied to all sloping surfaces at least in a general way. Unfortunately, the equation is derived exclusively on an empirical basis and cannot be utilized

without reservation for any sloping surface.

If the geometrical considerations of short wave diffuse radiation on slopes are compared to those of long wave radiation from the sky incident upon the same slope, without concern for anisotropy, then the similarities should be evident. Kondratyev (1965) presents an equation for net long wave radiation on a sloping surface and then provides measured values in support of the equation. The data can be reasonably well described by:

$$q_{LNS} = q_{LNH} \cos^2 a/2 \quad - - - [4.40]$$

where q_{LNS} and q_{LNH} are the net long wave radiative fluxes on sloping and horizontal surfaces respectively. It follows that the short wave diffuse component may be expressed as:

$$q_{dSS} = q_{dSH} \cos^2 a/2 \quad - - - [4.41]$$

This equation indicates that a vertical face will receive one-half the diffuse radiation of a horizontal surface.

Although this equation is not rigorously correct, its simplicity makes it attractive for use in the solution of field problems. However, care should be exercised in its use, for it unequivocally indicates that the diffuse radiation falling on a sloping surface is always less than that of a horizontal surface. Garnier and Ohmura (1969) compare values computed from equation [4.41] with those measured on north, east and south facing slopes with a shielded Eppley pyranometer. They indicate that this equation produces overestimates of 56% to underestimates of 26%. Overestimates are more frequent on north facing than on east or south facing slopes. Data for the east facing slope appears to be scattered

equally between over and under estimates, while the data computed for the south facing slope appears to predominantly underestimate the measured values. However, their measurements were restricted to a slope angle of 20° and the correlation between computed and measured values were evaluated solely on that basis. In view of these results, it appears that equation [4.41] may be used to give reasonable estimates of diffuse radiation on sloping surfaces.

4.3.4 Short Wave Component Reflected to the Surface by Surrounding Surfaces (q_{RSS})

Objects or surfaces may reflect diffusely or specularly to the surface of interest. Diffuse reflection occurs from irregular or roughened surfaces and the reflected radiation will be distributed in all directions. On the other hand, specular reflection (from the direct beam) will occur from surfaces such as glass, polished metals or very still water. Real surfaces will exhibit neither purely diffuse nor purely specular reflection and most natural surfaces may be treated as diffuse reflectors (Threlkeld, 1962). Therefore, both direct beam and diffuse radiation will be reflected diffusely by these natural surfaces.

The amount of radiation reflected to a surface by another is a function of the amount of radiation incident upon the first surface and a geometric view factor which relates the size and orientation of the two surfaces. If the adjacent or reflecting surface is designated (1) and the surface receiving the reflected radiation is (2), then the amount of reflected radiation which is incident upon unit surface dA_2 is:

$$q_{RSS}(2) = \alpha_1 (q_{DS} + q_{dS}) (1) V_f / \pi \quad - - - [4.42]$$

where α_1 = albedo of surface (1)
 $(q_{DS} + q_{dS}) (1)$ = total short wave radiation incident upon surface (1).

V_f = dimension less geometric view or configuration factor which describes the fraction of energy directly incident on one surface from another surface assumed to be reflecting or emitting energy diffusely (Wiebelt, 1966).

A completely general evaluation for V_f must involve a relationship combining the geometry of the areas and the orientation of the unit normals of the areas in one co-ordinate system. Preliminary investigations suggest that this solution is too complex to be of practical value for most engineering applications. However, useable, but restrictive solutions are available for some problems associated with heating and ventilation system design. Threlkeld (1970) provides an acceptable approach to a number of specific problems. However, care must be exercised regarding the geometry of one surface relative to the other. The choice of the co-ordinate system is dependent upon the orientation of the areas. This aspect does not create problems for situations of windows or walls facing parking lots or large court yards and where hand calculations are used for each problem. In cases of complex geometry, it appears unlikely that the form of this solution is amenable for use with computerized techniques in evaluating radiation on sloping surfaces.

Nonetheless, the procedure taken from Threlkeld (1970) is developed and included in Appendix C. It is left for the reader to decide if his particular problem can be modelled to meet the conditions imposed by this solution.

The solution may be categorized into three general cases (A, B and C) with specific situations arising in each case. For conditions described in Case A, surface dA_2 cannot "see" surface A_1 and thus no radiation is reflected from A_1 to dA_2 . In Case C, the surface dA_2 is "facing" A_1 . Surface dA_2 is either parallel to or forms an acute angle with surface A_1 . This condition would rarely be of significance in nature and would occur only when there was an overhanging bank or canopy of trees.

Case B is the most important and probably the only significant one of the three conditions described in the general solution. If Case B₍₂₎ is considered for the condition of a horizontal surface in front of sloping ground, the view factor may be expressed as:

$$V_f = \pi/2 (1 - \cos a) = \pi/2 \sin^2 a/2 \quad - - - [4.43]$$

where a = inclination of the slope.

$$\text{Then } q_{RSS} = \alpha_1 (q_{DSH} + q_{dSH})_1 \sin^2 a/2 \quad - - - [4.44]$$

This equation is also in agreement with Kondratyev (1965).

Threlkeld (1970) performs a sample calculation to show that the reflected radiation intercepted by a vertical south facing window on June 1 at noon, positioned 6 ft. above a 50 x 100 ft. concrete parking lot, represents 26% of the total radiation incident upon the window. This is obviously of significant magnitude and the designer must therefore consider each situation on its own merit and perform at least perfunctory calculations before dismissing this component of radiation as being unimportant.

4.3.5 Short wave Component of Radiation Reflected by the Surface (q_{RS})

The short wave radiation reflected from a sloping surface will be equal to the product of the albedo of the surface and the sum of all short wave radiation incident upon it. The equation to express this value may be written as:

$$q_{RS} = \alpha(q_{DSS} + q_{dSS} + q_{RSS}) \quad - - - [4.45]$$

This equation differs from that of a horizontal surface only in the addition of the last term which represents the short wave radiation that is reflected to the slope by other surfaces.

4.3.6 Downward Longwave Component of Radiation Falling on the Slope (q_{LDS})

Long wave radiative flux from the sky is not isotropic, increasing from the zenith to the horizon. Gardeners and agriculturalists observe this phenomenon in the late stages of the growing season when early morning air temperatures hover near the freezing point. Vegetation on sloping surfaces and regions partially sheltered from the zenith by buildings, trees or canopies will often remain unharmed by otherwise killing frosts. Kondratyev (1965) proposes that the equation to describe the amount of long-wave radiation falling on the slope take the form:

$$q_{LDS} = q_{LDH} \cos^2 a/2 \quad - - - [4.46]$$

The equation suggests that the downward longwave component decreases as the slope angle increases. This is not strictly correct because anisotropy effects will modify this relationship.

Additional equations and further details concerning anisotropy may be found in Sellers (1965). This author suggests that little error will result if equation [4.46] is adopted for use in general

field conditions if it becomes necessary to independently estimate this component of radiation.

4.3.7 Downward Long Wave Component Reflected to the Surface by Surrounding Surfaces (q_{LDR})

This component of radiation will be reflected diffusely to the sloping surface from adjacent surfaces in the same manner that short wave radiation is scattered and reflected. The treatment will, therefore, be identical to that described in section 4.3.4. Equation [4.42] must be rewritten as:

$$q_{LDR(2)} = \alpha_1 (q_{LD})_1 \frac{V_f}{\pi} \quad - - - [4.46]$$

where α_1 = infrared albedo of surface 1.

$(q_{LD})_1$ = long wave radiation falling on surface 1.

The writer suggests that a rigorous treatment of view factors is unwarranted for this relatively small component of radiation. It is, therefore, suggested that equation [4.46] be modified for general use as:

$$q_{LDR} = \alpha_1 (q_{LDH}) \sin^2 a/2 \quad - - - [4.47]$$

where q_{LDH} = long wave radiation falling on a horizontal surface in front of the slope

α_1 = infrared albedo

a = angle of slope with the horizontal

4.3.8 Upward Component of Long wave Radiation Reflected onto the Slope by Surrounding Surfaces (q_{LUR})

Strictly speaking, this radiative component should also be dealt with in the same manner as reflected short wave radiation on

a slope. Again it is the author's opinion that such a rigorous treatment of this radiative component is unjustified in view of its small contribution to the radiation balance at the surface.

Kondratyev (1965) suggests:

$$q_{LUR} = q_{LUH} \sin^2 a/2 \quad - - - [4.47]$$

where q_{LUH} = long wave radiation emitted by the surface
in front of the slope.

a = angle of slope with horizontal.

4.3.9 Long wave Radiation Emitted by the Surface (q_{LUS})

The theory involved in the computation of this portion of radiation falling on the slope is identical to that outlined in section 4.2.8 dealing with horizontal surfaces. Equation [4.17] may be used to describe this component with slight modifications to the nomenclature.

$$q_{LUS} = \epsilon_s \sigma T_{ss}^4 \quad - - - [4.48]$$

where T_{ss} = temperature of the sloping surface rather than
that of the horizontal adjacent surfaces. The magnitude of this term may experience a substantial diurnal variation as the slope comes into direct contact with the sun during certain periods of the day.

4.3.10 Summary of Components

The following treatment will attempt to briefly summarize the radiation balance on slopes and group the terms into net short wave and net long wave categories.

i) q_{DSS} = complex expression relating the unit normal of the slope to the rays of the sun.

$$ii) q_{dSS} = q_{dSH} \cos^2 a/2$$

$$iii) q_{RSS} = \alpha (q_{DSH} + q_{dSH}) \sin^2 a/2$$

$$iv) q_{RS} = -\alpha (q_{DSS} + q_{dSH} + q_{RSS})$$

$$v) q_{LDS} = q_{LDH} \cos^2 a/2$$

$$vi) q_{LDR} = \alpha_1 (q_{LDH}) \sin^2 a/2$$

$$vii) q_{LUR} = q_{LUH} \sin^2 a/2$$

$$viii) q_{LUS} = -\epsilon_s \sigma T_{ss}^4 \approx q_{LUH}$$

Grouping expression i), ii), iii) and iv)

$$q_{NSS} = \{q_{DSS} + q_{dSH} + \alpha \sin^2 a/2 (q_{DSH} + q_{dSH})\}(1-\alpha) - q_{dSH} \sin^2 a/2 \quad - - - [4.49]$$

where q_{NSS} = net short wave radiation on the sloping surface.

This is a suitable form of the equation if all components are to be calculated separately. However, if calculations are based on measured total values then the equation should be recast into the following form:

$$q_{NSS} = \{q_{DSHA} \frac{\cos \lambda}{\cos z} + q_{dSH} + \alpha \sin^2 a/2 (q_{STHA})\} (1-\alpha) - q_{dSH} \sin^2 a/2 \quad - - - [4.50]$$

where q_{DSHA} = actual direct beam short wave radiation on a horizontal surface.

q_{dSH} = diffuse radiation on a horizontal surface.

q_{STHA} = total short wave radiation recorded on a horizontal surface.

α , $\cos \Lambda$ and $\cos z$ are as previously defined.

Components v), vi), vii), and viii) may be grouped as follows:

$$q_{LNS} = q_{LDH} (\cos^2 a/2 + \alpha_1 \sin^2 a/2) + q_{LUH} \sin^2 a/2 - q_{LUH}$$

If $\alpha_1 = 1.0$,

$$\begin{aligned} q_{LNS} &= (\epsilon_s q_{LDH} - q_{LUH}) + \epsilon_s q_{LUH} \sin^2 a/2 \\ &= q_{LNH} + \epsilon_s q_{LUH} \sin^2 a/2 \quad - - - \quad 4.51 \end{aligned}$$

If the value of q_{LN} from equation 4.24 is substituted into equation 4.51, then

$$q_{LNS} = \epsilon_s \sigma \{T_a^4 (a+b\sqrt{e}) - T_s^4 (1-\epsilon_s \sin^2 a/2)\} \quad - - - \quad 4.52$$

If the value of q_{LN} from equation 4.28 is substituted into equation 4.51, then

$$q_{LNS} = \epsilon_s \sigma \left\{ T_s^4 \frac{G_s}{G_a} \epsilon_s - T_s^4 (1-\epsilon_s \sin^2 a/2) \right\} \quad - - - \quad 4.53$$

Equations 4.52 and 4.53 indicate that in general the net long wave radiation on short slopes facing a horizontal surface will change from negative to positive values at slope angles of 60 degrees or greater. This observation may not be true where slopes are warmed well above the prevailing air temperatures. Under these conditions a very strong negative component may be emitted from the surface of the soil. However, data collected at Fort Simpson, N.W.T. indicate that the net radiometers installed on sloping surfaces rarely recorded negative values of net radiation while those placed over horizontal terrain consistently monitored negative values in the early morning hours of clear days. An example of this data is included in Appen-

dix D.

4.4 Turbulent Transfer Processes

Transfer of water vapour, heat, and momentum within the atmosphere plays a significant role in maintaining the heat balance at the surface of the earth. This transfer process is generally accomplished by turbulent mixing in the atmosphere even when the air mass is very stable. However, this activity cannot extend to the ground surface and a laminar boundary layer of a few millimeters in thickness is present between the surface of the earth and the turbulent activity in the atmosphere above. If the temperature and vapour pressure gradients within this thin layer can be accurately established, then the amount of heat, vapour and momentum in motion could be computed by boundary layer theory (Sellers, 1965). Such measurements are, at worst unobtainable, and at best impractical. The alternative has, therefore, been to measure temperature and vapour pressure gradients at higher levels and to use turbulent transfer theories to estimate the flux of heat or vapour at the surface.

4.5 Evaporation and Condensation

Evaporation occurs when vapour moves from the surface to the atmosphere in response to a gradient, while condensation is simply the reverse of this process. It is, therefore, more reasonable to consider nomenclature that describes heat transfer only, in terms of the latent heat of vaporization or condensation, and to let the sign of the vapour pressure gradient determine whether the net effect is evaporation or condensation.

There are two general procedures utilizing turbulent

theory to estimate this component of the heat balance. The first of these is the eddy flux or eddy correlation technique which assumes that quantities measured at the one meter level will give reliable values of the surface fluxes. Swinbank (1955), Dyer (1961), and Frankenberg (1960) have attempted to use these approaches with varying degrees of success. The equations which describe this process are of the form

$$q_L = L_e \bar{w} \bar{q} \quad (\text{Sellers, 1965}) \quad - - - [4.54]$$

where L = latent heat of vaporization
 e = density of the air
 \bar{w} = mean or average vertical eddy velocity
 \bar{q} = mean or average specific humidity

However, Sellers (1965) states, "it is very doubtful that they will ever come into general use".

The second of the turbulent transfer methods is that of aerodynamic or profile techniques. The general form of the equation is

$$q_L = \rho L k^2 \frac{(u_2 - u_1)(q_2 - q_1)}{(f_n z_2 - f_n z_1)^2} \quad \text{Ibid} \quad - - - [4.55]$$

where k = von Karman's coefficient ($=0.41$).
 u_1 and u_2 = wind velocities at levels z_1 and z_2
 q_1 and q_2 = specific humidities at levels z_1 and z_2

Various functions are used to model the wind-humidity profiles. Thornthwaite and Holzman (1939) suggest that under adiabatic, fully turbulent conditions with logarithmic wind profiles, the function of z_1 and z_2 is logarithmic and the denominator in

equation [4.55] is $\ln (z_2/z_1)^2$. A variety of specific equations using a combination of empirical and theoretical techniques are available for estimating q_L . O'Neill (1973) provides an excellent review of the background and theory and lists a number of the more popular equations.

In summary, the gain or loss of heat associated with vapour transport can be described as:

$$q_L = fn(u) (e_a - e_s) \quad - - - [4.56]$$

where $fn(u)$ may be a partially empirical and partially theoretical function of the wind profile and where e_a and e_s are the vapour pressures of the air and surface respectively.

It is of interest to note the relative magnitudes of e_a and e_s and to consider their variation over typical weather conditions during the thaw season with specific boundary conditions. The vapour pressure of the surface (e_s) is the saturated vapour pressure at the prevailing surface temperature provided the surface is fully saturated. This relationship is well known and is shown in Figure 4-6. Note that the saturated vapour pressure of water at 0°C is 6.1 mb. The partial pressure of water vapour in the air (e_a) is related to the air temperature and the amount of water vapour present in the atmosphere. This vapour pressure can be determined by various psychrometric techniques, which include a variety of humidity sensors and wet and dry bulb temperature relationships. The term relative humidity is used to describe the ratio of the amount of water vapour in the air at a given temperature to the amount of water vapour the air is capable of holding at the same temperature. Table 4-3 shows some typical values of water vapour pressure for various air temp-

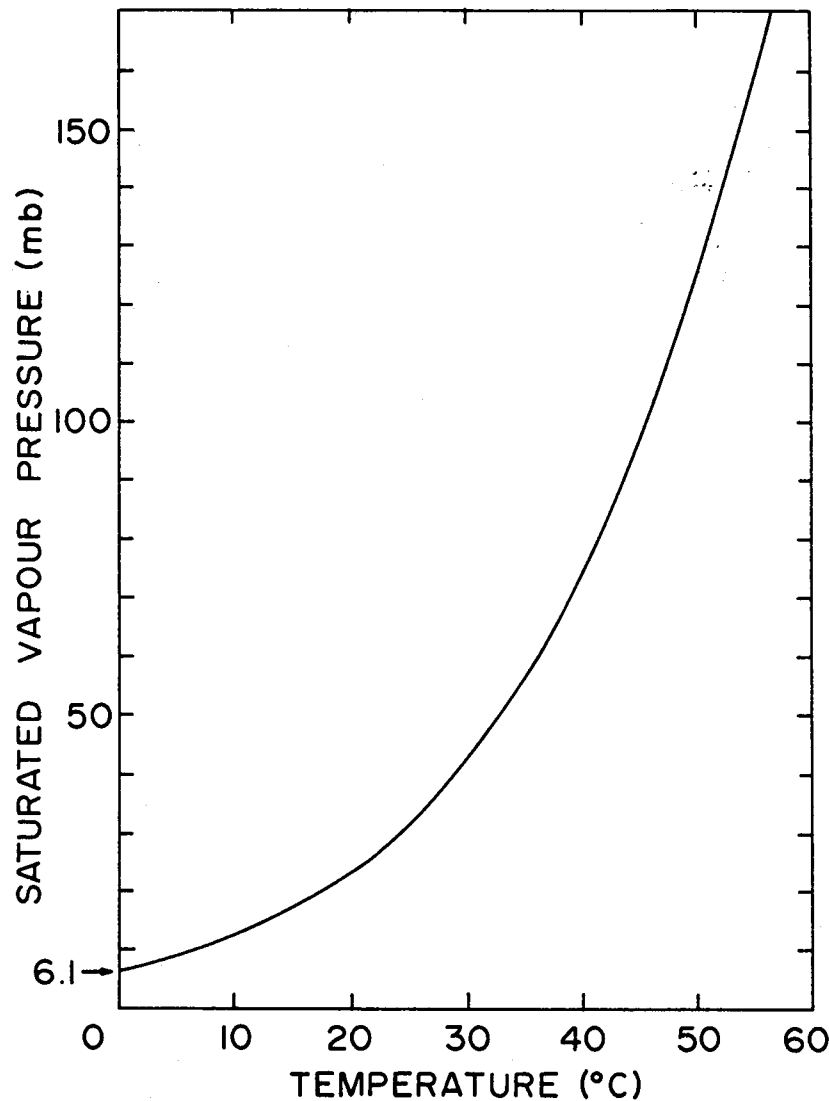


Fig. 4.6 Saturated Vapour Pressure vs Temperature
eratures and relative humidities.

In general the earth's surface is warmer than the air above it so that even with high relative humidities the vapour pressure gradient is from the surface to the air indicating the presence of evaporation. However, there are interesting observations to be made regarding cold surfaces such as glaciers, melting snow packs and exposed permafrost that exist even during the summer months. If the air temperature is 10°C then the relative humidity must drop below 50% before the vapour

TABLE 4-3

AIR TEMPERATURE, RELATIVE HUMIDITY AND VAPOUR PRESSURE

AIR TEMPERATURE °C	RELATIVE HUMIDITY %	VAPOUR PRES- SURE mb
5	70	6.1
10	80	9.8
↓	70	8.4
↓	50	6.1
20	80	18.3
↓	70	16.4
↓	60	14.2
↓	40	9.1
↓	30	7.2
↓	26	6.1

pressure gradient becomes negative and at 20°C the relative humidity must drop below 26% before evaporation will occur (Table 4-3). At relative humidities above these values, which are the rule rather than the exception, the gradient is positive and vapour is moving from the air, condensing on the surface resulting in a positive heat flux of $600 \frac{\text{cal}}{\text{cm}^2}$ for 1 cm. of condensate.

It is important to realize that all techniques discussed above for estimating q_L are contingent upon the ability to predict, model and maintain a wind and vapour pressure profile over the terrain in question. This is often possible over snow fields, lakes and reservoirs, deserts, and other extensive and reasonably uniform surfaces. However, this is not the case where the area of interest exists as an isolated entity within a totally different environment such as a remaining snowpatch in a bare field, an oasis in a desert or an exposed face of melting permafrost contained with an otherwise warmed surface. Under these conditions, the only alternative is to physically measure the amount of vapour transferred either to or from the surface by a process called lysimetry. The procedure requires that the soil, ice or snow surface be isolated, but remain in contact with the surroundings. Measurements are made at frequent intervals to determine the loss or gain of weight resulting from evaporation or condensation respectively. Countless researchers have employed different techniques for lysimetric measurements with varying degrees of success. The greatest problem associated with this technique appears to be the difficulty associated with installing and maintaining the device without disturbing the heat balance within the lysimeter in comparison to the surrounding terrain. The reader is referred to Technical Note No. 83, WMO (1966), and Nyeburg (1965)

for details regarding various types of lysimeter design and operation.

4.6 Sensible Heat Transfer

The second major activity associated with turbulent motion in the atmosphere is the vertical flux of sensible heat. This term, in the heat balance equation, although usually small and negative, may on some occasions be as large as, and of the same sign as the net radiation (Treidl, 1970). The equations which describe this transfer process are essentially of the same form as those used to describe or predict the transport of water vapour.

The appropriate equation is

$$q_s = \rho C_p \bar{W} \bar{T} \quad (\text{Sellers, 1965}) \quad - - - [4.57]$$

where ρ = the density of the air

C_p = the specific heat of the air at constant pressure
($\approx 0.24 \text{ cal/gm.}^\circ\text{C}$)

\bar{T} = mean or average temperature

(strictly speaking this is the potential temperature, i.e. the temperature of a body of air brought adabatically to a standard pressure)

\bar{W} = mean or average vertical eddy velocity

The limitations of this equation, discussed in reference to vapour transport, are also true for sensible heat transfer.

A variety of relationships exhibiting minor variations in the form of wind and height functions express the aerodynamic and profile methods for estimating the vertical flux of sensible heat. They take the general form of

$$q_s = \rho C_p k^2 \frac{f_n(U) (T_2 - T_1)}{f_n(z_2 - z_1)} \quad - - - [4.58]$$

The reader is again referred to O'Neill (1973), Sellers (1965) or any of the classic texts dealing with climatology and micro-meteorology for a complete treatment of the theory and background regarding sensible heat transfer predictions.

The simple semi-empirical approach is again useful in describing the fundamentals and the variation in magnitude and sign that may exist under specific atmospheric and terrain conditions. This relationship is quantified by the equation

$$q_s = fn(u) (T_a - T_s) \quad - - - [4.59]$$

Since the surface temperature is in general somewhat greater than the air temperature, the temperature gradient is negative and the surface of the earth is cooled as heat is transferred to the atmosphere. There are, of course, many exceptions to the above statement one of which occurs at night when temperature inversions are frequent. Other more important exceptions may be noted when the surface temperatures are consistently lower than the air temperatures. These situations are again in evidence during the time of snow melt in the spring and on glaciers and exposed permafrost surfaces in the summer. Under these conditions significant amounts of sensible heat may be utilized in sustaining the melting process (Treidl, 1970; Muller and Keeler, 1969; Streten and Wendler, 1968).

It must be noted, with some emphasis, that the predictive capabilities of these formulae are predicated upon being able to model and maintain the wind and temperature profiles over reasonably uniform surfaces. When the areas of interest are isolated or appear as islands in a substantially different environment, then large amounts of sensible heat will be horizontally advected into this

zone causing an accelerated rate of melting and making prediction almost impossible.

Since the process of evaporation and diffusion of water vapour from any water surface is similar to the conduction or diffusion of specific heat from the same water surface, Bowen (1926) has suggested that it may be represented as a ratio $R = q_S/q_L$, and that

$$R = 0.46 \frac{(T_w - T_a)}{(P_w - P_a)} \frac{P}{760} \quad - - - [4.60]$$

where T_w and T_a = temperatures of the water surface and air respectively in $^{\circ}\text{C}$.

P_w and P_a = vapour pressures of the water and air respectively in mm. of Hg.

P = total pressure of the atmosphere in mm. of Hg.

This equation supposedly reflects the difference in the transfer coefficients associated with the flux of sensible heat and water vapour. However, if the transfer coefficients are considered to be equal the equation takes the form

$$R = 0.501 \frac{(T_w - T_a)}{(P_w - P_a)} \frac{P}{760} \quad - - - [4.61]$$

Obviously the 8% difference in these two equations can hardly be considered significant.

If the ratio is defined simply as $R = q_S/q_L$, and when q_L can be measured and q_S calculated as the residual in the heat balance equation from ablation measurements, then the ratio may be evaluated and compared to the ratios obtained by other researchers. Table 4-4 summarizes the values of R that might be anticipated for the

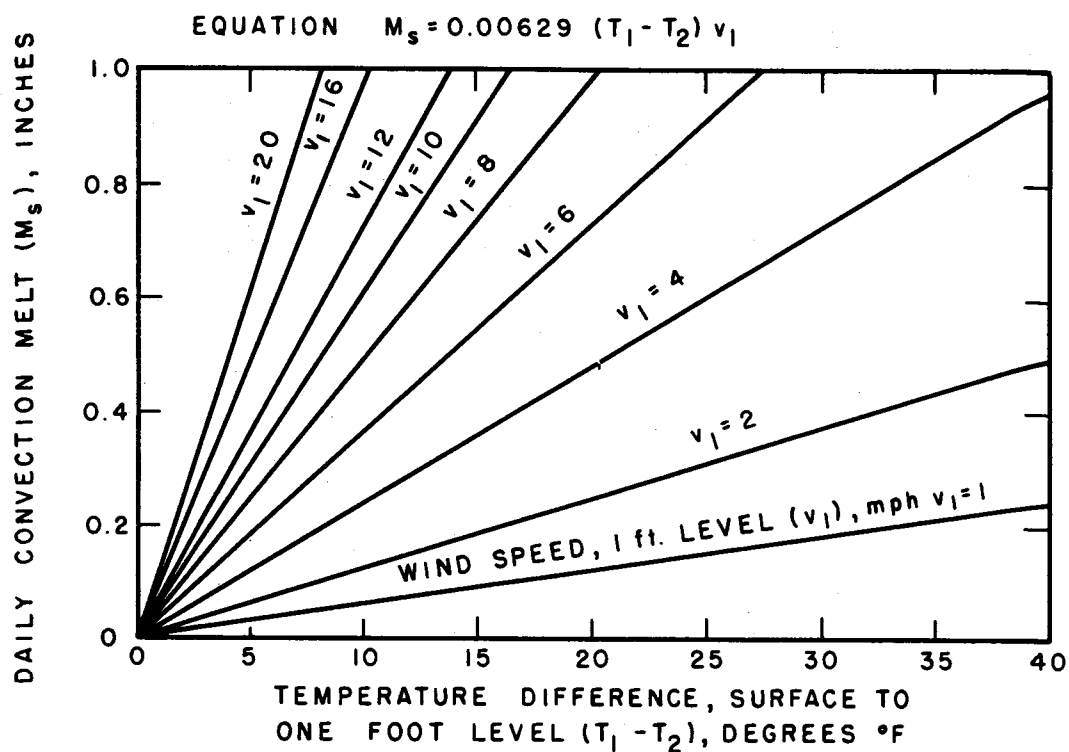


Fig. 4.7 Convection Melt (computed) (After U.S. Army Corps of Eng., 1956)

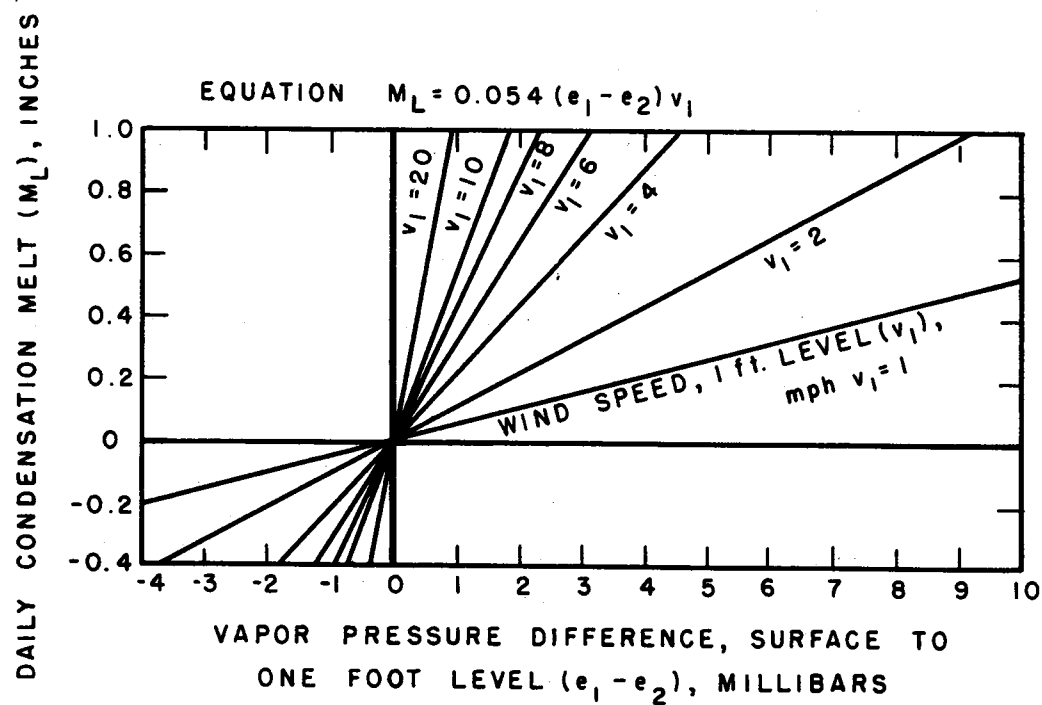


Fig. 4.8 Condensation Melt (computed) (After U.S. Army Corps of Eng., 1956)

TABLE 4-4
 SNOW MELT DUE TO SENSIBLE & CONVECTIVE HEAT TRANSFER AND BOWEN'S RATIO
 (AFTER U.S. ARMY CORPS OF ENG., 1956)

Temp. Diff. °C	Humidity %	M sensible in/day	M latent in/day	$\frac{M \text{ sensible}}{M \text{ latent}}$	R'	R
5	40	0.05	-0.08	-.63	-0.71	-1.2
	50		-0.05	-1.0	-1.13	-1.8
	60		0	0	0	-3.8
	80		+0.10	0.5	.56	+3.8
	100	0.05	.2	.25	.28	+1.2
10	40	0.11	.05	2.2	2.5	-5.1
	50		.10	1.1	1.13	-460
	60		.20	.55	.62	+4.4
	80		.31	.36	.41	1.7
	100	0.11	.43	.26	.29	1.0
15	40	0.18	.21	.86	.97	8.4
	50		.30	.60	.68	4.0
	60		.40	.45	.51	2.2
	80		.60	.30	.34	1.0
	100	0.18	.78	.23	.26	.85
20	40	0.21	.40	.53	.60	4.2
	50		.54	.39	.44	2.1
	60		.65	.32	.36	1.5
	80	0.21	.90	.23	.26	1.0

* NOTE: Values of M_S and M_L have been established from the accompanying
 Figures 4-6 and 4-7

equations predicting snow melt supplied by U.S. Army (1956). The snow melt due to sensible and latent heat transfer has been determined partly by theory and partly by empirical procedures (Fig. 4.7 and Fig. 4.8).

$$M_S = 0.00629 (P/P_0) (Z_a/Z_b)^{-1/6} (T_a - T_s) V_b \quad - - - \quad 4.68$$

$$M_L = 0.054 (Z_a - Z_b)^{-1/6} (e_a - e_s) V_b \quad - - - \quad 4.63$$

where M_S and M_L are the magnitudes of snow melts in inches/day due to sensible and latent heat transfer respectively; P and P_0 are the actual and reference atmospheric pressures respectively; Z_a and Z_b are the heights of the sensors above the surface; V_b = the wind velocity at level b (mph); T_a and T_s are the air and surface temperatures respectively ($^{\circ}\text{F}$); e_a and e_s are the vapour pressures of the air and surface (mb). The magnitudes of heat flux required to produce M_S and M_L are:

$$q_S = M_S \times 80 \times 2.54 = 203 M_S \text{ langley/day}$$

$$q_L = M_L \times \frac{600}{8.5} \times 2.54 = 180 M_L \text{ langley/day and}$$

$$R = q_S/q_L = 1.13 M_S/M_L$$

It is evident that R calculated from equation 4.60 bears little if any relation to R' . It will subsequently be shown that ratios of q_S to q_L obtained from the Fort Simpson research project agree reasonably well with the ratios calculated from meteorological data.

The author, therefore, concludes that the Bowen Ratio may be a satisfactory means of estimating q_s from measured values of q_L in the general case. However, there appears to be a strong indication that it should not be applied indiscriminantly to specific cases that involve unique or unusual boundary conditions.

4.7 Energy Transfer Due to Precipitation (q_p)

Energy may be transported to or from the surface of the earth by precipitation that is cooler or warmer than the surface. If the precipitation does not change phase as it comes into contact with the surface, the equation describing the heat exchange is:

$$q_p = C_w \rho (T_p - T_s) P \quad - - - [4.64]$$

where C_w = specific heat of water ($\frac{\text{cal}}{\text{gm } ^\circ\text{C}}$);

ρ = density of water gm/cm^3 ;

T_p and T_s = temperature of the precipitation and surface respectively;

P = the amount of precipitation received in a given period of time.

Generally speaking the surface of the earth will be cooled by precipitation during the summer. However, many exceptions again exist when the surface temperature remains at or near 0°C . Under these conditions the heat exchange will be positive. Since the magnitude of this term is small, its sign is of little significance. If, for example, the temperature difference is 5°C and 10 cm. of rain fall on the surface in a 24-hour period, then only 50 langley's per day are involved in the heat balance equation. Although this is

significant on the day of occurrence, accumulated values are of little importance over the entire thaw season.

4.8 Soil Heat Transfer (q_s)

In many projects dealing with agricultural, biological or engineering studies, the soil heat flux is the term in the heat balance equation that is the major item of interest. It can rarely be calculated as the residual in the equation, with any degree of accuracy, because it represents a relatively small difference of comparatively large numbers. The magnitude of this term varies greatly depending on the type of terrain. Arctic and desert regions will exhibit substantial soil heating while more southerly vegetated regions will show considerably less. Field (1967) suggests that this term is usually not larger than ten percent of the net radiation. However, the limits may range from as little as two percent of the net radiation (Williams, 1967) to values in excess of twenty five percent (Gill, 1971).

Occasionally, attempts are made to measure this component directly by using heat flux plates buried in the soil or below a pavement (Monteith, 1958; Johnston, 1974)*. Problems arise in this procedure due to disturbance and more importantly from the difference in thermal conductivity of the plates and the soil. The equation describing heat flow in a homogeneous, isotropic medium for steady state conditions is:

$$q_G = ks \frac{\partial T}{\partial Z} \quad - - - [4.65]$$

where ks = the thermal conductivity;

T = soil temperature;

Z = depth below the surface.

* Johnson, H personal communication

CHAPTER V

HEAT FLUX MEASUREMENTS AT THE HEAD SCARP

5.1 Introduction

The fundamental terms in the heat balance equation have been discussed for both horizontal and sloping surfaces. The magnitude of these quantities described thus far refer primarily to terrain normally encountered throughout the region of interest and therefore synoptic estimates of these terms are generally applicable. In addition, situations involving specific boundary conditions (namely cold surfaces) have been discussed that exist during the summer months. The following deals with the heat balance that exists at a typical head scarp of a bimodal flow slide in the subarctic. A description of the site and equipment used for the data acquisition is also given. The data will be presented and analyzed in relation to the various terms in the heat balance equation. Computed values will be compared to those measured whenever possible.

5.2 Site Location and Description

The field work was performed at a large landslide approximately 18 miles downstream from Fort Simpson, N.W.T. on the Mackenzie River ($61^{\circ} 50' \text{ N}$; $121^{\circ} 21' \text{ W}$; elev. 432 ft. M.S.L.). The site is shown in Figure 5-1. McRoberts (1973) has provided a preliminary description of this landslide but more recent information introduces two notable alterations. Measurements made in the course of this study would indicate that the average slope of the profile shown in Figure 5-2 is 13.5° rather than the 19° angle suggested previously. The age of white spruce trees along the head scarp was determined by counting annual rings. They were found to be in excess of 140 years old, which is older than that



Fig. 5-1 Aerial View of Fort Simpson Landslide

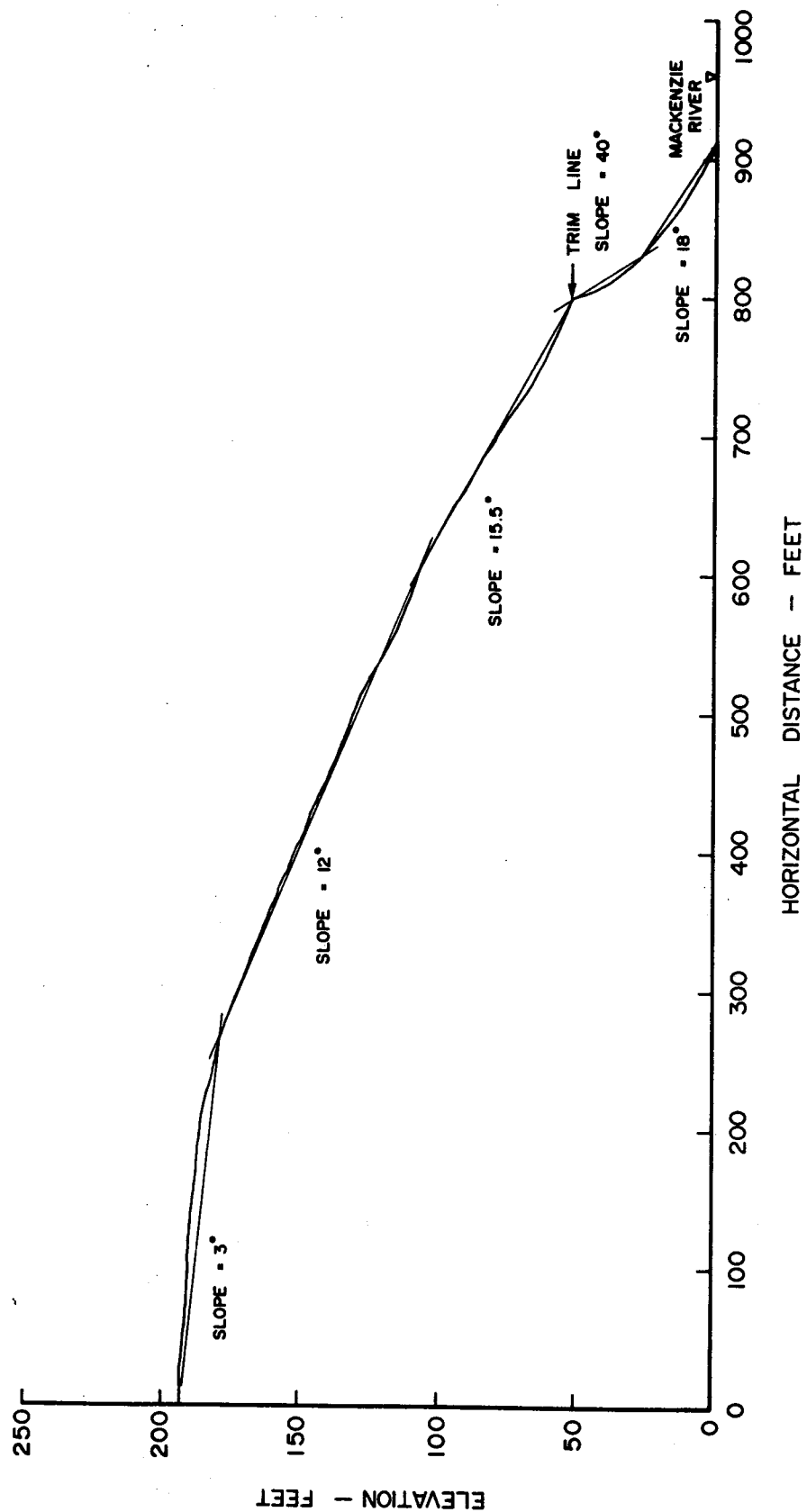


Fig. 5.2 Bank Profile of Mackenzie River Immediately East of Fort Simpson Landslide

reported by McRoberts (1973).

The rotted and charred remains of timber are evident beneath the forest litter, indicating the action of ancient forest fires. The last severe fire apparently occurred approximately 140 years ago and in all probability denuded the area of all trees and shrubs as no fire scars are evident on any of the standing vegetation. The date of the fire has been inferred by determining the age of some of the largest trees on the site. If indeed the fire was hot enough to fell the majority of the trees, then it would logically destroy the insulative quality of the moss cover and precipitate mass movements characteristic of burned over slopes in permafrost regions (Heginbottom, 1971). The action of flow slides does not appear to be consistent with the existing angle of the river bank. Mud flows within the slide area stabilize at angles considerably less than 10° to the horizontal. The question then remains as to why the inferred destruction of the moss cover did not trigger massive flow slides in this region. On the other hand, if flow slides were initiated, why did they stabilize at these relatively steep angles?

The writer makes no attempt to analyse the principal causes of the slide or the different modes of failure that have occurred over the recent period of instability. McRoberts (1973) has described what appear to be the dominant processes involved within the landslide activity. The immediate concern is centered around the southeast portion of the slide. This area is retreating rapidly due to the ablation of the exposed permafrost and forming the classic features characteristic of bimodal flow slides in the Mackenzie River Valley (ibid).

It may be noted from Figures 5-3 and 5-4 that a series of these bowl shaped flow slides have developed, giving the east and

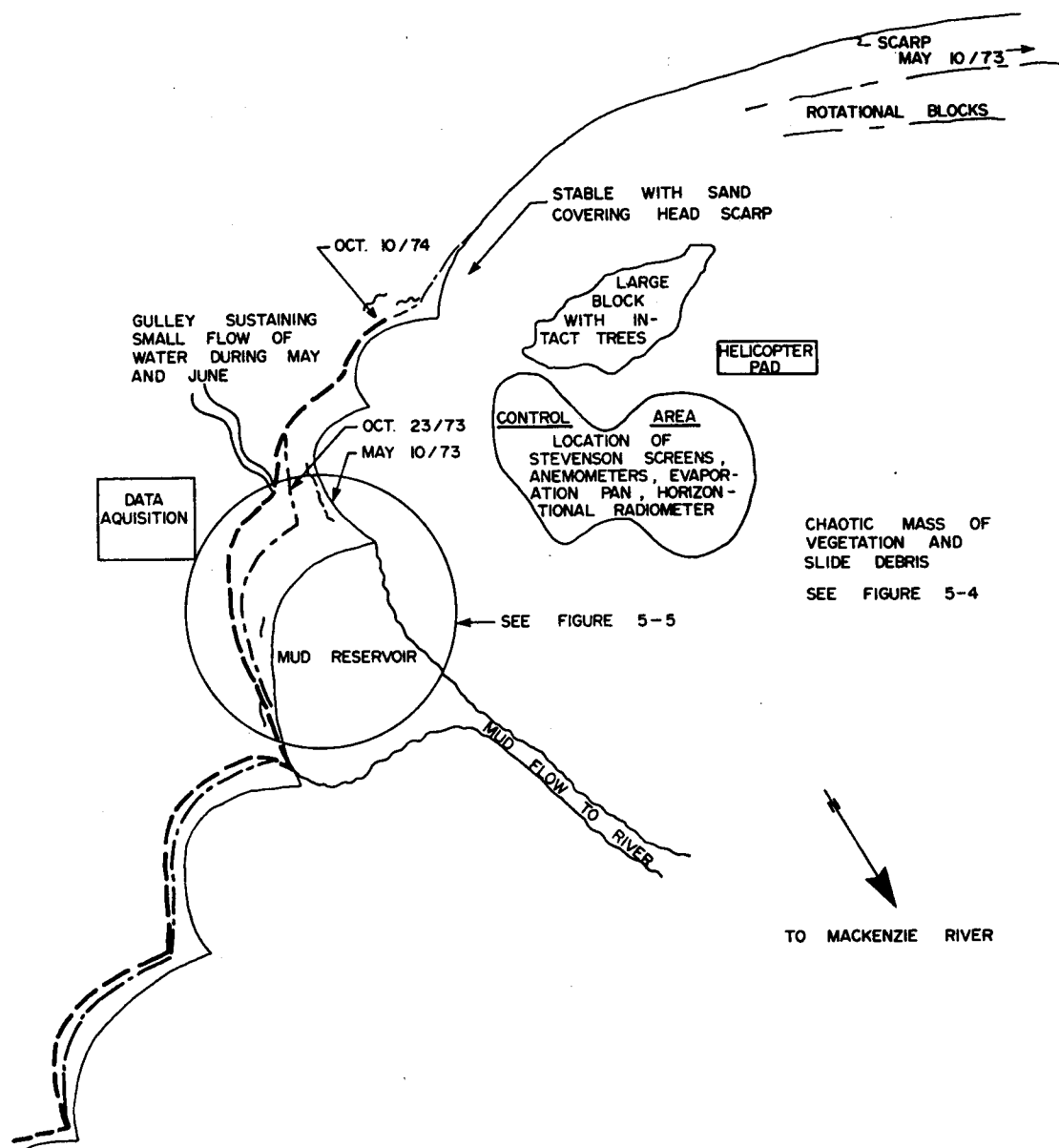


Fig. 5.3 Plan View of Fort Simpson Landslide

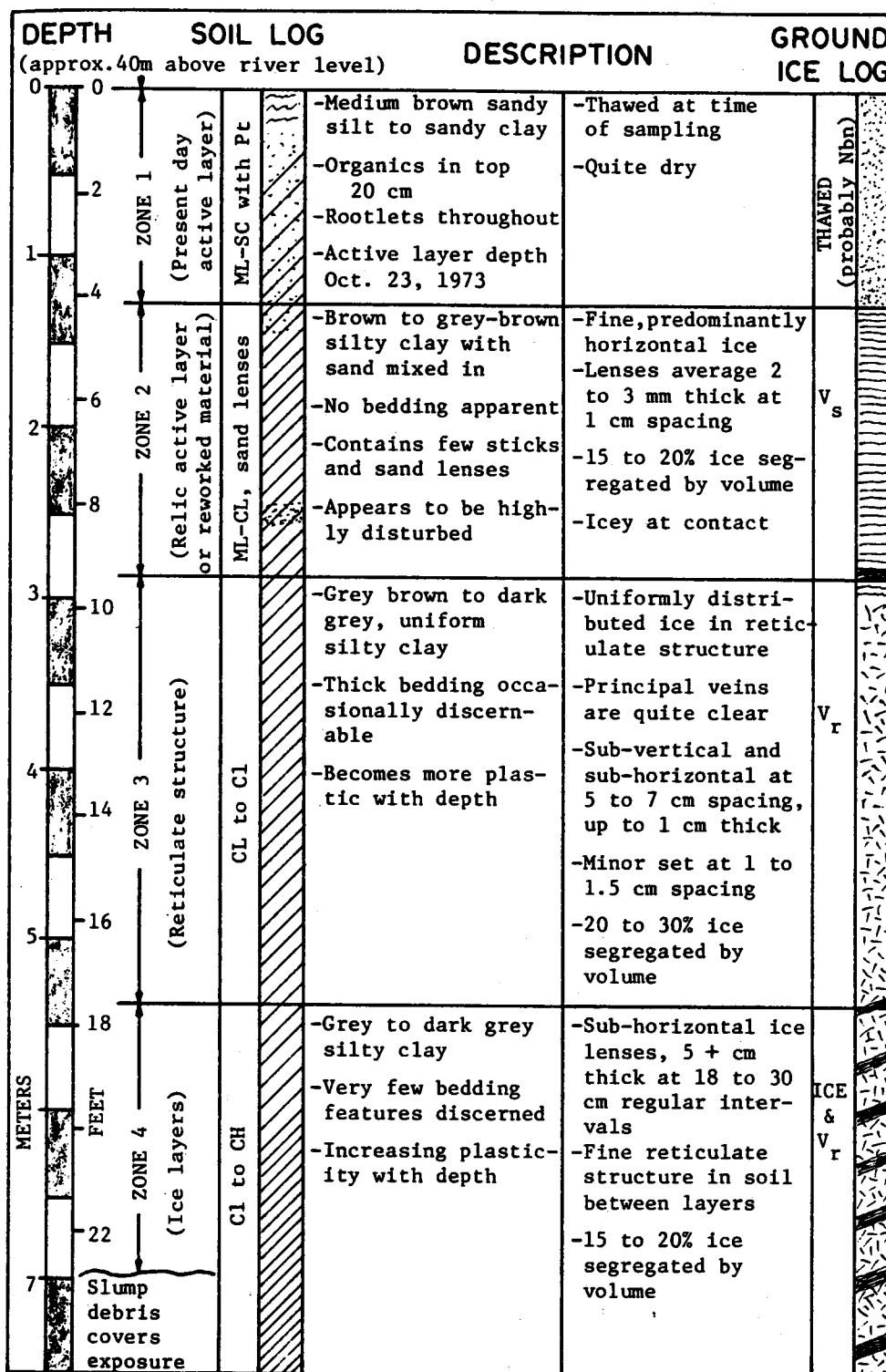


Fig. 5-3(a) Description of Sediments of Fort Simpson Landslide

After Roggensack (1975).



Fig. 5-4 Aerial View of East Flank of Fort Simpson Landslide

southeast flank of the slide a cusped appearance. It is the area circled "A" in Figure 5-3 and enlarged in Figure 5-5 that was studied in detail in this project.

The shape of this immediate region varies substantially from time to time depending upon the soil-ice stratigraphy and the profile of the bank above the slide. During the summer of 1974 the headscarp varied from 20 to 40 feet in height and sloped at 45° to near vertical. The main part of the ablating face is north facing. However, the flanks of the bowl face east and west and recession of these faces proceeds at a rate comparable to that of the north slope. Figure 5-6 provides a view of the head scarp as it existed in July, 1974. As the permafrost melts, it sloughs off the face and the debris slides down the slope on the frozen surface of the underlying soil. It appears that an exposed face of frozen soil and the pore water pressures that are generated by an advancing thaw front are required to maintain the active retreat of the headscarp. Otherwise, the debris becomes lodged on the face of the headscarp and it will not readily move downslope. A small reservoir of mud, exhibiting a consistency near to that of the liquid limit of the soil forms at the base of the headscarp. When a sufficient volume of this material has accumulated it gradually moves down slope forming a typical mud flow as described by Kerfoot (1969). Figure 5-7 illustrates the mud flow that had developed at the Fort Simpson slide in July, 1974.

The head scarp exposure reveals the presence of an upper layer of sand of varying thickness but generally increasing in thickness with distance from the river. Below this sandy layer lies a silty clay or clayey silt with intrusions of sand pockets. The thickness of the sorted materials appears to be in the order of one hundred

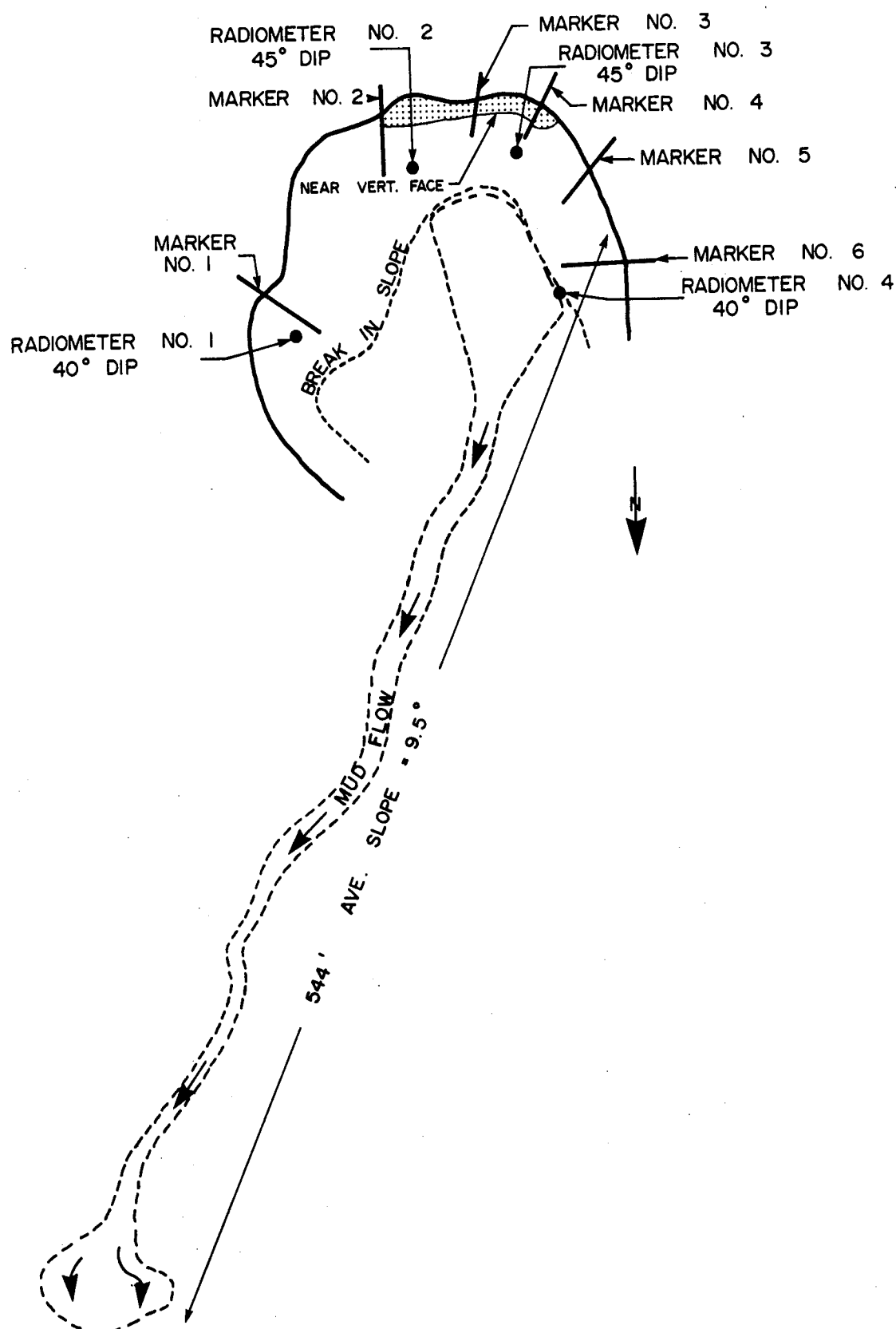


Fig. 5.5 Plan View and Instrumentation of Headscarp of Bimodal Flow at Fort Simpson Landslide

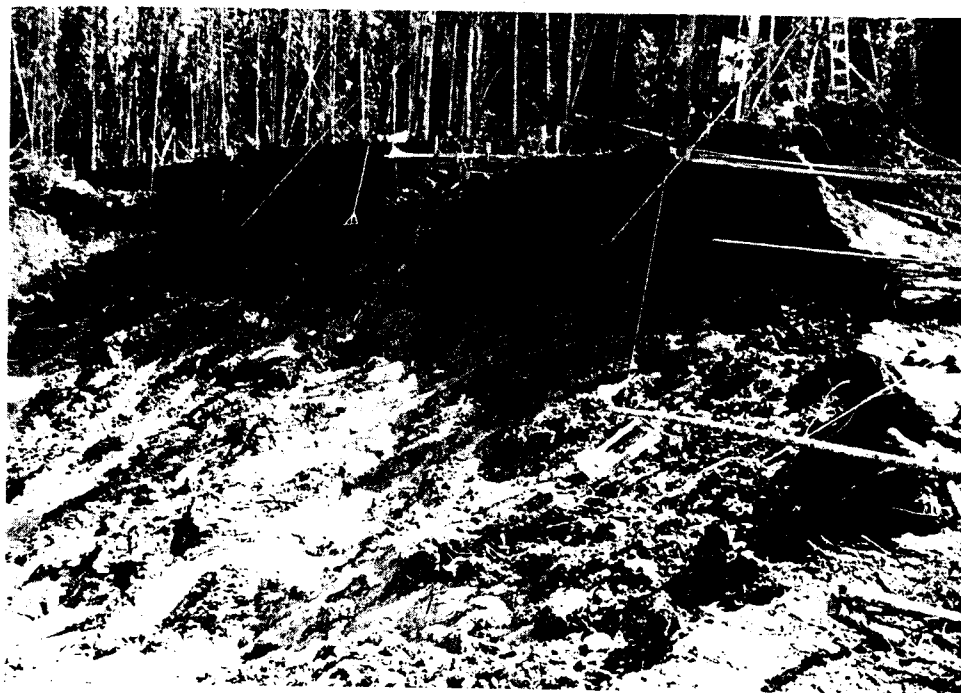


Fig. 5-6 View of Headscarp (July 1974)



Fig. 5-7 Mudflow at the Base of the Headscarp

and fifty feet at a distance one thousand feet back from the shoreline. This layer of material appears to pinch out near the shoreline of the river.

The upper sand layer is quite variable in thickness throughout its areal extent. It is largely absent in the area where severe ablation is presently in progress. The other areas of the slide are essentially stable because the retreating headscarps have encountered reasonably thick beds of sand. This granular material is thaw stable and as melting occurs it sloughs down over the face of the lower ice rich sediments forming a stable active layer.

The stratigraphic profile shown in Figure 5-3(a) of the head scarp may be most easily described by recognizing four reasonably distinct zones, differentiated on the basis of the amount and type of ground ice. The active layer has been designated as Zone 1 and it is approximately one metre (3 feet) in thickness, as determined from a test pit dug at the top of the head scarp in Oct. of 1973. The thawed soil consisted of clayey sand grading into sandy to silty clay with increasing depth. Zone 2 is considered to be an extended relic active layer. Generally the soil is a silty clay with rhythmically banded ice lenses of from 2 to 5 mm. in thickness. The water contents in this zone are extremely variable, depending on the location and the size of the sample. Occasional lenses of sand and local thick ice lenses are evident in this zone. Water contents as listed in Table 5-1 indicate variations of from 20 to 125%. However, the writer recommends that these high values should not be considered in determining a representative water content for this zone. Zone 3 consists of 4 to 5 meters of medium to highly plastic clay extending across the face of the head scarp. The ground ice is essentially a fine reticulate network occasionally ex-

TABLE 5-1

SUMMARY OF SOIL DATA AT FORT SIMPSON LANDSLIDE

Location	Soil Type	Liquid Limit %	Plastic Limit %	Gross Nat. Water Content %	Specific Gravity	Unit Weight kN/m^3	% Silt	% Clay	Undrained Strength kN/m^2
Zone 1 Active Layer	Clayey sand to sandy clay	-	-	20 to 40	-	-	-	-	-
	silty clay with pockets of sand	39 40 46 42	23 24 25 24	20 - 125 34 - 38 31 - 40 36	2.75	17.4-17.8 16.8-18.1 17.5	35-40	60-65	
Zone 2 Relic Layer	silty clay	41 37 50 43	23 24 25 24	37 - 72	2.75	15 - 18 14 - 17 16.4	35-45	55-65	variable, may be up to 10 - 15
Zone 3	silty clay	40 33 41 37 38	22 22 24 22 22.5	28 - 53	2.75	16 - 18	35-45	55-65	19.0 to 48.0
Zone 4									

posing repeating horizontal ice lenses of 5 to 10 mm. (2 to 4 in.) in thickness. The unit weight of this material ranges from 14 to 18 kN/m³ (90 to 115 pcf) with typical water contents of 37 to 72%. This zone is occasionally very ice rich with the lenses ranging from 5 to 25 cm. (2 to 10 in.) in thickness. These lenses appear to dip sub-parallel to the face of the scarp. Bedding planes, although obscure, within the soil mass between the lenses are essentially horizontal. Undrained strength tests performed on this material were extremely variable and generally quite low. Strengths ranged from near zero to as high as 10 to 15 kN/m² (200 to 300 psf). Zone 4 is essentially unexposed at the head scarp and exists to an unknown depth below the upper materials. This soil (between the ice lenses) is a high density, medium to highly plastic clay. It has a total unit weight of from 16 to 18 kN/m³ (102 to 115 pcf) with water contents ranging from 28 to 53%. Undrained strengths of this material range from 5 to 10 kN/m² (1000 to 2000 psf), (Roggen-sack, 1975)*. This layer of competent material may well play an important role in limiting the depth to which the flow slide has developed at this site. The soil is dense enough and of sufficiently low water content to render it reasonably stable when thawed. If this material does not slough and fall away during the ablation process, then it will form the base of the flow slide. The above statements are only speculation and a comprehensive drilling program would be essential to establish the location of this material relative to the base of the mud flow throughout the existing slide. Figures 5-8, 5-9 and 5-10 indicate the different zones described above.

The index properties and soil gradation are given in Table 5-1. It is interesting and of significance to note that the index properties



Fig. 5-8 Soil Profile Zone 1, 2 & 3 (Oct. 1973)



Fig. 5-9 Soil in Zone 3

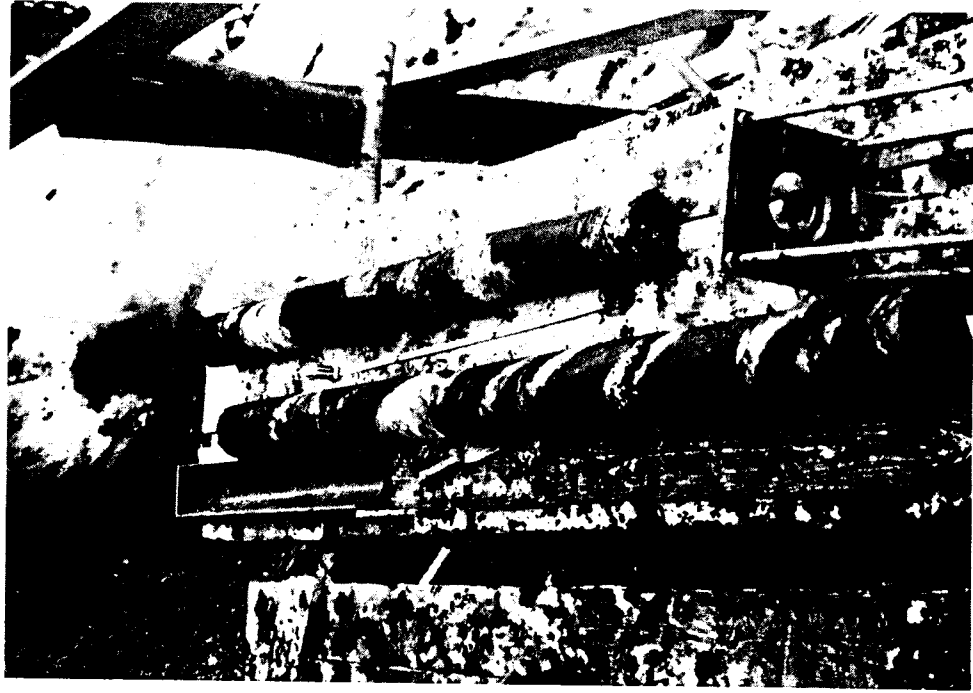


Fig. 5-10 Frozen Core Removed From Zone 4

and grain size distribution of the soil within the zones are essentially the same. Only the amount and nature of the ground ice differentiates the visual classification and behavior of the different zones. The numbers set within the boxes are considered to be the most representative of the values recorded for any listed property.

5.3 Ablation Rates

5.3.1 Measurement Techniques

The rate at which the head scarp retreated was determined from physical measurements taken daily around its perimeter at six different stations. A technique was developed that enabled all activity associated with the measurement to be performed from the top of the escarpment. Slender timber rails were extended over the edge and secured in a horizontal position. A plumb bob was permanently fastened to each rail so that it swung freely a few cm. from the face of the soil (Figure 5-11 and 5-12). A light cord was threaded through a hollow conduit and another weight fastened to this cord. At the time of measurement, the conduit was extended along the rail to the point where the plumb bob was fastened. The weight on the cord in the conduit was lowered until it coincided with the level of the plumb bob. The cord was held securely and the conduit was moved back horizontally along the rail until the weight came into contact with the face of the soil. The end of the conduit was marked on the timber rail and thus the movement of the face was established each day at the same level. The weight was lifted an arbitrary amount and a similar measurement taken part way up the slope. All of the stations did not always provide reliable daily ablation rates. Occasionally the melted soil became lodged on the face of the slope indicating that melting was not occurring for

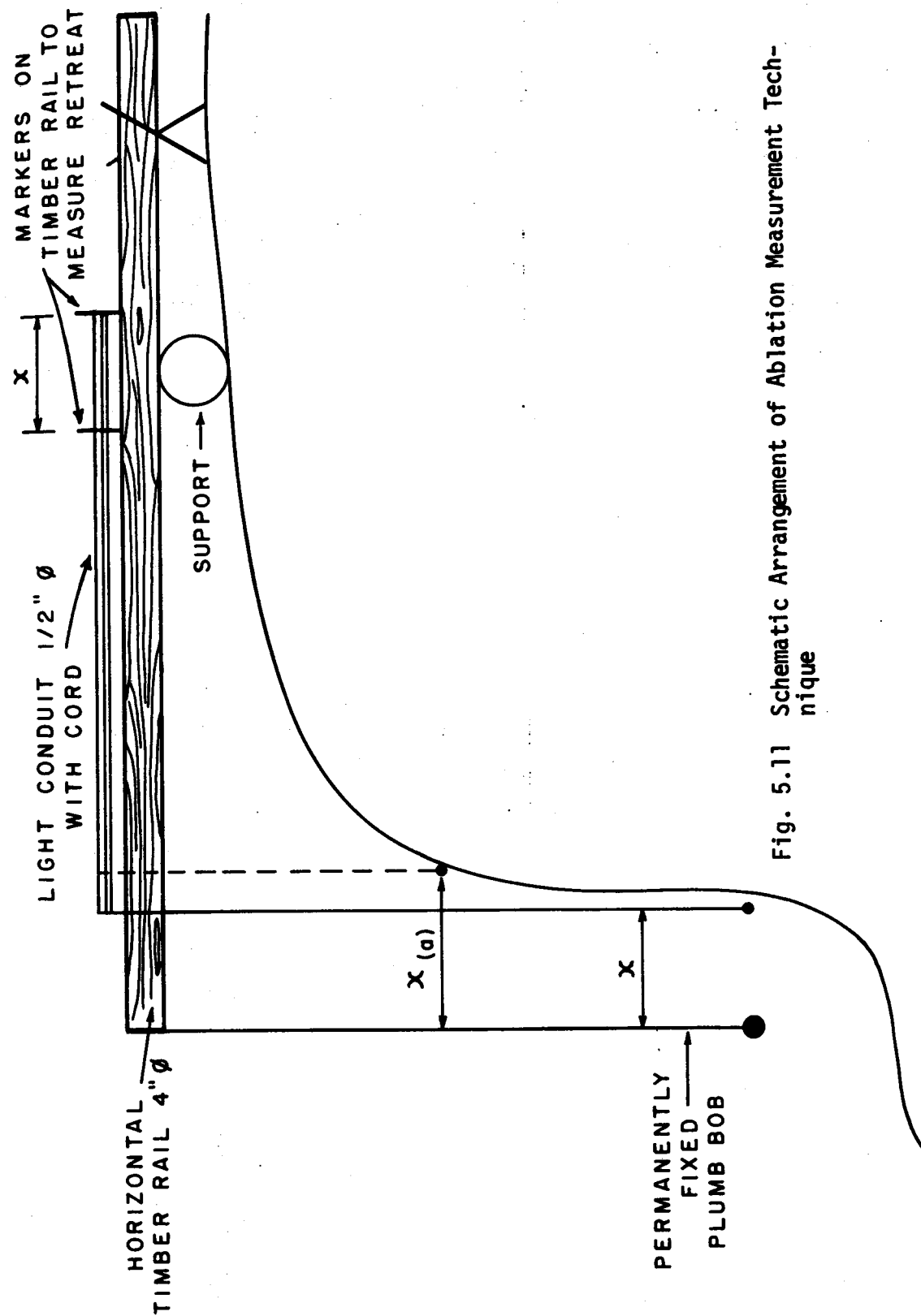


Fig. 5.11 Schematic Arrangement of Ablation Measurement Technique

a number of days. However, when the weight of the melted material became sufficiently large to overcome the shearing strength of the soil at the thaw front, the material would slough off and move down the slope exposing the frozen face to a new cycle of ablation.

5.3.2 Magnitude and Heat Requirements

Ablation measurements were taken from June 21, 1974 to July 21, 1974. The retreat ranged from a minimum of 256 cm. to a maximum of 455 cm. The larger numbers are associated with stations where the ground ice was relatively uniform and rhythmically banded. These soil conditions allowed the material to fall away from the face as quickly as it melted providing a truer indication of the ablation rate than areas that retained the melted soil. The recorded data are presented in Figures 5-13 to 5-18. Figures 5-13, 5-14, 5-16 and 5-17 indicate ablation rates at stations 1 and 1(a), 2 and 2(a), etc. The subscript "a" indicates a measurement taken approximately 1 metre above the break in the slope of the head scarp at the same station. The data presented in Figures 5-15, 5-16, and 5-17 provide the most reliable data and will therefore be used to compute the amount of heat utilized in maintaining this rate of melting. The average rate of retreat for stations 3, 4 and 5 for the time period of measurement was 14 cm/day.

A representative water content of the soil from this body of permafrost is very difficult to determine. This is largely due to the variability of the material and the presence of large ice lenses. Sampling was not attempted during the summer while the remainder of the experimental work was being conducted. Obtaining frozen cores from the face of the melting head scarp was not feasible. Frozen



Fig. 5-12 Ablation Measurement Technique

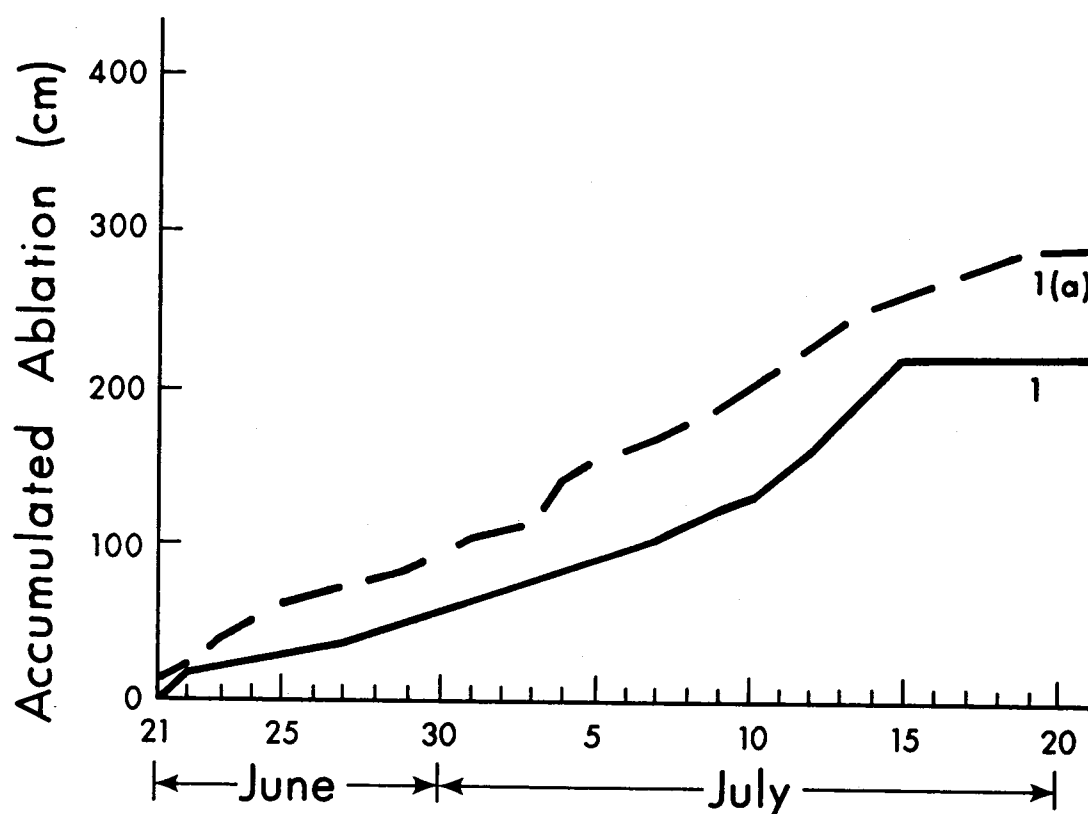


Fig. 5.13 Accumulated Ablation at Sta.1

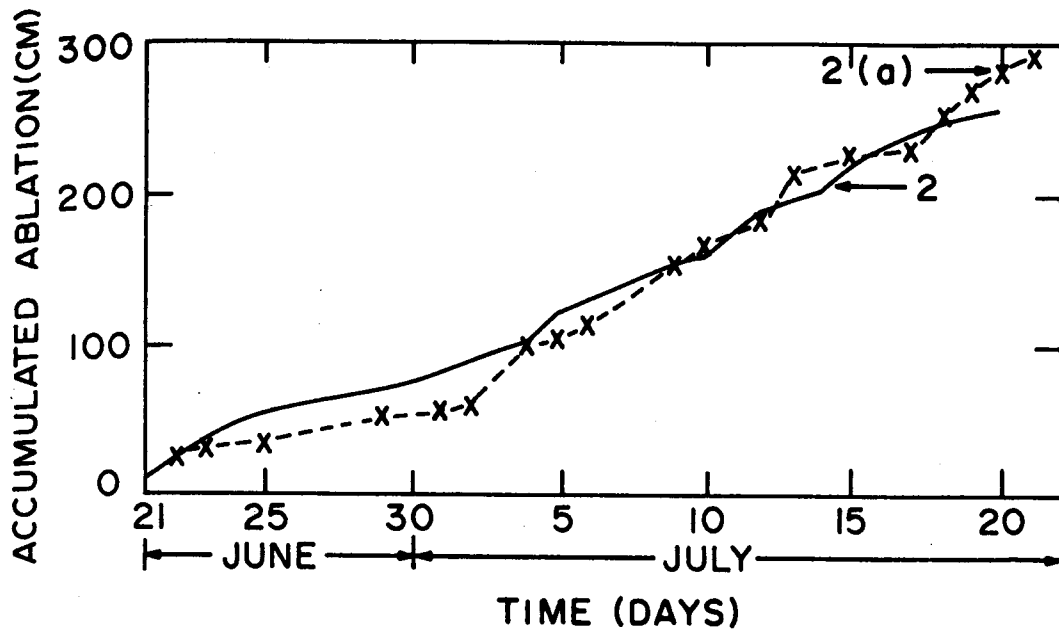


Fig. 5.14 Accumulated Ablation at Sta. 2

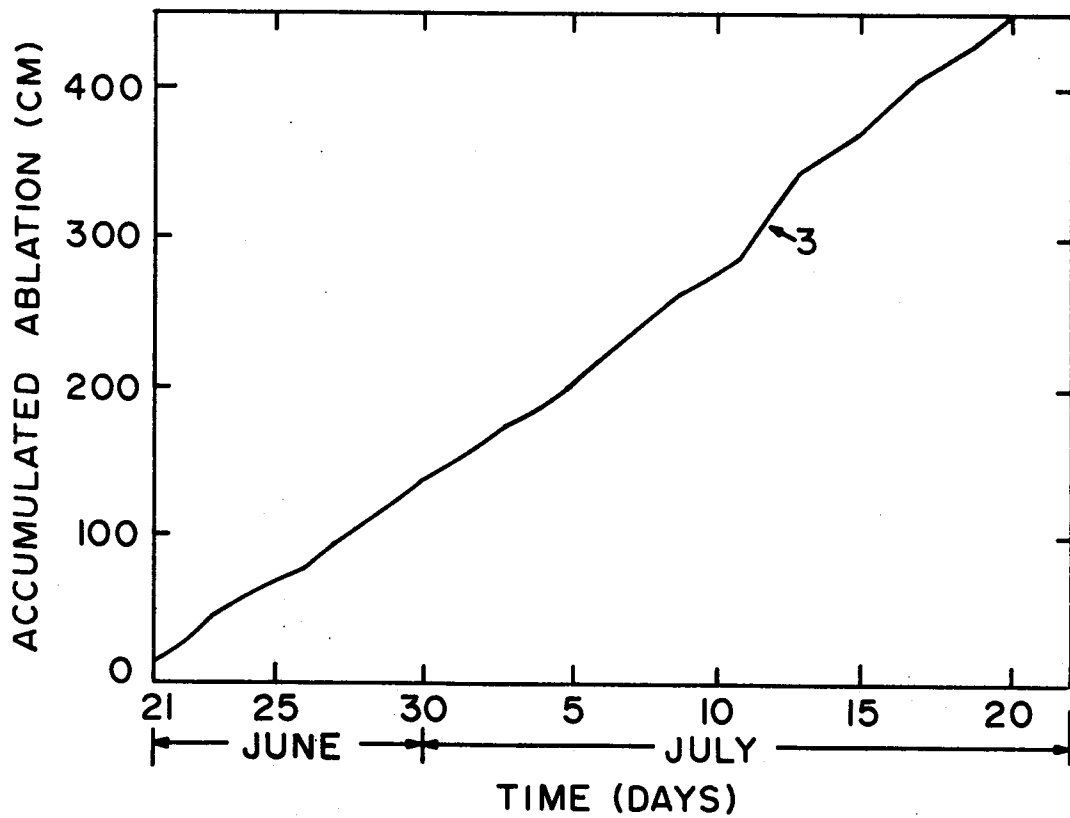


Fig. 5.15 Accumulated Ablation at Sta. 3



Fig. A.1 Mile 222 Alaska Highway (Backslope instability during construction, July 1973).

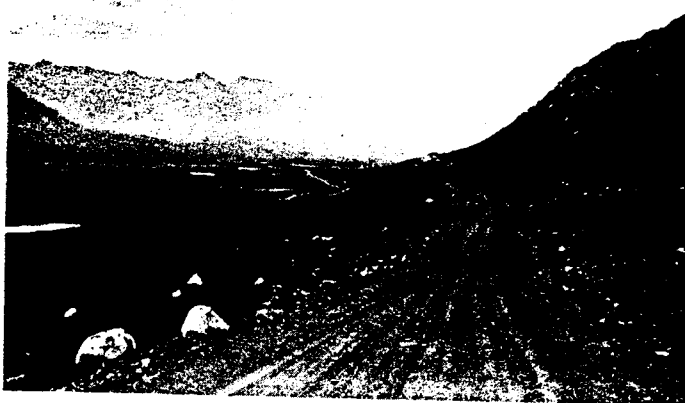


Fig. A.2 Mile 50 Dempster Highway (Headwaters of the East Blackstone River. Road built at very modest geometric design standards).

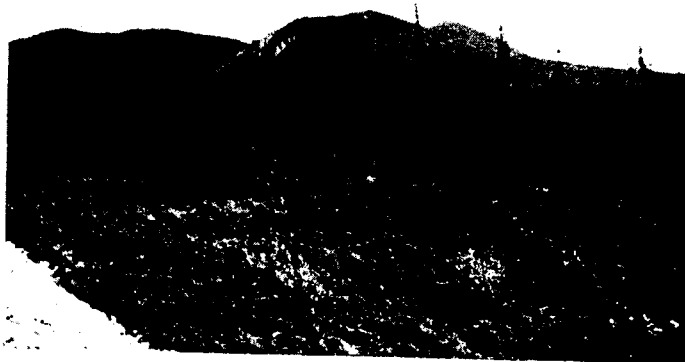


Fig. A.3 Mile 124 Dempster Highway (Typical view of the Ogilvie physiographic unit).



Fig. A.4 Mile 80 Dempster Highway
(Improved geometric design standards).



Fig. A.5 Mile 109 Dempster Highway (Biangular profile of
backslope due to permafrost degradation).



Fig. A.6 Mile 114 Dempster Highway (Large thermal degradation
scar - 150 ft. wide and 15 to 20 ft. deep).



Fig. A .7 Mile 120.7 Dempster Highway (Ten ft. cut with 2:1 backslopes made into ice rich organic silt.



Fig. A .8 Mile 153 Dempster Highway (Melting of large ice wedges caused slope degradation).



Fig. A.9 Mile 153 Dempster Highway
(View from top dressed backslope).



Fig. A.10 Mile 175 Dempster Highway (Backslope and shoulder failure
due to melting of a large ice lense).



Fig. A.11 Mile 175 Dempster Highway (Severe cracking of shoulder due
to differential thermal subsidence caused by construction).



Fig. A.12 Mile 343 Dempster Highway- Large cut between Arctic Red River and Fort McPherson (Looking west).



Fig. A.13 Mile 343 Dempster Highway - Stabilized backslope. (Hand placed vegetation to control rate of thaw).



Fig. A.14 Bimodal flow in the Richardson Mountains.

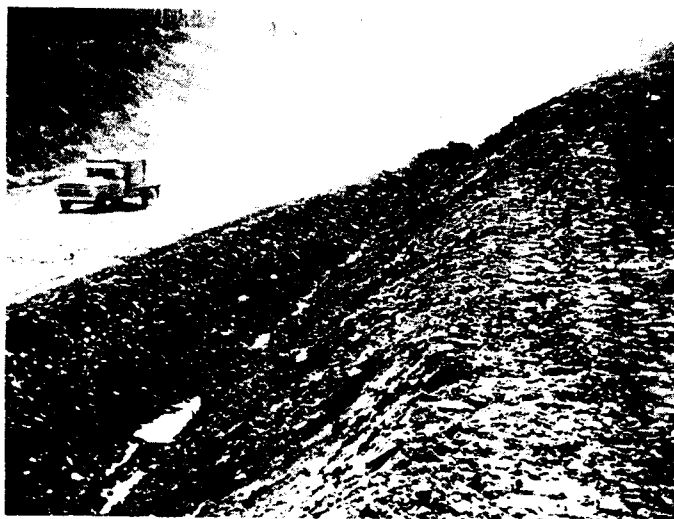


Fig. A15 Approach cut to Mackenzie River crossing at Arctic Red River.



Fig. A.16 Typical vegetation patterns at southern end of TAPS Haul Road.



Fig. A.17 Mile 14 TAPS Haul Road (July 1973).

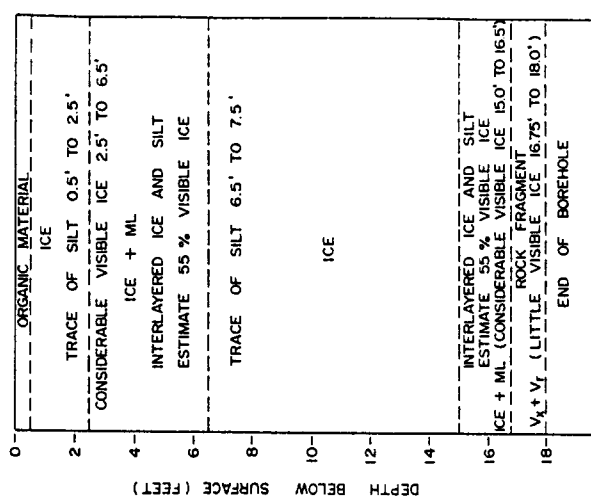


Fig. A.18 Mile 20 TAPS Haul Road - Typical Bore Hole Log (After Smith & Berg 1972).



Fig. A.19 Mile 19.6 (31.6 km) TAPS Haul Road (July 1973).



Fig. A.20 Mile 20.3 (32.6 km) TAPS Haul Road (July 1973).



Fig. A.21 Mile 22.9 TAPS Haul Road (April 1970)
(After Smith & Berg 1972).



Fig. A.22 Mile 22.9 TAPS Haul Road (July 1973).



Fig. A.23 Mile 23.4 TAPS Haul Road. Approach to Hess Creek
(April 1970).



Fig. A.24 Mile 23.4 TAPS Haul Road. Approach to Hess Creek (July 1973).



Fig. A.25 Mile 33 TAPS Haul Road (July 1973).



Fig. A.26 Mile 54.4 TAPS Haul Road (July 1973).

APPENDIX B

The following appendix contains a computer program that was used in Chapter III of this thesis.

This program may be utilized in the design of insulation thickness and surcharge loading for the stabilization of planar landslides in thawing soils. The insulation used in this example is woodchips. The input for trial one is:

Thermal conductivity of gravel	(K1)	= 0.0065 cal/deg C cm s
Thermal conductivity of woodchips	(K2)	= 0.00030 cal/deg C cm s
Thermal conductivity of thawed soil	(K3)	= 0.0030 cal/deg C cm s
Insulation thickness	(H)	= 0.15 m
Surface temperature	(TS)	= 16.9° C
Length of thaw season	(TF)	= 130 days
Coeff. of consolidation	(Cv)	= 0.002 cm ² /sec
Grid spacing	(Dx)	= 0.040 m
Depth of surcharge	(DEP)	= 0.91 m
Unit wt. of G amt 1		= 19.65 kN/m ³
Specific gravity of parent material	(GS)	= 2.70
Water content of parent material	(W)	= 35%
Unfrozen water content of parent material		= 0%
Friction angle of parent material	(Ø)	= 22
Slope angle (beta)		= 12%
Number of times output is produced	(IO)	= 5

Trial number two has increased insulation thickness and decreased surcharge load. All other parameters remain constant.

Insulation thickness	(H)	= 0.23 m
Depth of surcharge	(DEP)	= 0.61 m

The elapsed time, the thaw depth, the number of depth increments, the pore pressure-depth increment profile, the pore pressure at the thaw front, the effective normal stress at the thaw front, the shearing stress at the thaw front and the factor of safety are listed in the output.

```

MTS  FORTAN IV G COMPILER (C/S REL 21.7)          MAIN          12-27-75    08:45:02    PAGE 0001

C----- PROGRAM TO CALCULATE THE PORE PRESSURES AND THE FACTOR OF SAFETY
C----- OF A THAWING SLOPE WITH INSULATION AND SURCHARGE LOADING
C----- THE PROGRAM USES THE CRANK-NICHOLSON FINITE DIFFERENCE METHOD..
C----- IT IS A FIXED GRID. MOVING BOUNDARY SITUATION. AND THE SOIL IS
C----- ASSURED HOMOGENEOUS... ONE DIMENSIONAL FLOW IS PERMITTED. AND
C----- THE PROGRAM CAN INCORPORATE ANY SPECIFIED RATE OF THAW....
C----- KM/SQ M MAY BE CONVERTED TO PSF BY MULTIPLYING BY 20.89
C----- KM/CM H ( KN/FT ) MAY BE CONVERTED TO PCF BY MULTIPLYING BY 6.37
C-----
COMMON U(500),A(500),B(500),C(500),D(500),EOUT(500),DX,P0,M1,V1,X
COMMON GAMSUB,GAMT1,GAMT3,CV,TIME,PHI,BETA,DEFIV,CB,CN,DEP,CB1
PEAL K1,K2,K3,L
C-----
C----- ENTER THE PARAMETERS NECESSARY FOR SOLUTION
99  READ(5,101)K1,K2,K3,H,TS,TF,CV3,DX,DEP,GAMT1,GS,W,U,PHI,BETA,IO
101  FORMAT(8F10.0,/,7F10.0,I3)
IF(H.LE.C.0) K2=K3
WRITE(6,102)K1,K2,K3,H,TS,TF,CV3,DX,DEP,GAMT1,GS,W,U,PHI,BETA,IO
102  FORMAT(11,/,102)
1X(T)=SQRT(K3/K2+H*2*K3*TS/L*TIME)-K3/K2*H,/, THE RATE OF THAW IS GIVEN BY:
2F TH SURCHARGE=,F7.5,CAL/DEG C CM S,/, THE THERMAL COND.O
3THE INSULATION=,F7.5,CAL/DEG C CM S,/, THE THERMAL COND. OF
4HE LOWER SOIL =,F7.5,CAL/DEG C CM S,/, THE THICKNESS OF INSUL
5ATION=,F7.2, H,/, THE AVE AIR TEMP=,F7.2, DEG C,/, THE
6SOIL WILL TERMINATE AT TIME=,F7.1, DAYS,/, THE CORRP OF CONSOL
7=,F9.4, CM SQ/SEC,/, THE DEPTH OF SURCHARGE =,F7.2, H,/, THE TOTAL
8.3, H,/, THE SURCHARGE NATRL=,F7.2, FM/M3,/, THE SPECIFIC
91 UNIT WT.OF THE SURCHARGE =,F7.2,/, THE WATER CONTENT OF THE LOWER SOI
10FAVITY OF THE SOIL=,F7.2,/, THE UNFROZEN WATER CONTENT OF THE LOWER SOI
2L=,F7.2,/, THE FRICTION ANGLE OF THE SOIL=,F7.2, DEGREES,/, THE SLO
3, THE ANGLE OF THE SOIL=,F7.2, DEGREES,/, THE DESIGD NO. OF TIMES OUTPUT
4PE ANGLE=,F7.2, DEGREES,/, THE DESIGD NO. OF TIMES OUTPUT
5WILL BE PRODUCED OVER THE THAW PERIOD=,F7.2,/,
6-----
HE=K2/F1*DEP
GAMTCG=GS*(1+W)/(1+GS*W)
GAMDF=GAMTCG/(1+W)
L=GAMDP*(W-WU)*79.6
CB=K3/K2*HF
CR1=K3/K1*DEP
CN=2*K3*TS/L*8.64
GAMSUB=(GAMTCG-1.0)*9.8066
GAMT3=GAMTCG*9.8066
C----- CHANGE DEGREES TO RADIANS FOR COMPUTATIONS
BETA=BETA*3.1415927/180.
PHI=PHI*3.1415927/180.
C----- CHANGE CV UNITS FROM CM SQ/SEC TO M SQ/DAY
CV=CV*8.64
PO=DEP*GAMT1
C----- THE DENOMINATOR OF THE FOLLOWING STATEMENT INDICATES NUMBER OF TIMES
C----- OUTPUT WILL BE GENERATED FOR THE TOTAL TIME OF THAW
TOUT=TF/IO
TOUTP=TOUT
XC=2.1*DX
C----- CALCULATE TIME TO THAW THROUGH 2.1 DEPTH INCREMENTS

```

HTS FORTRAN IV G COMPILER (O/S REL 21.7) HAIN 12-27-75 08:45:02 PAGE 0002

```

0025 IF (H) 6C,60,70
0026 60 TO=((X0*CB1)*(X0*CB1)-CB1*CB1)/CM
0027 GOTO 71
0028 70 TO=((X0*CB)*(X0*CB)-CB*CB)/CM
0029 71 TIME=TC
C----- ESTIMATE OF PORE PRESSURES FOR THIS THAW DEPTH
0030 U(1)=C-2*P(PC,GANSUB,X0,BETR)
0031 U(2)=U(1)
0032 DT=TC/20.
0033 X=TC
0034 DERIV=X/TIMP
0035 CALL POSIT(N,V,NP)
0036 N1=NP
0037 V1=V
0038 N=N1+1
0039 U(N)=U(1)
0040 CALL OUTPUT
C----- THIS PROGRAM DOES NOT RETURN ABOVE THIS STATEMENT UNTIL A NEW SET
C----- OF DATA IS READ
0041 25 IF (TIME.GT.TF) GO TO 99
0042 TIMP=TIME+DT
0043 RT=CV*DT/(DX*DX)
C----- STUFF X AND DX/DT AT THE JTH TIME STEP.....
0044 XJ=X
0045 DERJ=DERIV
C----- CALCULATE X AND DX/DT AT THE (J+1)TH TIME STPP.....
0046 IF (H) 65,65,75
0047 65 CALL THAW1
0048 GOTO 85
0049 75 CALL THAW
0050 85 XJ1=X
0051 DERJ1=DERIV
0052 CALL POSIT(N2,V2,NP)
0053 MARK=0
0054 N2=NP
0055 IREM=0
0056 IF (N2.EQ.N1) GO TO 1
0057 IREM=N2-N1
0058 V2=V2+IREM
0059 MARK=1
0060 1 D(1)=2.*(1.-BT)*U(1)+BT*U(2)
0061 N=N1+1
0062 NL2=N-2
0063 IF (NL2.LF.1) GO TO 4
0064 DO 2 I=2,NL2
0065 D(I)=BT*(U(I+1)+U(I-1)) +2.*(1.-BT)*U(I)
0066 D(N-1)=BT*V1+U(N-2)/(1.+V1) + (1.-BT)*U(N-1) + PT*U(N)/(1.+V1)
0067 DO 3 I=1,NL2
0068 A(I)=2.*(1.+BT)
0069 B(I)=BT
0070 C(I)=BT
0071 C(1)=C.
0072 A(N-1)=1.+BT
0073 C(N-1)=BT*V2/(1.+V2)
0074 B(N-1)=PT/(1.+V2)

```



```

NTS  FORTRAN IV G COMPILER (O/S REL 21.7)          MAIN          12-27-75    08:45:02    PAGE 0003

C-----CALCULATE THE COEFFICIENTS FOR THE FINITE DIFFERENCE EQUATION
C-----AT THE BOUNDARY(NTH) NODE .....
0075  BJ=CV*DT/(V1*V1+DX*DX)
0076  BJ1=CV*DT/(V2*V2+DX*DX)
0077  PJ=P(P0,GANSUR,XJ,BETR)
0078  PJ1=P(P0,GANSUR,XJ1,BETR)
0079  CJ=V1+DX*DEFJ/CV
0080  CJ1=V2+DX*DEFJ1/CV
0081  A(N)=1.+PJ1*(1.+CJ1)
0082  C(N)=RJ1
0083  B(N)=0.
0084  D(N)=(1.-BJ-BJ1)*U(N)+BJ*(N-1)+BJ1*(N-1)+BJ+CJ*PJ
C-----SOLVE THE ESTABLISHED FINITE DIFFERENCE EQUATIONS
      CALL GAUSSL(N)
      DO 8 I=1,N
0085  8  U(I)=C(I)
0086  8  IF(MARK.FO.C) GO TO 10
0087  8  DIST=V2*DX
0088  8  GRAD=(U(N)-U(N1))/DIST
0089  8  UX=U(N)
0090  8  DO 5 I=N,N2
0091  5  U(I)=U(N1)+GRAD*(I-N1)*DX
0092  5  U(N2+1)=UX
0093  5  N1=N2
0094  5  V1=V2-IRFM
0095  5  IF(V1.LE.C.C) V1=0.0000000001
0096  5  MARK=0
0097  5  C-----ESTABLISH APPROPRIATE TIME STEP
0098  5  NG=300
0099  5  DT=DX/(NG*DERIV)
0100  5  TIME2=TIME/2.
0101  5  IF(DT.LT.TIME2) GO TO 30
0102  5  DT=TIME2
0103  5  IF (TIME.LT.TOUTP) GO TO 25
0104  5  TOUTP=TOUTP+TOUT
0105  5  CALL OUTPUT
0106  5  WRITE(6,108)
0107  5  FORMAT('C',)
0108  5  GO TO 25
0109  5  END
0110

```

```

MTS  FORTPAN IV G COMPILER (O/S REL 21.7)          GAUSEL      12-27-75      08:45:02      PAGE 0001

0001      SUBROUTINE GAUSEL(N)
0002      COMMON U(500),A(500),B(500),C(500),D(500),GOUT(500),IX,PC,N1,V1,X
0003      COMMON GANSUR,GANT1,GANT3,CV,TIME,PHR,BETR,DERIV,CB,CM,DEP,CB1
C-----
C----- THIS SUBROUTINE SOLVES 'N' LINEAR SIMULTANEOUS TRIAGONAL
C----- EQUATIONS, AND STORES THE RESULT IN THE ARRAY C(I).....
C-----
0004      IF(N.GT.1)GO TO 8
0005      C(N)=D(N)/A(N)
0006      GO TO 6
C----- TO CHANGE TO UPPER TRIANGULAR FORM.
0007      DO 5 I=2,N
0008      A(I)=A(I)-B(I-1)*C(I)/A(I-1)
0009      D(I)=D(I)-D(I-1)*C(I)/A(I-1)
0010      C(I)=0.
C----- BACK SUBSTITUTION..
0011      C(N+1)=0.
0012      I=N
0013      C(I)=(D(I)-B(I)*C(I+1))/A(I)
0014      IF(I.LE.1)GO TO 6
0015      I=I-1
0016      GO TO 4
0017      6  RETURN
0018      END

```

```

MTS FORTRAN IV G COMPILER (O/S FPL 21.7)                OUTPUT      12-27-75    08:45:02    PAGE 0001

0001      SUBROUTINE OUTPUT
0002      COMMON U(500),A(500),B(500),C(500),D(500),UOUT(500),DI,PC,N1,V1,X
0003      COMMON GMSUB,GANT3,CV,TIME,PHR,BETR,DERIV,CB,CN,DEP,CB1
0004      N1=N1-1
0005      TIMDAY=TIME
0006      V1=N1-V1
0007      V1=N1-V1
0008      WRITE(6,8)TIMDAY,X,V1N1
0009      8   FORMAT('C',, THE ELAPSED TIME FOR THIS CALCULATION =',F9.2,' DA
0010      IYS',/10.,, THE THAW DEPTH =',F7.2,' M. ',/10.,, THE NUMBER OF
0011      1DEPTH INCREMENTS =',F10.2)
0012      IF (N1.LE.1) WRITE(6,10)
0013      10  FORMAT('C',, PORE PRESSURES ARE NOT VALID FOR THIS THAW DEPTH
0014      1AND FACTOR OF SAFETY WILL NOT BE CALCULATED',/ *****
0015      2*****
0016      3*****
0017      N=N1+1
0018      IF (N1.LE.1) GOTO 12
0019      WRITE(6,10C5)
0020      10C5 FORMAT('C',, THE PORE PRESSURE-DEPTH INCREMENT PROFILE IS AS FOL
0021      1LLOWS: UNITS ARE IN KM/50 M ')
0022      3   WRITE(6,3) (U(I),I=1,N)
0023      3   FORMAT('O',10F10.2)
0024      IF (BETR.LE.0) GOTO 12
0025      CALL SSAN(N)
0026      12 RETURN
0027      END

```

```

0001      SUBROUTINE THAW1
0002      COMMON U(500),A(500),B(500),C(500),D(500),UOUT(500),DX,PC,M1,V1,X
0003      COMMON GANSUR,GANT1,GANT3,CV,TIME,FHM,BETR,DERIV,CB,CN,DEP,CB1
C----- THIS SUBROUTINE CALCULATES THE DEPTH OF THAW FROM THE EQUATION
C-----  $X = \sqrt{CB1 + CB1 \cdot CN \cdot TIME}$  -CB1
C----- THE ROUTINE ALSO CALCULATES THE DERIVATIVE DX/DT...
C----- *****
0004      X=SQRT(CB1+CB1*CN*TIME)-CB1
0005      DERIV=CN/(2.*SQRT(CB1+CB1*CN*TIME))
0006      RETURN
0007      END

```

HTS FORTRAN IV G COMPILER (O/S REL 21.7) THAW 12-27-75 08:45:02 PAGE 0001
 0001 SUBROUTINE THAW
 0002 COMMON U(500),A(500),B(500),C(500),D(500),ROUT(500),DX,P0,M1,V1,X
 0003 COMMON GANSUB,GANT1,GANT3,CV,TIME,PFR,BETR,DEIV,CB,CH,DEP,CB1
 C---- THIS SUBROUTINE CALCULATES THE DEPTH OF THAW FROM THE EQUATION
 C---- X=SQRT(CB*CB+CM*TIME)-CB
 C---- THE ROUTINE ALSO CALCULATES THE DERIVATIVE DX/DT...
 C---- *****
 0004 X=SQRT(CB*CB+CM*TIME)-CB
 0005 DERIV=CM/(2.*SQRT(CB*CB+CM*TIME))
 0006 RETURN
 0007 END

```

NTS  FORTRAN IV G COMPILER (O/S REL 21.7)          POSIT          12-27-75    08:45:03    PAGE 0001

0001      SUBROUTINE POSIT(N,V,NP)
0002      COMMON U(SOC),A(500),B(500),C(500),D(500),UOUT(SOC),DX,PO,N1,V1,X
0003      COMMON GANSUP,GANT1,GANT3,CV,TIME,PHR,BETR,DERIV,CB,CN,DEP,CB1
C-----THIS ROUTINE GIVES THE POSITION OF THE FREEZE-THAW INTERFACE
0004      NP=X/DX
0005      V=X/DX-NP
0006      N=NP+1
0007      RETURN
0008      END

```

```

0001      SUBROUTINE SSAM(N)
0002      C----- THIS SUBROUTINE CALCULATES THE FACTOR OF SAFETY OF A THAWING SLOPE
0003      C-----
0004      COMMON U(500),A(500),B(500),C(500),D(500),UOUT(500),DX,P0,M1,V1,X
0005      ENS=(DEP*GAMT1+X*GANSUB)/COS(BETR)  U(N)
0006      PS=TAN(PHR)/TAN(BETR)*(GAMT1+DEP*GANSUB*X-(U(N)/COS(BETR)))/(GAMT1
0007      1+DEP*GAMT3*X)
0008      WRITE(6,105)U(N),ENS,SS,PS
0009      FORMAT('C',10X,'THP SORE PRESSURE ACTING AT THE BASE OF THE THAW DE
0010      1PTH =',F10.2,'KN /SQ M','0',10X,'THE EFFECTIVE NORMAL STRESS AT TH
0011      2E BASE OF THE THAW DEPTH =',F10.2,'KN/SQ M','0',10X,'THE SHEARING
0012      3STRESS AT THE BASE OF THE THAW DEPTH =',F10.2,'KN/SQ M','0',10X,'T
0013      4HE FACTOR OF SAFETY =',F10.2)
0014      RETURN
0015      END

```

```

HTS  FORTRAN IV G COMPILEP (O/S REL 21.7)      P      12-27-75      08:45:03      PAGE 0001
0001      PEAL FUNCTION P(PO,GANSUB,X,BETP)
C-----THIS FUNCTION CALCULATES THE NORMAL EFFECTIVE OVERBURDEN STRESS
C-----AT THE PEETP-THAN INTERFACE....
0002      P=(PC+GANSUB*X)*COS(BETP)
0003      RETURN
0004      END

```


DATA INPUT:

THE RATE OF THAW IS GIVEN BY: $X(T) = \sqrt{\text{SORT}(K3/K2 \cdot H \cdot 2 \cdot K3 \cdot TS / (L \cdot \text{TIME})) - K3/K2} \cdot H$
 THE THERMAL COND. OF THE SURCHARGE = 0.00650 CAL/DEG C CM S
 THE THERMAL COND. OF THE INSULATION = 0.00300 CAL/DEG C CM S
 THE THERMAL COND. OF THE LOWER SOIL = 0.00300 CAL/DEG C CM S
 THE THICKNESS OF INSULATION = 0.15 M.
 THE AVE AIR TEMP = 16.90 DEG C
 THE SOIL WILL TERMINATE AT TIME = 130.0 DAYS
 THE COEFF OF CONSOL = 0.0020 CM SQ/SEC
 THE GRID SPACING IN THE X-DIRECTION = 0.040 M.
 THE DEPTH OF SURCHARGE = 0.91 M.
 THE TOTAL UNIT WT. OF THE SURCHARGE MATRL = 19.65 KN/M³
 THE SPECIFIC GRAVITY OF THE SOIL = 2.70
 THE WATER CONTENT OF THE LOWER SOIL = 0.35
 THE UNFROZEN WATER CONTENT OF THE LOWER SOIL = 0.0
 THE FRICTION ANGLE OF THE SOIL = 22.00 DEGREES
 THE SLOPE ANGLE = 12.00 DEGREES
 THE DESIRED NO. OF TIMES OUTPUT WILL BE PRODUCED OVER THE THAW PERIOD = 5

THE ELAPSED TIME FOR THIS CALCULATION = 14.70 DAYS

THE THAW DEPTH = 0.08 M.

THE NUMBER OF DEPTH INCREMENTS = 2.10

PORE PRESSURES ARE NOT VALID FOR THIS THAW DEPTH AND FACTOR OF SAFETY WILL NOT BE CALCULATED *****

THE ELAPSED TIME FOR THIS CALCULATION = 26.01 DAYS

THE THAW DEPTH = 0.15 M.

THE NUMBER OF DEPTH INCREMENTS = 3.66

THE PORE PRESSURE-DEPTH INCREMENT PROFILE IS AS FOLLOWS: UNITS ARE IN KN/SQ M

0.22 0.45 0.67 0.82

THE PORE PRESSURE ACTING AT THE BASE OF THE THAW DEPTH = 0.82 KN/SQ M

THE EFFECTIVE NORMAL STRESS AT THE BASE OF THE THAW DEPTH = 17.90 KN/SQ M

THE SHEARING STRESS AT THE BASE OF THE THAW DEPTH = 4.28 KN/SQ M

THE FACTOR OF SAFETY = 1.69

THE ELAPSED TIME FOR THIS CALCULATION = 52.00 DAYS

THE THAW DEPTH = 0.28 M.

THE NUMBER OF DEPTH INCREMENTS = 7.07

THE PORE PRESSURE-DEPTH INCREMENT PROFILE IS AS FOLLOWS: UNITS ARE IN KN/SQ M

C.22 0.43 0.65 0.86 1.08 1.30 1.51 1.52
 THE PORE PRESSURE ACTING AT THE BASE OF THE THAW DEPTH = 1.52KN /SQ M
 THE EFFECTIVE NORMAL STRESS AT THE BASE OF THE THAW DEPTH = 18.34KN/SQ M
 THE SHEARING STRESS AT THE BASE OF THE THAW DEPTH = 4.80KN/SQ M
 THE FACTOR OF SAFETY = 1.54

THE ELAPSED TIME FOR THIS CALCULATION = 78.01 DAYS

THE THAW DEPTH = 0.41 M.

THE NUMBER OF DEPTH INCREMENTS = 10.29

THE PORE PRESSURE-DEPTH INCREMENT PROFILE IS AS FOLLOWS: UNITS ARE IN KN/SQ M

0.21	0.42	0.63	0.84	1.05	1.26	1.47	1.68	1.89	2.10
2.16									

THE PORE PRESSURE ACTING AT THE BASE OF THE THAW DEPTH = 2.16KN /SQ M

THE EFFECTIVE NORMAL STRESS AT THE BASE OF THE THAW DEPTH = 18.78KN/SQ M

THE SHEARING STRESS AT THE BASE OF THE THAW DEPTH = 5.29KN/SQ M

THE FACTOR OF SAFETY = 1.43

THE ELAPSED TIME FOR THIS CALCULATION = 104.01 DAYS

THE THAW DEPTH = 0.53 M.

THE NUMBER OF DEPTH INCREMENTS = 13.35

THE PORE PRESSURE-DEPTH INCREMENT PROFILE IS AS FOLLOWS: UNITS ARE IN KN/SQ M

C.20	0.41	0.61	0.82	1.02	1.23	1.43	1.64	1.84	2.05
2.25	2.46	2.66	2.73						

THE PORE PRESSURE ACTING AT THE BASE OF THE THAW DEPTH = 2.73KN /SQ M

THE EFFECTIVE NORMAL STRESS AT THE BASE OF THE THAW DEPTH = 19.24KN/SQ M

THE SHEARING STRESS AT THE BASE OF THE THAW DEPTH = 5.76KN/SQ M

THE FACTOR OF SAFETY = 1.35

THE ELAPSED TIME FOR THIS CALCULATION = 110.03 DAYS

THE THAW DEPTH = 0.65 M.

THE NUMBER OF DEPTH INCREMENTS = 16.26

THE POPE PRESSURE-DEPTH INCREMENT PROFILE IS AS FOLLOWS: UNITS ARE IN KN/SQ M

0.20	0.40	0.60	0.80	1.00	1.20	1.40	1.60	1.80	2.00
2.20	2.40	2.60	2.80	3.00	3.20	3.25			

THE POPE PRESSURE ACTING AT THE BASE OF THE THAW DEPTH = 3.25KN /SQ M

THE EFFECTIVE NORMAL STRESS AT THE BASE OF THE THAW DEPTH = 19.69KN/SQ M

THE SHEARING STRESS AT THE BASE OF THE THAW DEPTH = 6.20KN/SQ M

THE FACTOR OF SAFETY = 1.28

DATA INPUT:

THE RATE OF THAW IS GIVEN BY: $K(T) = \text{SQRT}(K3/K2 \cdot H + 2 \cdot K3 \cdot TS / L \cdot \text{TIME}) - K3/K2 \cdot H$
 THE THERMAL COND. OF THE SURCHARGE = 0.006500 CAL/DEG C CM S
 THE THERMAL COND. OF THE INSULATION = 0.000300 CAL/DEG C CM S
 THE THERMAL COND. OF THE LOWER SOIL = 0.003000 CAL/DEG C CM S
 THE THICKNESS OF INSULATION = 0.23 M.
 THE AVE AIR TEMP = 16.90 DEG C
 THE SOLN WILL TERMINATE AT TIME = 130.0 DAYS
 THE COEFF OF CONSOL = 0.00200 CM SQ/SEC
 THE GRID SPACING IN THE X-DIRECTION = 0.040 M.
 THE DEPTH OF SURCHARGE = 0.61 M.
 THE TOTAL UNIT WT. OF THE SURCHARGE MATRL = 19.65 KN/M³
 THE SPECIFIC GRAVITY OF THE SOIL = 2.70
 THE WATER CONTENT OF THE LOWER SOIL = 0.35
 THE UNFROZEN WATER CONTENT OF THE LOWER SOIL = 0.0
 THE FRICTION ANGLE OF THE SOIL = 22.00 DEGREES
 THE SLOPE ANGLE = 12.00 DEGREES
 THE DESIRED NO. OF TIMES OUTPUT WILL BE PRODUCED OVER THE THAW PERIOD = 5

THE ELAPSED TIME FOR THIS CALCULATION = 19.46 DAYS

THE THAW DEPTH = 0.08 M.

THE NUMBER OF DEPTH INCREMENTS = 2.10

PORE PRESSURES ARE NOT VALID FOR THIS THAW DEPTH AND FACTOR OF SAFETY WILL NOT BE CALCULATED

THE ELAPSED TIME FOR THIS CALCULATION = 26.02 DAYS

THE THAW DEPTH = 0.11 M.

THE NUMBER OF DEPTH INCREMENTS = 2.79

PORE PRESSURES ARE NOT VALID FOR THIS THAW DEPTH AND FACTOR OF SAFETY WILL NOT BE CALCULATED

THE ELAPSED TIME FOR THIS CALCULATION = 52.01 DAYS

THE THAW DEPTH = 0.22 M.

THE NUMBER OF DEPTH INCREMENTS = 5.47

THE PORE PRESSURE-DEPTH INCREMENT PROFILE IS AS FOLLOWS: UNITS ARE IN KN/SQ M

0.12	0.24	0.36	0.48	0.60	0.66
------	------	------	------	------	------

THE PORE PRESSURE ACTING AT THE BASE OF THE THAW DEPTH = 0.66 KN/SQ M

THE EFFECTIVE NOMINAL STRESS AT THE BASE OF THE THAW DEPTH = 12.90 KN/SQ M

THE SHEARING STRESS AT THE BASE OF THE THAW DEPTH = 3.33 KN/SQ M

THE FACTOR OF SAFETY = 1.57

THE ELAPSED TIME FOR THIS CALCULATION = 78.02 DAYS

THE THAW DEPTH = 0.32 M.

THE NUMBER OF DEPTH INCREMENTS = 8.06

THE PORE PRESSURE-DEPTH INCREMENT PROFILE IS AS FOLLOWS: UNITS ARE IN KN/SQ M

0.12	0.24	0.36	0.48	0.60	0.73	0.85	0.97	0.97
------	------	------	------	------	------	------	------	------

THE PORE PRESSURE ACTING AT THE BASE OF THE THAW DEPTH = 0.97 KN /SQ M

THE EFFECTIVE NORMAL STRESS AT THE BASE OF THE THAW DEPTH = 13.45 KN/SQ M

THE SHEARING STRESS AT THE BASE OF THE THAW DEPTH = 3.72 KN/SQ M

THE FACTOR OF SAFETY = 1.46

THE ELAPSED TIME FOR THIS CALCULATION = 104.02 DAYS

THE THAW DEPTH = 0.42 M.

THE NUMBER OF DEPTH INCREMENTS = 10.55

THE PORE PRESSURE-DEPTH INCREMENT PROFILE IS AS FOLLOWS: UNITS ARE IN KN/SQ M

0.12	0.24	0.36	0.49	0.61	0.73	0.85	0.97	1.09	1.22
------	------	------	------	------	------	------	------	------	------

THE PORE PRESSURE ACTING AT THE BASE OF THE THAW DEPTH = 1.28 KN /SQ M

THE EFFECTIVE NORMAL STRESS AT THE BASE OF THE THAW DEPTH = 13.98 KN/SQ M

THE SHEARING STRESS AT THE BASE OF THE THAW DEPTH = 4.10 KN/SQ M

THE FACTOR OF SAFETY = 1.38

THE ELAPSED TIME FOR THIS CALCULATION = 130.02 DAYS

THE THAW DEPTH = 0.52 M.

THE NUMBER OF DEPTH INCREMENTS = 12.96

THE PORE PRESSURE-DEPTH INCREMENT PROFILE IS AS FOLLOWS: UNITS ARE IN KN/SQ M

0.12	0.24	0.37	0.49	0.61	0.73	0.85	0.98	1.10	1.22
------	------	------	------	------	------	------	------	------	------

1.34 1.46 1.58

THE PORE PRESSURE ACTING AT THE BASE OF THE THAW DEPTH = 1.58 KN /SQ M

THE EFFECTIVE NORMAL STRESS AT THE BASE OF THE THAW DEPTH = 14.40 KN/SQ M

THE SHAPING STRESS AT THE BASE OF THE THAW DEPTH = 4.07MN/SQ M

THE FACTOR OF SAFETY = 1.31

.....

APPENDIX C

This appendix contains two computer programs that may be utilized in computing the amount of solar radiation encountered by a sloping surface. It also contains the details for computing the amount of radiation reflected from one surface to another.

C.1 Program 1:

This program computes the length of a shadow cast by a sky line obstruction on a sloping surface. Figure C-1 illustrates the configuration. The symbols in the figure are defined as:

\hat{S}_u = a unit vector along the rays of the sun.

\hat{S}_L = a unit vector normal to the slope.

\hat{O}_b = a unit vector along the base line of the obstruction.

\bar{S}_H = the length of the shadow measured on the slope along the azimuth of the sun.

\bar{P} = the length of the shadow measured perpendicular to the obstruction on the slope.

\bar{H} = height of the obstruction.

are: Direction cosines for the sun and the normal to the slope

	Sun (\hat{S}_u)	Slope \hat{S}_l
x axis	$\sin Z \cos a_{su}$	$-\cos a_{sl} \sin b$
y axis	$-\sin Z \sin a_{su}$	$\sin a_{sl} \sin b$
z axis	$-\cos Z$	$\cos b$

where

a_{su} = azimuth of the sun

a_{sl} = azimuth of the normal to the slope

Z = zenith angle of the sun

b = zenith angle of the normal to the slope or the slope angle measured from the horizontal

Let \bar{E} be a vector in the plane of the slope along the base of the obstruction and, therefore, perpendicular to the unit normal of the slope.

$$\bar{E} = \{1 + \tan^2 b [\cos^2 (a_{ob} - a_{s1})]\}^{1/2} \quad - - - [C.1]$$

where a_{ob} = the azimuth of the obstruction

$$\bar{N} = \left\{ \frac{H^2 \tan^2 z}{[\bar{E} (1+c)]^2} [2.0 \tan^2 b \cos^2 (a_{s1} - a_{su}) (1 - \cos(a_{su} - a_{ob})) + \sin^2 (a_{su} - a_{ob})] \right\}^{1/2} \quad - - - [C.2]$$

where $c = \tan Z \tan b [(\cos (a_{s1} - a_{su}))] \quad - - - [C.3]$

$$Z = \arccos [\cos \delta \cos \phi \cos w + \sin \delta \sin \phi]$$

where δ = declination of the sun (degrees)

ϕ = latitude of the site (degrees)

w = hour angle of the sun measured positively to the west of the solar noon or negatively to the east (degrees)

The input parameters for the program are:

- i) Declination of the sun in degrees (DECLIN) (F6.2 format)
- ii) Latitude of the site in degrees (ALAT) (F6.2 format)
- iii) Height of obstruction in meters (H) (F5.1 format)
- iv) Azimuth of obstruction in degrees (AOB) (F7.2 format)
- v) Azimuth of slope in degrees (ASL) (F7.2 format)
- vi) Slope angle in degrees (B) (F7.2 format)
- vii) Hour angle in degrees (HRANGL) (F7.2 format)

The listing and a sample of the output are included.

C.2 Program 2:

This program computes the daily direct beam radiation and the total solar daily radiation on a slope. It also computes the average daily direct beam radiation and the average total solar daily radiation on a slope for the time period of interest.

The expression for the angle between the rays of the sun and the normal to the slope:

$$\cos \Lambda = \cos \delta (-\cos w \sin \phi \cos a \sin b - \sin w \sin a \sin b + \cos b \cos w \cos \phi) + \sin \delta (\cos \phi \cos a \sin b + \sin \phi \cos b) \quad - - - [C.4]$$

δ = declination of the sun
 w = hour angle of sun (measured positively to the west of solar noon)
 ϕ = latitude of the site
 a = azimuth of a unit normal to the slope
 b = angle of slope to the horizontal

The input parameters for the program are contained on two cards.

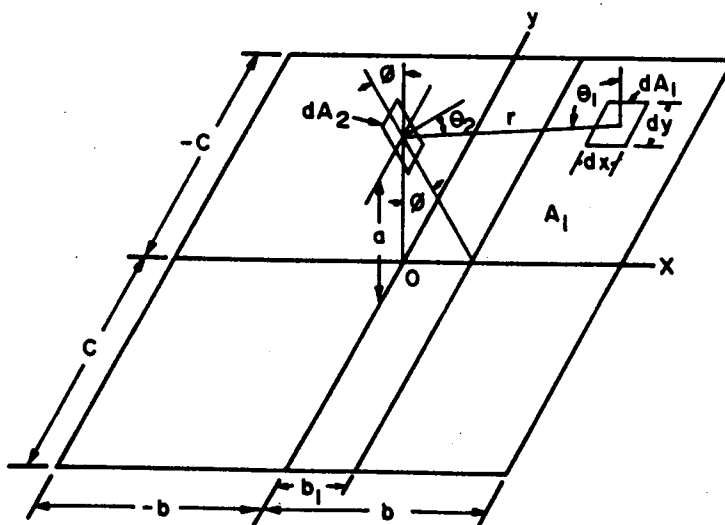
Card 1: number of cards (N) (I10 format)

Card 2: i) latitude of the site (A1at) (F10.2 format)
 ii) azimuth of the normal to the slope (Azs1) (F10.2 format)
 iii) slope angle in degrees (S1a) (F10.2 format)
 iv) time to begin calculations; measured from Mar 21 in days (T1) (I10 format)
 v) final time of calculations in days (T2) (I10 format)
 vi) total solar radiation on a horizontal surface at the site (QHT) (F10.0 format)

A sample of the output follows the computer listing.

C.3 Reflected Radiation from Surface 1 to Surface 2 (After Threlkeld 1970)

The following provides a basis for computing the amount of radiation diffusely reflected from one surface to another.



C.2 Relation of a Small Surface dA_2 to a Diffusely Reflecting Large Surface A_1 (After Threlkeld, 1963).

Figure C.2 illustrates a small surface dA_2 whose plane is inclined by an angle θ to a perpendicular position with respect to surface A_1 . The distance between the two surfaces is a . The surface A_1 is rectangular and reflects radiation diffusely. The albedo of this surface is α_1 . The amount of radiation reflected by surface A_1 is given by:

$$dq = \alpha_1 I_1 dA_1 \quad - - - [C.5]$$

where dq = the radiation in ly/hr diffusely reflected by dA_1 upon a hemisphere of radius r

I_1 = the intensity of solar radiation on surface A_1

Since A_1 is assumed to be a pure diffuse reflector,

$$dq = \pi r^2 I_{rn} \quad - - - [C.6]$$

where I_{rn} is the intensity of reflected radiation along the normal to dA_1 and at a distance r away.

$$dI_r = I_{rn} \cos \theta_1 \cos \theta_2 \quad - - - [C.7]$$

where dI_r = the intensity of radiation incident upon dA_2 due to radiation diffusely reflected by dA_1 .

$$dI_r = \frac{\alpha_1 I_1 dA_1 \cos \theta_1 \cos \theta_2}{\pi r^2} \quad - - - [C.8]$$

$$dA_1 = dx dy$$

$$\cos \theta_1 = a/r$$

$$\cos \theta_2 = x/r \cos \theta - a/r \sin \theta$$

$$r = \sqrt{x^2 + y^2 + a^2}$$

Integration of equation [C.8] gives

$$I_r = \frac{\alpha_1 I_1 a}{\pi} \int_{-c}^c \int_{b_1}^b \frac{(x \cos \theta - a \sin \theta)}{(x^2 + y^2 + a^2)^2} dx dy \quad - - [C.9]$$

$$I_r = \frac{\alpha_1 I_1}{\pi} F \quad - - - [C.10]$$

$$\text{where } F = a \int_{-c}^c \int_{b_1}^b \frac{(x \cos \theta - a \sin \theta)}{(x^2 + y^2 + a^2)^2} dx dy \quad - - - [C.11]$$

The solution for F for several special cases is contained in Table C-1.

TABLE C-1

FACTOR F IN EQ. (C.10) FOR SEVERAL SPECIAL CASES

CASE	F
A. $\tan \phi \geq b/a$, $b_1 = b$	$F = 0$
B. $-b/a \leq \tan \phi \leq b/a$, $b_1 = a \tan \phi$	$F = \tan^{-1} \frac{c \cos \phi}{a} - \frac{(a \cos \phi + b \sin \phi)}{\sqrt{a^2 + b^2}} \tan^{-1} \frac{c}{\sqrt{a^2 + b^2}}$ $+ \frac{c \sin \phi}{\sqrt{a^2 + c^2}} (\tan^{-1} \frac{a \tan \phi}{\sqrt{a^2 + c^2}} - \tan^{-1} \frac{b}{\sqrt{a^2 + c^2}})$
1. General case	
2. Same as Case B-1 with b and c infinitely large and a finite	$F = \frac{\pi}{2} (1 - \sin \phi)$
3. $\phi = 0$, $b_1 = 0$ (Plane of dA_2 perpendicular to A_1)	$F = \tan^{-1} \frac{c}{a} - \frac{a}{\sqrt{a^2 + b^2}} \tan^{-1} \frac{c}{\sqrt{a^2 + b^2}}$
4. Same as Case B-3 but with b and c infinitely large and a finite	$F = \frac{\pi}{2}$
C. $\tan \phi \leq -b/a$, $b_1 = -b$	$F = -2 \sin \phi \left(\frac{b}{\sqrt{a^2 + b^2}} \tan^{-1} \frac{c}{\sqrt{a^2 + b^2}} \right.$ $\left. + \frac{c}{\sqrt{a^2 + c^2}} \tan^{-1} \frac{b}{\sqrt{a^2 + c^2}} \right)$
1. General case	
2. $\phi = -\pi/2$ (dA_2 parallel to and facing A_1)	$F = \frac{2b}{\sqrt{a^2 + b^2}} \tan^{-1} \frac{c}{\sqrt{a^2 + b^2}}$ $+ \frac{2c}{\sqrt{a^2 + c^2}} \tan^{-1} \frac{b}{\sqrt{a^2 + c^2}}$
3. Same as Case C-2 but with b and c infinitely large and a finite	$F = \pi$

MTS FORTRAN IV G COMPILER (O/S REL 21.7)

MAIN

12-27-75

08:44:32

PAGE 0001

```

0001 C**** PROGRAM TO COMPUTE SHADOW LENGTH ON SLOPING GROUND
0002 1 READ(5,2)DECLIN,ALAT,H,AOB,ASL,B,HRANGL
0003 2 FORMAT(2F6.2,P5.1,4F7.2)
0004 WRITE(6,3)DECLIN,ALAT,H,AOB,ASL,B,HRANGL
0005 3 FORMAT('0',,DECLINATION OF THE SUN =',F7.2,'DEG',/,LATIT
0006 1UDE OF THE SITE =',F7.2,'DEG',/,HEIGHT OF OBSTRUCTION =',F7.2,
0007 2,'M',/,AZIMUTH OF OBSTRUCTION =',F7.2,'DEG',/,AZIMUTH OF SL
0008 3OPE =',F7.2,'DEG',/,SLOPE ANGLE =',F7.2,'DEG',/,HRANGL =',
0009 4F7.2)
0010 CONV=3.1415927/180.0
0011 DECLIN=DECLIN*CONV
0012 ALAT=ALAT*CONV
0013 AOB=AOB*CONV
0014 ASL=ASL*CONV
0015 B=B*CONV
0016 HRANGL=HRANGL*CONV
0017 Z=ARCOS(COS(DECLIN)*COS(ALAT)*COS(HRANGL)+SIN(DECLIN)*SIN(ALAT))
0018 ASU=ARSIN(SIN(HRANGL)*COS(DECLIN)*1.0/SIN(Z))
0019 SUY=SIN(Z)*COS(ASU)
0020 SUZ=-SIN(Z)*SIN(ASU)
0021 SLX=-COS(ASL)*SIN(B)
0022 SLY=SIN(ASL)*SIN(B)
0023 SLZ=COS(B)
0024 EX=-COS(AOB)
0025 EY=SIN(AOB)
0026 EZ=(COS(AOB)*SLX-SIN(AOB)*SLY)/SLZ
0027 E=SQRT(EX**2+EY**2+EZ**2)
0028 OBY=-COS(AOB)/E
0029 OBY=SIN(AOB)/E
0030 OBY= (-TAN(B)*COS(AOB-ASL))/E
0031 C=TAN(Z)*TAN(B)*COS(ASL-ASU)
0032 SHZ= (-H*C)/(1+C)
0033 SHY= (H/(1+C))*TAN(Z)*SIN(ASU)
0034 SHX= (H/(1+C))*COS(ASU)*TAN(Z)
0035 ANX=SHY*OBY-SHZ*OBY
0036 ANY=SHZ*OBY-SHX*OBY
0037 ANZ=SHX*OBY-SHY*OBY
0038 AN=SQRT(ANX**2+ANY**2+ANZ**2)
0039 WRITE(6,20)ANX,ANY,ANZ,AN
0040 20 FORMAT('0',10X,' NX=',F7.2,3X,' NY=',F7.2,3X,' NZ=',F7.2,3X,
0041 1N=',F7.2)
0042 GO TO 1
0043 END

```

\$RUN -LOAD#
08:44:33

DECLINATION OF THE SUN = 23.50DEG
LATITUDE OF THE SITE = 60.00DEG
HEIGHT OF OBSTRUCTION = 30.00M
AZIMUTH OF OBSTRUCTION = 0.0 DEG
AZIMUTH OF SLOPE = 180.00DEG
SLOPE ANGLE = 20.00DEG
HRANGL = 75.34

NX= 19.76 NY= -0.07 NZ= 54.28 N= 57.77

DECLINATION OF THE SUN = 23.50DEG
LATITUDE OF THE SITE = 60.00DEG
HEIGHT OF OBSTRUCTION = 30.0CM
AZIMUTH OF OBSTRUCTION = 0.0 DEG
AZIMUTH OF SLOPE = 270.00DEG
SLOPE ANGLE = 20.00DEG
HRANGL = 75.34

*** NX= 0.00 NY= -69.97 NZ= 192.23 N= 204.57 ***

```

HTS  FORTRAN IV G COMPILER (O/S REL 21.7)          MAIN          12-27-75    08:43:49    PAGE 0001

C-----PROGRAM TO DETERMINE SHORT WAVE RADIATION ON A SLOPE FROM VALUES ON
C-----A HORIZONTAL SURFACE
      DIMENSION COPR(365)
      INTEGER T1,T2
      CONV=3.1415927/180.
      8C READ(5,100)ALAT,AZSL,SLA,T1,T2,QHT,P,AL
      100 FORMAT(3F10.0,2I10,3F10.0)
      AZSL=90.0
      DO 30 N=1,3
      AZSL=AZSL+90.0
      P=0.30
      DO 30 L=1,4
      R=R+0.65
      SLA=-10.0
      DO 20 M=1,9
      SLA=SLA+10.0
      101 WRITE(6,101)ALAT,AZSL,SLA,T1,T2,QHT,P,AL
      101 FORMAT('11.0 DATA INPUT :',11.0, ' THE LATITUDE OF THE SITE IS',
      1P7.2,'DEGREES',/ ' THE AZIMUTH OF THE SLOPE IS',P7.2,'DEGREES',/ '
      2 THE ANGLE OF THE SLOPE IS',P7.2,'DEGREES',/ ' TIME TO BEGIN CA
      3LCULATIONS (COUNTED IN DAYS FROM MAR.21) IS',I10,' DAYS',/ ' FINA
      4L TIME OF CALCULATIONS',I10,' DAYS',/ ' AVERAGE TOTAL RADIATION O
      5N A HORIZONTAL SURFACE FOR THIS PERIOD OF TIME',P7.2,' LANGLEYS PER
      6 DAY',/ ' THE RATIO OF DIFFUSE SKY RADIATION TO TOTAL RADIATION =
      7,P7.2/ ' THE ALBEDO OF THE TERRAIN IS ',P7.2)
C-----ESTABLISH SINES AND COSINES
      SLAT=SIN(ALAT*CONV)
      SAZSL=SIN(AZSL*CONV)
      SSLA=SIN(SLA*CONV)
      CLAT=COS(ALAT*CONV)
      CAZSL=COS(AZSL*CONV)
      CSLA=COS(SLA*CONV)
      CSQSLA=COS(SLA/2.0*CONV)**2.0
      SSQSLA=SIN(SLA/2.0*CONV)**2.0
      SUN=C
      QDR=QHT*(1.-P)
C-----BEGIN CALCULATIONS
      DO 93 I=T1,T2
      WRITE(6,102)I
      102 FORMAT('C',7X,'DAY',I4,' ',/ ' *****')
      DECL=23.5*CONV*SIN(2.*CONV*180./365.*I)
      SDECL=SIN(DECL)
      CDECL=COS(DECL)
      SCOSZT=C
      SCOSST=C
      ICOUNT=0
      X=CAZSL*SSLA
      Y=SSLA*SAZSL
      Z=CSLA
      TT1=(X*SLAT+Y*CLAT)*CDECL
      TT2=(-X*CLAT+Y*SLAT)*SDECL
C-----SET HOUR ANGLE TO 00:00 HOURS
      H=-CONV*180.
      ITMP=0100
C-----INCREMENT HOUR ANGLE BY 20 MINUTRS

```



```

NTS FORTRAN IV G COMPILER (O/S REL 21.7)          MAIN          12-27-75    08:43:49    PAGE 0002

0043      97  W=0.087265
0044      ICOUNT=ICOUNT+1
0045      C----- DETERMINE COSINE OF SUN'S ZENITH ANGLE
0046      COSZ=CDECL*CLAT+COS(W)*SDECL*SLAT
0047      C----- TEST WHETHER SUN IS ABOVE HORIZON
0048      IF(COSZ.LE.0.0) GOTO 96
0049      C----- CALCULATE AREA UNDER COSZ VS TIME PLOT
0050      SCOSZT=SCOSZT+COSZ*0.087265
0051      Q2=-Y*SIN(W)*CDECL+T1*COS(W)
0052      C----- DETERMINE COSINE OF ANGLE BETWEEN SOLAR BEAM AND THE NORMAL TO THE SLOPE
0053      C----- COSSS=Q2*TT2
0054      C----- CHECK THAT SLOPE IS NOT IN SHADOW
0055      IF(COSSS.LE.0.0) COSSS=0.0
0056      C----- CALCULATE AREA UNDER COSSS VS TIME PLOT
0057      SCOSST=SCOSST+COSSS*0.087265
0058      96  IF(ICOUNT.NE.3) GOTO 97
0059      ICOUNT=0
0060      ITIME=ITIME+100
0061      IF(LTIME.LE.2400) GOTO 97
0062      CORR(I)=SCOSST/SCOSZT
0063      WRITE(6,104) CORR(I)
0064      104  FORMAT(' ',24X,' THE DAILY CORRECTION =',F7.2)
0065      QDS=QDS+CORR(I)
0066      WRITE(6,105) QDS
0067      105  FORMAT(' ',24X,' THE DAILY DIRECT BEAM RADIATION =',F7.2,' LY/DAY')
0068      QTS=QDS+QHT*R*CSQSLA
0069      WRITE(6,106) QTS
0070      106  FORMAT(' ',24X,' THE TOTAL RADIATION ON THE SLOPE =',F7.2,' LY/DAY'
0071      1)
0072      SUN=SUN+CORR(I)
0073      AVCORR=SUN/(T2-T1+1)
0074      WRITE(6,107) AVCORR
0075      107  FORMAT(' ',24X,' THE AVE. CORR. FOR TIME PERIOD T2-T1=',F7.2)
0076      QDSAV=QDS+AVCORR
0077      WRITE(6,108) QDSAV
0078      108  FORMAT(' ',24X,' THE AVE DAILY DIRECT BEAM RADIATION FOR TIME PERI
0079      QTSAV=QDSAV+QHT*R*CSQSLA
0080      WRITE(6,109) QTSAV
0081      109  FORMAT(' ',24X,' THE AVE TOTAL RADIATION ON THE SLOPE FOR THE TIME
0082      1 PERIOD T2-T1=',F7.2,' LY/DAY')
0083      QNSS=(QDSAV+SSQSLA*AL*QHT+QHT*P)*(1.C-AL)-QHT*R*SSQSLA
0084      WRITE(6,113) QNSS
0085      113  FORMAT(' ',24X,' THE AVE. NET SHORT WAVE RADIATION FOR TIME PERIOD
0086      1 T2-T1=',F7.2,' LY/DAY')
0087      2C  WRITE(6,112)
0088      112  FORMAT(' ',10X,' *****')
0089      3C  CONTINUE
0090      GO TO 80
0091      END

```

DATA INPUT :

THE LATITUDE OF THE SITE IS 68.30DEGREES
 THE AZIMUTH OF THE SLOPE IS 0.C DEGREES
 THE ANGLE OF THE SLOPE IS 20.00DEGREES
 TIME TO BEGIN CALCULATIONS (COUNTED IN DAYS FROM MAR.21) IS 86 DAYS
 FINAL TIME OF CALCULATIONS 121 DAYS
 AVERAGE TOTAL RADIATION ON A HORIZONTAL SURFACE FOR THIS PERIOD OF TIME 473.00LANGLEYS PER DAY
 THE RATIO OF DIFFUSE SKY RADIATION TO TOTAL RADIATION = 0.35
 THE ALBEDO OF THE TERRAIN IS 0.13

DAY 86

THE DAILY CORRECTION = 1.08

THE DAILY DIRECT BEAM RADIATION = 330.75LY/DAY

THE TOTAL RADIATION ON THE SLOPE = 491.31LY/DAY

DAY 87

THE DAILY CORRECTION = 1.08

THE DAILY DIRECT BEAM RADIATION = 330.75LY/DAY

THE TOTAL RADIATION ON THE SLOPE = 491.31LY/DAY

DAY 88

THE DAILY CORRECTION = 1.08

THE DAILY DIRECT BEAM RADIATION = 330.75LY/DAY

THE TOTAL RADIATION ON THE SLOPE = 491.31LY/DAY

DAY 89

THE DAILY CORRECTION = 1.08

THE DAILY DIRECT BEAM RADIATION = 330.75LY/DAY

THE TOTAL RADIATION ON THE SLOPE = 491.31LY/DAY

DAY 90

THE DAILY CORRECTION = 1.08

THE DAILY DIRECT BEAM RADIATION = 330.751Y/DAY

THE TOTAL RADIATION ON THE SLOPE = 491.311Y/DAY

DAY 91

THE DAILY CORRECTION = 1.08

THE DAILY DIRECT BEAM RADIATION = 330.751Y/DAY

THE TOTAL RADIATION ON THE SLOPE = 491.311Y/DAY

DAY 92

THE DAILY CORRECTION = 1.08

THE DAILY DIRECT BEAM RADIATION = 330.751Y/DAY

THE TOTAL RADIATION ON THE SLOPE = 491.311Y/DAY

DAY 93

THE DAILY CORRECTION = 1.08

THE DAILY DIRECT BEAM RADIATION = 330.751Y/DAY

THE TOTAL RADIATION ON THE SLOPE = 491.311Y/DAY

DAY 94

THE DAILY CORRECTION = 1.08

THE DAILY DIRECT BEAM RADIATION = 330.751Y/DAY

THE TOTAL RADIATION ON THE SLOPE = 491.311Y/DAY

DAY 95

THE DAILY CORRECTION = 1.08
THE DAILY DIRECT BEAM RADIATION = 330.75LY/DAY
THE TOTAL RADIATION ON THE SLOPE = 491.31LY/DAY

DAY 96

THE DAILY CORRECTION = 1.08
THE DAILY DIRECT BEAM RADIATION = 330.75LY/DAY
THE TOTAL RADIATION ON THE SLOPE = 491.31LY/DAY

DAY 97

THE DAILY CORRECTION = 1.08
THE DAILY DIRECT BEAM RADIATION = 330.75LY/DAY
THE TOTAL RADIATION ON THE SLOPE = 491.31LY/DAY

DAY 98

THE DAILY CORRECTION = 1.08
THE DAILY DIRECT BEAM RADIATION = 330.75LY/DAY
THE TOTAL RADIATION ON THE SLOPE = 491.31LY/DAY

DAY 99

THE DAILY CORRECTION = 1.08
THE DAILY DIRECT BEAM RADIATION = 330.75LY/DAY
THE TOTAL RADIATION ON THE SLOPE = 491.31LY/DAY

DAY 100

THE DAILY CORRECTION = 1.08
THE DAILY DIRECT BEAM RADIATION = 330.751Y/DAY
THE TOTAL RADIATION ON THE SLOPE = 491.311Y/DAY

DAY 101

THE DAILY CORRECTION = 1.08
THE DAILY DIRECT BEAM RADIATION = 330.751Y/DAY
THE TOTAL RADIATION ON THE SLOPE = 491.311Y/DAY

DAY 102

THE DAILY CORRECTION = 1.08
THE DAILY DIRECT BEAM RADIATION = 330.751Y/DAY
THE TOTAL RADIATION ON THE SLOPE = 491.311Y/DAY

DAY 103

THE DAILY CORRECTION = 1.08
THE DAILY DIRECT BEAM RADIATION = 330.751Y/DAY
THE TOTAL RADIATION ON THE SLOPE = 491.311Y/DAY

DAY 104

THE DAILY CORRECTION = 1.08
THE DAILY DIRECT BEAM RADIATION = 330.751Y/DAY
THE TOTAL RADIATION ON THE SLOPE = 491.311Y/DAY

DAY 105

THE DAILY CORRECTION = 1.08
THE DAILY DIRECT BEAM RADIATION = 330.75LY/DAY
THE TOTAL RADIATION ON THE SLOPE = 491.31LY/DAY

DAY 106

THE DAILY CORRECTION = 1.08
THE DAILY DIRECT BEAM RADIATION = 330.75LY/DAY
THE TOTAL RADIATION ON THE SLOPE = 491.31LY/DAY

DAY 107

THE DAILY CORRECTION = 1.08
THE DAILY DIRECT BEAM RADIATION = 330.75LY/DAY
THE TOTAL RADIATION ON THE SLOPE = 491.31LY/DAY

DAY 108

THE DAILY CORRECTION = 1.08
THE DAILY DIRECT BEAM RADIATION = 330.75LY/DAY
THE TOTAL RADIATION ON THE SLOPE = 491.31LY/DAY

DAY 109

THE DAILY CORRECTION = 1.08
THE DAILY DIRECT BEAM RADIATION = 330.75LY/DAY
THE TOTAL RADIATION ON THE SLOPE = 491.31LY/DAY

DAY 110

THE DAILY CORRECTION = 1.08

THE DAILY DIRECT BEAM RADIATION = 330.75LY/DAY

THE TOTAL RADIATION ON THE SLOPE = 491.31LY/DAY

DAY 111

THE DAILY CORRECTION = 1.08

THE DAILY DIRECT BEAM RADIATION = 330.75LY/DAY

THE TOTAL RADIATION ON THE SLOPE = 491.31LY/DAY

DAY 112

THE DAILY CORRECTION = 1.08

THE DAILY DIRECT BEAM RADIATION = 330.75LY/DAY

THE TOTAL RADIATION ON THE SLOPE = 491.31LY/DAY

DAY 113

THE DAILY CORRECTION = 1.08

THE DAILY DIRECT BEAM RADIATION = 330.75LY/DAY

THE TOTAL RADIATION ON THE SLOPE = 491.31LY/DAY

DAY 114

THE DAILY CORRECTION = 1.08

THE DAILY DIRECT BEAM RADIATION = 330.75LY/DAY

THE TOTAL RADIATION ON THE SLOPE = 491.31LY/DAY

DAY 115

THE DAILY CORRECTION = 1.03
THE DAILY DIRECT BEAM RADIATION = 317.94LY/DAY
THE TOTAL RADIATION ON THE SLOPE = 478.50LY/DAY

DAY 116

THE DAILY CORRECTION = 1.01
THE DAILY DIRECT BEAM RADIATION = 309.34LY/DAY
THE TOTAL RADIATION ON THE SLOPE = 469.90LY/DAY

DAY 117

THE DAILY CORRECTION = 1.01
THE DAILY DIRECT BEAM RADIATION = 309.16LY/DAY
THE TOTAL RADIATION ON THE SLOPE = 469.72LY/DAY

DAY 118

THE DAILY CORRECTION = 1.00
THE DAILY DIRECT BEAM RADIATION = 308.98LY/DAY
THE TOTAL RADIATION ON THE SLOPE = 469.54LY/DAY

DAY 119

THE DAILY CORRECTION = 0.98
THE DAILY DIRECT BEAM RADIATION = 300.24LY/DAY
THE TOTAL RADIATION ON THE SLOPE = 460.80LY/DAY

DAY 120

THE DAILY CORRECTION = 0.98
THE DAILY DIRECT BEAM RADIATION = 299.97LY/DAY
THE TOTAL RADIATION ON THE SLOPP = 460.52LY/DAY

DAY 121

THE DAILY CORRECTION = 0.95
THE DAILY DIRECT BEAM RADIATION = 291.21LY/DAY
THE TOTAL RADIATION ON THE SLOPE = 451.77LY/DAY
THE AVE. CORR. FOR TIME PERIOD T2-T1= 1.06
THE AVE DAILY DIRECT BEAM RADIATION FOR TIME PERIOD T2-T1 = 325.79LY/DAY
THE AVE TOTAL RADIATION ON THE SLOPE FOR THE TIME PERIOD T2-T1= 486.35LY/DAY
THE AVE. NET SHORT WAVE RADIATION FOR TIME PERIOD T2-T1= 424.09LY/DAY

APPENDIX D

Appendix D contains a computer program for the computation of vapor pressures, vapor pressure gradients and temperature gradients above the headscarp at the Fort Simpson landslide. Typical values of wet and dry bulb temperatures are included. Some selected values of net radiation are also listed in this Appendix. They indicate typical hourly intensities during the day and at night for both horizontal and sloped surfaces. They are listed in Table D-1.

D.1 This program computes vapor pressure, vapor pressure gradients and temperature gradients.

The vapor pressure is computed using the equations listed in lines 18, 19, and 20 of the program.

The variables in these equations are the wet bulb temperature (WBT), the dry bulb temperature (DBT), and the barometric pressure (BP). The steam point temperature (STMPT) = 373.16° K.

The data cards are assembled in groups of three. The first card provides the data at the 1 m level, the second at the 3 m level and the third at the 6 m level. The variables on each card are the same.

- i) Date (MDATE1, MDATE2) (A2,A4 format)
- ii) Time (ITIME 1, ITIME 2) (A4, A3 format)
- iii) Level (L(I)) (F6.2 format)
- iv) Dry bulb temperature (DBT(I)) (F6.2 format)
- v) Wet bulb temperature (WBT) (F6.2 format)
- vi) Barometric pressure (BP) (F8.2 format)
- vii) Temperature scale (ISCALE) (C or F, A2 format)

The listing and output are contained in the following pages.

FORTRAN IV G1 RELEASE 2.0 MAIN DATE = 76194 11/17/04 PAGE 0001

```

C**** PROGRAM TO COMPUTE VAPOR PRESSURES,VAPOR PPESSURE GRADIENTS AND
C**** TEMP. GRADIENTS
C**** VP GRAD1=VAPOR PPESSURE GRAD. FROM SURFACE TO 1 METER LEVEL
C**** VP GRAD2=VAPOR PPESSURE GRAD. FROM 1 METER LEVEL TO 3 METER LEVEL
C**** VP GRAD3=VAPOR PPESSURE GRAD. FROM 3 METER LEVEL TO 6 METER LEVEL
C**** T GRAD1=TEMP GRAD. FROM SURFACE TO 1 METER LEVEL
C**** T GRAD2=TEMP GRAD. FROM 1 METER LEVEL TO 3 METER LEVEL
C**** T GRAD3=TEMP GRAD. FROM 3 METER LEVEL TO 6 METER LEVEL
C**** VAPOR PPESSURE GRADS. ARE IN MB/METER
C**** TEMP. GRADS. ARE IN DEG C/METER
C**** WRITE HEADINGS
IMPLICIT REAL*8(A-H,O-Z)
DIMENSION VP(10),L(10),DBT(10)
INTEGER C/C%, ISCALE/'.'/
REAL L
WRITE(6,22)
12 FORMAT(' ',, *****
1 *****
2.)
22 FORMAT('1',4X,'DATE',4X,'TIME',4X,'LEVEL',3X,'DB TEMP',2X,'WB TEMP
1',2X,'B.PRES',2X,'VP PRES',2X,'VP GRAD1',2X,'VP GRAD2',2X,'VP GRA
2DB',2X,'T GRAD1',2X,'T GRAD2',2X,'T GRAD3')
32 DO 30 I=1,3
READ(5,23)MDATE1,MDATE2,ITIME1,ITIME2,L(1),DBT(1),WB*,BP,ISCALE
23 FORMAT(A2,A4,A4,A3,3F6.2,F8.2,A2)
IF(1 ISCALE.EQ.C)GOTO 36
DBT(1)=(DBT(1)-32.0)*5.0/9.0
WB*=(WB*-32.0)*5.0/9.0
36 STMP1=373.16
IF(BP.NE.0.0) GOTO 5
BP=1000.0
5 EPRIME=7.95357242D10*DEXP(-18.1972839*(STMP1/(WB*+273.16)))+5.32809
1*DLG(STMP1/(WB*+273.16))-70242.1852*DEXP(-26.1205253/(STMP1/(WB*+
2273.16)))+58.0691913*DEXP(-8.03945282*(STMP1/(WB*+273.16)))
DELTA E=(0.00666*(1.0+0.00115*WB*))*BP*(DBT(1)-WB*)
VP(1)=EPRIME-DELTA E
WRITE(6,25)MDATE1,MDATE2,ITIME1,ITIME2,L(1),DBT(1),WB*,BP,VP(1)
IF(1.EQ.3) GCTO31
30 CONTINUE
C
C COMPUTE GRADIENTS
31 VPGL=(VP(1)-8.7)/(L(1)-0.0)
VPGL2=(VP(2)-VP(1))/(L(2)-L(1))
VPGL3=(VP(3)-VP(2))/(L(3)-L(2))
TEGL=(DBT(1)-5.0)/(L(1)-0.0)
TEGL2=(DBT(2)-DBT(1))/(L(2)-L(1))
TEGL3=(DBT(3)-DBT(2))/(L(3)-L(2))
WRITE(6,24)VPGL,VPGL2,VPGL3,TEGL,TEGL2,TEGL3
GOTO 32
24 FORMAT('0',64X,F6.2,5X,F6.2,4X,F6.2,4X,F6.2,3X,F6.2,3X,F6.2,2X,F6.2,
25 FORMAT('0',3X,A2,A4,2X,A4,A3,1X,F5.2,3X,F6.2,3X,F6.2,3X,F7.2,4X,F6
1.2)
END
0004
0005
0006
0007
0008
0009
0010
0011
0012
0013
0014
0015
0016
0017
0018
0019
0020
0021
0022
0023
0024
0025
0026
0027
0028
0029
0030
0031
0032
0033
0034

```

DATE	TIME	LEVEL	DB TEMP	WB TEMP	B. PRES.	VP PRES	VP GRAD1	VP GRAD2	VP GRAD3	T GRAD1	T GRAD2	T GRAD3
JUN19	18:00	1.00	16.25	12.78	996.18	12.44						
JUN19	18:00	3.00	16.83	13.11	996.18	12.59						
JUN19	18:00	6.00	17.19	13.22	996.18	12.54						
JUN21	08:20	1.00	12.17	10.69	996.18	11.88	3.74	0.08	-0.02	11.25	0.20	0.12
JUN21	08:20	3.00	13.22	11.31	996.18	12.11						
JUN21	08:20	6.00	13.31	11.50	996.18	12.36						
JUN21	10:00	1.00	16.11	12.78	996.18	12.53	3.18	0.12	0.08	7.17	0.53	0.03
JUN21	10:00	3.00	16.72	13.39	996.18	13.13						
JUN21	10:00	6.00	17.11	13.61	996.18	13.24						
JUN21	12:00	1.00	18.06	13.61	996.18	12.61	3.83	0.30	0.04	11.11	0.31	0.13
JUN21	12:00	3.00	18.61	14.03	996.18	12.94						
JUN21	12:00	6.00	19.08	14.29	996.18	13.06						
JUN21	14:00	1.00	20.56	14.28	996.18	12.07	3.91	0.17	0.04	13.06	0.28	0.16
JUN21	14:00	3.00	20.94	14.44	996.18	12.10						
JUN21	14:00	6.00	22.06	14.61	996.18	11.64						
JUN21	16:00	1.00	20.22	14.28	996.18	12.29	3.37	0.01	-0.15	15.56	0.10	0.37
JUN21	16:00	3.00	21.44	14.44	996.18	11.76						
JUN21	16:00	6.00	21.67	14.67	996.18	12.00						
JUN22	04:00	1.00	14.44	12.39	996.59	13.01	3.59	-0.26	0.08	15.22	0.61	0.07
JUN22	04:00	3.00	14.44	13.44	996.59	14.74						
JUN22	04:00	6.00	15.00	13.72	996.59	14.84						
JUN22	09:40	1.00	11.72	11.53	996.59	13.46	4.31	0.87	0.03	9.44	0.0	0.10
JUN22	09:40	3.00	11.89	11.89	996.59	13.91						

JUL 5	41:00	1.00	13.89	11.22	991.65	11.55	2.95	0.04	-0.02	12.44	0.08	0.07
JUL 5	21:00	3.00	14.00	11.28	991.65	11.56						
JUL 5	21:00	6.00	14.44	11.28	991.65	11.26						
JUL 5	24:00	1.00	12.50	10.28	991.65	11.03	2.85	0.01	-0.10	8.99	0.04	0.15
JUL 5	24:00	3.00	13.00	10.50	991.65	11.03						
JUL 5	24:00	6.00	13.06	10.56	991.65	11.08						
JUL 10	14:20	1.00	22.22	14.44	987.52	11.29	2.33	0.00	0.02	7.50	0.25	0.02
JUL 10	14:20	3.00	22.50	14.72	987.52	11.59						
JUL 10	14:20	6.00	22.72	15.50	987.52	12.81						
JUL 10	16:00	1.00	22.22	14.94	987.52	12.16	2.59	0.15	0.41	17.22	0.14	0.07
JUL 10	16:00	3.00	22.56	15.11	987.52	12.23						
JUL 10	16:00	6.00	22.83	15.33	987.52	12.44						
JUL 10	18:00	1.00	24.39	15.14	987.52	11.06	3.46	0.04	0.07	17.22	0.17	0.05
JUL 10	18:00	3.00	25.00	15.78	987.52	11.80						
JUL 10	19:00	6.00	25.22	15.94	987.52	11.95						
JUL 10	20:00	1.00	23.89	15.00	987.52	11.15	2.36	0.37	0.05	19.30	0.31	0.07
JUL 10	20:00	3.00	24.56	15.17	987.52	11.00						
JUL 10	20:00	6.00	24.72	15.33	987.52	11.19						
JUL 10	22:00	1.00	22.33	15.00	987.52	11.85	2.45	-0.07	0.06	18.89	0.33	0.06
JUL 10	22:00	3.00	23.33	15.28	987.52	12.01						
JUL 10	22:00	6.00	25.78	15.56	987.52	12.21						
JUL 10	24:00	1.00	17.78	13.06	987.52	11.90	3.15	0.08	0.07	17.93	0.25	0.15
JUL 10	24:00	3.00	19.50	13.56	987.52	11.59						

JUL15	14:00	1.00	18.44	14.22	998.45	13.38	4.52	-0.11	0.04	10.61	0.64	0.17
JUL15	14:00	3.00	19.56	14.61	998.45	13.31						
JUL15	14:00	6.00	19.86	14.72	998.45	13.30						
JUL15	14:00	1.00	18.89	13.72	998.45	12.23	4.68	-0.04	-0.00	13.44	0.56	0.10
JUL15	16:00	3.00	19.44	14.39	998.45	13.00						
JUL15	16:00	6.00	20.00	14.50	998.45	12.82						
JUL15	18:00	1.00	19.61	14.50	998.45	13.08	3.53	0.38	-0.06	13.89	0.28	0.10
JUL15	18:00	3.00	20.00	14.67	998.45	13.11						
JUL15	18:00	6.00	20.83	14.72	998.45	12.65						
JUL15	20:00	1.00	19.72	14.11	998.45	12.33	4.38	0.01	-0.15	14.51	0.19	0.28
JUL15	20:00	3.00	20.57	14.33	998.45	12.08						
JUL15	20:00	6.00	21.67	14.33	998.45	11.41						
JUL15	22:00	1.00	20.17	13.33	998.45	10.73	3.63	-0.13	-0.22	14.72	0.47	0.33
JUL15	22:00	3.00	20.56	13.72	998.45	11.12						
JUL15	22:00	6.00	20.89	13.72	998.45	10.89						
JUL15	24:00	1.00	15.89	12.06	998.45	11.51	2.03	0.20	-0.07	15.17	0.19	0.11
JUL15	24:00	3.00	17.72	12.78	998.45	11.45						
JUL15	24:00	6.00	18.44	12.56	998.45	10.60						
JUL15	02:00	1.00	15.44	11.67	990.19	11.21	2.81	-0.03	-0.23	10.89	0.52	0.24
JUL15	02:00	3.00	16.00	11.67	990.19	10.84						
JUL15	02:00	6.00	16.17	11.72	990.19	10.82						
JUL15	04:00	1.00	13.33	9.83	990.19	9.82	2.51	-0.18	-0.31	10.44	0.28	0.04
JUL15	04:00	3.00	14.03	10.28	990.19	10.02						

JUL 16 04:00	6.00	14.17	10.29	990.19	9.93	1.12	0.10	-0.03	8.33	0.35	0.05
JUL 15 06:00	1.00	11.11	9.72	990.19	11.13						
JUL 16 06:00	3.00	11.78	9.72	990.19	10.69						
JUL 15 06:00	6.00	11.78	9.72	990.19	10.69						
JUL 16 08:00	1.00	13.44	9.94	990.19	9.91	2.43	-0.22	0.0	6.11	0.33	0.0
JUL 15 08:00	3.00	13.78	10.50	990.19	10.52						
JUL 16 08:00	6.00	13.94	10.50	990.19	10.41						
JUL 15 10:00	1.00	17.50	12.00	990.19	10.37	1.21	0.30	-0.04	8.44	0.17	0.06
JUL 16 10:00	3.00	18.19	12.33	990.19	10.44						
JUL 15 10:00	6.00	18.78	12.22	990.19	9.88						
JUL 15 12:00	1.00	19.89	13.33	990.19	10.95	1.67	0.04	-0.19	12.50	0.35	0.19
JUL 16 12:00	3.00	20.39	13.61	990.19	11.08						
JUL 15 12:00	6.00	20.61	13.33	990.19	10.47						
JUL 16 14:00	1.00	21.50	12.93	990.19	9.06	2.25	0.07	-0.20	14.89	0.25	0.07
JUL 16 14:00	3.00	22.56	13.22	990.19	9.00						
JUL 15 14:00	6.00	22.78	13.22	990.19	8.85						
JUL 15 15:00	1.00	22.22	13.28	990.19	9.31	0.35	-0.03	-0.05	16.50	0.53	0.07
JUL 16 16:00	3.00	23.22	13.75	990.19	9.43						
JUL 15 16:00	6.00	23.94	13.83	990.19	9.09						
JUL 16 18:20	1.00	17.44	13.22	990.19	12.39	0.61	0.06	-0.11	17.22	0.50	0.24
JUL 15 18:20	3.00	17.89	13.78	990.19	13.02						
JUL 15 18:20	6.00	18.44	13.33	990.19	11.91						
JUL 15 20:00	1.00	15.94	13.06	990.19	13.11	3.69	0.32	-0.37	12.44	0.22	0.19

TABLE D-1
RADIATION DATA JUNE 21/74 (LY/HR)
(FORT SIMPSON TEST SITE)

TIME (HOURS)	STA 1	STA 2	STA 3	STA 4	STA 5	STA 6
1:00	0.9	1.0	2.7	0.4	-2.0	0.1
2:00	1.5	1.8	3.6	1.1	-1.2	-
3:00	1.7	1.9	3.9	1.4	-0.6	-
4:00	0.9	1.1	5.8	0.6	-2.1	-
5:00	-0.4	-	2.5	0.9	-3.9	0.9
6:00	0.6	1.2	4.6	4.5	-2.0	3.6
7:00	1.7	3.1	10.2	13.3	-1.7	9.3
8:00	2.8	6.0	11.6	15.3	5.7	11.8
9:00	2.5	5.0	14.3	36.1	21.2	25.6
10:00	3.3	7.6	21.2	46.1	37.1	39.4
11:00	6.6	7.3	16.6	31.2	43.8	45.0
12:00	5.4	10.6	14.0	17.6	53.7	55.3
13:00	17.4	9.1	11.3	38.1	56.0	59.2
14:00	18.6	9.9	12.5	52.7	58.0	62.4
15:00	28.5	5.9	12.1	43.6	58.4	62.0
16:00	20.0	10.1	11.1	31.3	55.6	58.5
17:00	20.5	7.0	5.1	11.7	34.6	36.3
18:00	14.3	13.7	13.9	9.2	35.7	38.5
19:00	28.6	18.8	17.2	8.8	24.7	27.2
20:00	21.1	16.0	15.9	6.9	16.7	18.6
21:00	38.2	26.1	22.1	4.3	18.3	21.6
22:00	18.5	26.3	25.2	4.5	7.8	13.8
23:00	19.5	19.5	17.6	1.5	-2.1	6.0
24:00	3.5	5.1	7.9	-	-5.4	1.0
AVE	11.5	8.9	11.8	15.9	21.1	24.8

TABLE D-1 (CONTINUED)
RADIATION DATA JULY 11/74 (Ly/Hr)
(FORT SIMPSON TEST SITE)

TIME (HOURS)	STA 1	STA 2	STA 3	STA 4	STA 5	STA 6
1:00	0.9	-	-0.6	1.3	-5.1	1.9
2:00	1.1	-	-0.7	1.0	-4.8	1.9
3:00	1.5	0.2	-0.5	1.2	-4.3	1.9
4:00	2.1	0.8	-0.2	1.6	-3.7	1.9
5:00	2.1	0.7	-0.4	2.0	-3.9	2.3
6:00	2.9	1.6	0.7	7.3	1.3	5.1
7:00	3.4	2.6	2.0	15.6	2.2	12.2
8:00	4.3	4.1	4.0	10.0	2.8	10.3
9:00	5.5	5.2	8.1	19.1	11.7	18.7
10:00	7.4	7.6	12.1	24.0	19.2	26.4
11:00	7.6	7.1	18.6	30.9	38.0	44.5
12:00	7.4	6.6	16.2	23.8	44.0	52.0
13:00	13.3	11.5	16.1	29.8	46.0	55.6
14:00	15.3	12.0	29.0	33.2	49.9	59.3
15:00	14.6	10.5	29.6	24.4	38.0	47.4
16:00	21.1	9.9	53.2	17.9	45.0	54.1
17:00	8.2	4.4	10.8	4.4	2.2	4.7
18:00	15.0	14.0	20.3	11.4	16.3	22.3
19:00	18.6	15.5	18.1	11.5	13.5	19.4
20:00	32.1	22.2	25.7	8.2	17.9	24.1
21:00	41.5	30.0	29.2	8.1	17.8	24.1
22:00	19.8	16.4	13.1	6.5	5.5	12.4
23:00	10.3	9.7	4.7	3.7	-1.2	5.4
24:00	8.8	8.5	2.1	1.9	-3.6	3.0
AVE	10.9	8.5	13.1	12.6	14.6	21.6

TABLE D-1 (CONTINUED)

RADIATION DATA JULY 19/74
(FORT SIMPSON TEST SITE)

TIME (HOURS)	STA 1	STA 2	STA 3	STA 4	STA 5	STA 6
1:00	-1.6	0.8	0.3	-0.3	-5.9	1.9
2:00	-1.8	-1.0	-0.3	-0.7	-6.2	1.9
3:00	-1.8	-1.1	-0.6	-0.8	-6.2	1.9
4:00	-1.8	-1.1	-0.7	-1.0	-6.1	2.0
5:00	-1.6	-0.9	-0.6	-0.7	-5.6	2.1
6:00	-0.1	1.1	1.8	3.5	-3.2	4.8
7:00	1.9	3.2	4.0	4.4	-0.7	6.0
8:00	4.5	6.1	7.4	8.5	4.1	10.2
9:00	6.5	9.2	11.9	39.2	40.6	31.6
10:00	4.5	6.0	7.1	27.2	19.9	19.2
11:00	3.7	4.7	5.3	54.3	40.3	47.2
12:00	5.5	4.8	5.8	32.8	45.4	54.0
13:00	6.3	4.9	6.0	41.5	47.9	60.9
14:00	18.3	5.6	6.7	45.7	49.7	62.3
15:00	26.5	6.0	7.0	24.0	49.6	62.4
16:00	7.5	6.0	6.6	12.5	46.5	59.8
17:00	24.1	8.0	8.6	13.3	37.9	50.2
18:00	28.7	13.6	10.8	5.7	19.9	29.9
19:00	22.3	13.2	10.8	4.4	9.7	18.8
20:00	18.9	15.6	14.1	7.5	8.9	14.5
21:00	8.2	8.5	9.4	5.9	2.5	8.6
22:00	6.7	5.0	8.7	5.6	-1.9	5.6
23:00	2.1	3.4	4.2	2.3	-2.9	4.1
24:00	1.4	2.2	3.1	2.0	-2.7	2.1
AVE	7.9	5.2	5.8	14.2	16.1	23.7